AFOSR-TR- 85-0282

FINAL REPORT

on

SPARK GAP ELECTRODE EROSION

December 20, 1984

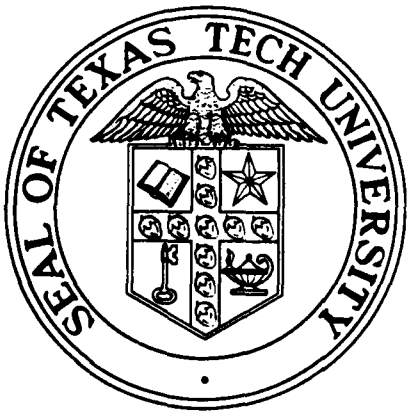

Air Force Office of Scientific Research
Grant No. 84-0015

PLASMA AND SWITCHING LABORATORY
LASER LABORATORY

Department of Electrical Engineering
TEXAS TECH UNIVERSITY

Lubbock, Texas 79409

Unclassified
SECURITY CLASSIFICATION OF THIS PAGE

REPORT DOCUMENTATION PAGE

1a. REPORT SECURITY CLASSIFICATION: Unclassified	1b. RESTRICTIVE MARKINGS
2a. SECURITY CLASSIFICATION AUTHORITY	3. DISTRIBUTION/AVAILABILITY OF REPORT: Approved for public release; Distribution Unlimited; distribution unlimited.
2b. DECLASSIFICATION/DOWNGRADING SCHEDULE: N/A	
4. PERFORMING ORGANIZATION REPORT NUMBER(S)	5. MONITORING ORGANIZATION REPORT NUMBER(S): AFOSR-TR- 85-0282
6a. NAME OF PERFORMING ORGANIZATION: Texas Tech University; 6b. OFFICE SYMBOL (If applicable): EE	7a. NAME OF MONITORING ORGANIZATION: Air Office of Scientific Research
6c. ADDRESS (City, State and ZIP Code): Dept. Electrical Engineering, P.O. Box 4439, Lubbock, TX 79409	7b. ADDRESS (City, State and ZIP Code): Bldg. 410, Bolling AFB, Washington, DC 20332
8a. NAME OF FUNDING/SPONSORING ORGANIZATION: Air Force Office of Scientific Res.; 8b. OFFICE SYMBOL (If applicable): NP	9. PROCUREMENT INSTRUMENT IDENTIFICATION NUMBER: AFOSR-84-0015
8c. ADDRESS (City, State and ZIP Code): Bldg. 410, Bolling AFB, Washington, DC 20332	10. SOURCE OF FUNDING NOS.

PROGRAM ELEMENT NO.	PROJECT NO.	TASK NO.	WORK UNIT NO.
61102F	2301	A7	

11. TITLE (Include Security Classification): Spark Gap Electrode Erosion

12. PERSONAL AUTHOR(S): H. Krompholz, M. Kristiansen

13a. TYPE OF REPORT	13b. TIME COVERED	14. DATE OF REPORT (Yr., Mo., Day)	15. PAGE COUNT
Final	FROM 10/1/83 TO 9/30/84	84/12/20	132

16. SUPPLEMENTARY NOTATION

17. COSATI CODES		
FIELD	GROUP	SUB. GR.
20	09	

18. SUBJECT TERMS (Continue on reverse if necessary and identify by block number): Breakdown, Recovery, Electrode, Erosion, Arc Voltage, Spark Gaps, ZIE (Jet Impact Erosion)

19. ABSTRACT (Continue on reverse if necessary and identify by block number)

The results of a one-year contract on electrode erosion phenomena are summarized. The arc voltage drop in a spark gap was measured for various electrode, gas, and pressure combinations. A previously developed model of self breakdown voltage distribution was extended. A jet model for electrode erosion was proposed and an experimental arrangement for testing the model was constructed. The effects of inhomogeneities and impurities in the electrodes were investigated.

20. DISTRIBUTION/AVAILABILITY OF ABSTRACT	21. ABSTRACT SECURITY CLASSIFICATION
UNCLASSIFIED/UNLIMITED ☑ SAME AS RPT. ☒ DTIC USERS ☐	Unclassified

22a. NAME OF RESPONSIBLE INDIVIDUAL	22b. TELEPHONE NUMBER (Include Area Code)	22c. OFFICE SYMBOL
Maj. H. Pugh	202/767-4906	AFOSR/NP

DD FORM 1473, 83 APR — EDITION OF 1 JAN 73 IS OBSOLETE

Final Report

SPARK GAP ELECTRODE EROSION

AFOSR Grant #84-0015

December 20, 1985

Principal Investigators: H. Krompholz
M. Kristiansen

Technician III: K. Zinsmeyer

Secretary: M. Byrd

Graduate Students: A. Donaldson
B. Maas
C. Yeh*

---

* Paid by the Republic of China (Taiwan)

INTRODUCTION

This report describes the work performed on a 1-year grant but also includes some related work, based on a previous AFOSR contract (F49620-79-C-0191), which was completed during this grant period. Some of the work described here is scheduled for completion in 1985 under a current grant (AFOSR #84-0032). The areas of investigation described here include:

1. Self breakdown voltage distributions
2. Electrode erosion
3. Spark gap voltage recovery

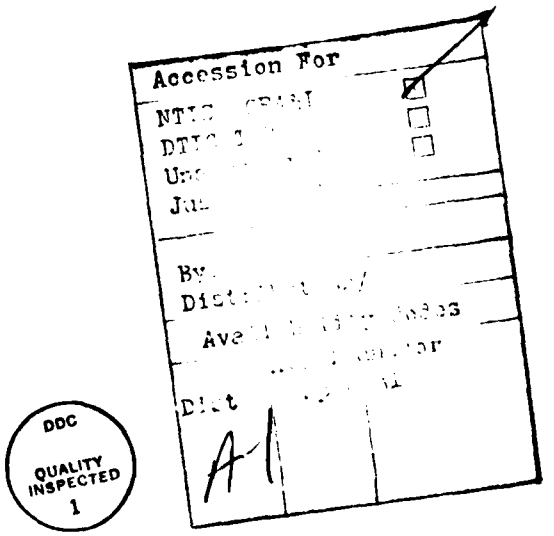

Table of Contents

Summary i

Spark Gap Electrode Erosion 1

References 21

Appendices 27

Publications and Inateractions 130

Spark Gap Electrode Erosion

A. SUMMARY

The work performed during this contract period has primarily been concerned with clarifying some of the remaining questions on performance limitations of high energy, rep-rated spark gap operation, i.e. voltage breakdown stability, electrode erosion, and voltage recovery. The accomplishments during the contract period include:

1. The theoretical model which had previously been developed to describe the self breakdown voltage distribution as a function of the relevant parameters (such as electrode surface conditions, gas type and pressure, and charging rate) has been extended to include effects caused by an inhomogeneous surface temperature distribution and by variations of the work function over the surface due to surface contaminations.
2. It has been found from a literature study, that one of the major physical mechanisms likely to contribute to erosion in all relevant parameter regimes is the impact of high temperature, supersonic "jets" - electrode material ejected from the opposite electrode surface. The characteristics of the jets, the process by which they are formed, and their influence on electrode erosion have mainly been discussed in early U.S., Soviet,

and Czech literature but have not been considered in our previous work or in any of the recent U.S. or Soviet literature on spark gaps. This provides new interpretations of our recent experimental results and may explain the major trends and parameter dependence of erosion on a physical basis. Futhermore, appropriate spark gap design offers promise for dramatically reducing the effect of erosion from this mechanism.

3. An experimental set up has been designed and tested which allows for a decoupling of breakdown conditions from the parameters relevant for erosion, i.e. gap distance, gas pressure, and current can be chosen independently.

4. Important background information for the quantitative analysis of erosion is a knowledge of the deposited energy in both the arc plasma and the electrode surface. Different diagnostic methods have been developed to measure these energies or the deposited power in the arc and in the electrodes. Measurements have been made for a sample space of 3 electrode materials, 3 gases, and 3 gas pressures.

5. Additional information concerning the basic erosion mechanisms in stainless steel, e.g. crack formation due to material inhomogeneities such as manganese stringers, has been obtained.

6. Studies concerning the voltage recovery mechanisms for rep rated spark gaps have been completed. For repetition rates on the order of kHz the voltage recovery is determined only by heat conduction in the electrodes and the surrounding gas. These mechanisms have been investigated by electrical diagnostics and interferometry, yielding complete information about the temperature distribution (temporal and spatial dependence) and its influence on the breakdown voltage. The results allow the development of scaling laws and design criteria for rep-rated spark gaps.
7. A facility for comparing high current, oscillatory discharge effects with those previously obtained for unipolar pulses has been constructed and instrumented.

B. MODELING OF SELF-BREAKDOWN VOLTAGE STATISTICS

Further development occurred on a model which relates the electrode surface structure produced by a high energy discharge to the self-breakdown voltage statistics. This model, previously described in Appendix I of the Fourth Annual Report [1] on AFOSR contract No. 49620-79-C-0191, has been modified to include the electrode surface temperature and work function as spatially dependent random variables. Details of this model are given in the Preprint of "Modeling of Self-Breakdown Voltage Statistics in High Energy Spark Gaps" in Appendix I and has been accepted for publication in the Journal of Applied Physics.

C. JET IMPACT EROSION (JIE)

During current conduction in a high energy spark gap high speed (10^4 m/s), directed streams of ionized electrode vapor ("jets") are produced in the space adjacent to the electrode surfaces. As the jets pass through the cathode and anode fall regions of the arc they are thought to become superheated (up to 40,000 °K) and upon impact with the opposite electrode produce macroscopic, crater-like, erosion. Numerous papers [2-25] have recently been found in the U.S., Soviet and Czech literature which describe both the means of jet production and its importance as a source of electrode erosion. The following includes a review of the important literature, and a description of the implications on more recent electrode erosion results at TTU and elsewhere.

1. Jet Production

Although the existence of high velocity jets of electrode vapor has been known since at least the 1920's, the mechanism of their production and acceleration has been a subject of considerable controversy since that time [2-9]. Starting with the work of Haynes [2] and Finkelnburg [3] in the 1940's serious attempts were made to explain the experimental findings in terms of the electrodynamic and thermal processes which occur in the region of the cathode and anode fall. A thorough review of the work done prior to 1972 is given by Holmes [7]. One of the most complete and tractable treatments of this problem for cathode jets was made by Minoo [6], and is

reproduced here. In his work, based on the transport equations of magnetogasdynamics in the cathode region, he derived an analytical expression for the plasma jet velocity v_1 at the end of the cathode region (assumed to be 10^{-3} cm from the cathode). It shows that v_1 strongly depends on the discharge current, I, and current density, J, the pressure, p_1, at the end of the cathode region, the ratio of the jet radius to the cathode spot radius, α, and the properties of the cathode material. To prove these dependencies he started with the equation for the the energy balance in the cathode region; given by

$$G = P_v + P_j + P_c + P_r, \tag{1}$$

where G is the source power (assumed to be $V_{arc}I$), and the components of the power dissipated are: P_v - by cathode heating and evaporation, P_j - by plasma jet heating and acceleration, P_c - by heat transfer to the electrode, and P_r - by cathode spot radiation. The following expression (Eq. 2) was then derived by a detailed analysis of Eq. (1) in the cathode region.

$$V_c\, I = \dot{m}(Q+h_1 + v_1^2/2) + (I/J)^{1/2}\, \lambda T_o + \varepsilon\sigma T_o^4\, (I/J) \tag{2}$$

$$\text{with } Q = L_f + L_b + \int_{T_i}^{T_b} c(t)dT \tag{3}$$

$$\text{and } h_1 = N_a(5kT_1 + eV_i)/M \tag{4}$$

In these equations T_o is the cathode temperature at the cathode surface, λ is the average thermal conductivity, is the total emissivity of the cathode surface, is the Stefan-Boltzmann constant, L_f and L_b are the latent heat of fusion and vaporization per unit mass, c(t) is the heat capacity per unit mass, T_i and T_b are the initial and the boiling temperatures of the cathode, h_1 is the enthalpy per unit mass of the jet at the edge of the cathode fall, N_a is Avagadro's number, M is the atomic mass of the ions, V_i is the ionization potential of the vapor atoms and T_1 the temperature of the plasma jet at the edge of the cathode fall.

From Eq. (2) and the other transport equations an expression for the velocity of the cathode jet was found which is highly dependent on pressure and current. It is hoped that a similar expression can be derived for anode jets as well.

2. Jet Characteristics

In order to substantiate a given mechanism which is responsible for the jet production and to apply this information to actual electrode erosion data the physical properties of the jet (temperature and velocity as a function of space and time) need to be determined for differing discharge conditions. Fortunately, many experiments have been performed which were designed to accomplish this and, although they were performed under a variety of conditions, the following list is a summary of those characteristics and trends applicable to high energy sparks.

- Initial jet temperature approaches 40,000 °K near the electrode surface [10], (10 kJ arc)
- Amount of jet material increases significantly with voltage (could be current) [11]
- Jet velocities increase with increasing current, and approach speeds of 2×10^4 m/sec [16, 22]
- Initial jet velocities are independent of the surrounding gas pressure [2]
- Jet emission occurs at high frequencies as a result of explosive emission of vapor from the electrode surface due to the transient nature of individual arc attachment points [13, 14, 20]
- Jets are always ejected perpendicular (within a very small solid angle) to the electrode surface regardless of the angle of the arc column gradient [2]
- Substitution of an oscillatory current pulse for a unipolar pulse produces little change in jet front velocity and, therefore, reversal of the electric field has little effect [2]
- Jets could be bent with an external magnetic field [2] and interact with the magnetic field produced by the arc current [23]
- Anode and cathode jets interact, forming regions of compression and rarefaction of the plasma which may move from electrode to electrode [12, 19-21]
- Periodicity of jet structure in the direction of propagation is inversely proportional to discharge volume [11]

- Properties for jet production between two electrodes is similar to processes occurring with an intense laser beam interacting with an electrode surface [13].

The discovery of several of these characteristics implied that the plasma jets could not only be a means of erosion, since material which makes up the jet is part of the electrode, but, more importantly, could act as a source of erosion as they impacted the opposite electrode surface.

3. Jet Influence on Erosion

Perhaps the first indication* that jet impact was a source of electrode erosion was reported by Zitka [15]. He concluded from experimental results that:

1. The wear of any electrode is influenced in most cases by the material of the opposing electrode.
2. The wear depends primarily on the energy transmitted by the vapor to the opposite electrode, and this energy increases rapidly as the gap distance decreases.
3. "One can expect that anode wear will be greater than the cathode wear in cases where the effect of the sprays (jets) does not exceed the effect of the energies which enter the electrodes by other paths".

---

* Earlier work is often referenced but, at this time, translations have not been obtained. See, for example S.L. Mandel'shtam and S.M. Raiskii, Izv. AN SSSR, ser.fizich., 13, 5, 549-565 (1949).

Although these experiments were conducted at low levels of energy (60 joules for a 500 V, 5 kA discharge) they were important in that they suggested a "new" mechanism (JIE) which could account for electrode erosion under certain conditions. Beginning in the 1960's Sultanov and others [16-21] started to study the effect of JIE for high energy discharges. Although much of their work made use of an electrode-insulator arrangement which was designed to act as a nozzle for the vapor jets, they reported that the results were similar for more conventional electrode arrangements. The principle findings of their work included:

1. The erosion pattern was essentially the same with or without the pulse current actually entering the electrode.
2. The amount of energy transferred to the electrode by the jet is given by the following proportionality

$$W \alpha vT \left(1 + \frac{\gamma-1}{2} M_a^2\right)$$

where v is the jet velocity, T is the jet temperature, γ is the ratio of specific heats, c_p/c_v, and M_a is the Mach number.

3. Regions of compression and rarefaction in the plasma between the electrodes (produced by the interaction of the sporadic emission of cathode and anode jets) moved back and forth between the electrodes and their "contact" with the electrodes was likely to be as important a factor on electrode erosion as the initial jet impact.

A theoretical comparison of the relative contributions of several sources (jet impact, charged particle impact, joule heating in the electrode, radiation from the arc) to the energy delivered to the electrode surface was done by Kalyatskiy et al. [24]. They found that the energy delivered by the jets represented the largest source by one to two orders of magnitude. Their calculations were done for breakdown through a solid dielectric but it is quite possible that the same trend would be true in gases (although probably not as large a difference).

It should be noted that Belkin and Kiselev, who are responsible for a large portion of the Soviet electrode erosion work, did mention JIE as a possible erosion factor in one of their brief papers [25], but it is interesting that they and others (Il'in and Lebedev [26]) reference some of the literature mentioned above but never used this information to explain quantitatively their results.

4. Implications on Previous Erosion Results

The mechanism of electrode erosion by jet impact possibly explains several phenomena which have defied adequate explanation in the past:

Material removal parallel to the electrode surface - It has been reported for a wide variety of conditions that the bulk of the electrode material is removed in droplet form parallel to the electrode surface [27-31]. Several theories were developed [32,33] which explained droplet formation in terms of various mechanisms for material removal from the microscopic craters formed by the individual points of current

attachment in the arc. However, Daalder [27] showed that the droplets were often considerably larger that the craters and thus, their origin must be from another source. Although several suggestions have been given to explain the removal of the molten material - $\bar{J} \times \bar{B}$ forces (Belkin [34]), thermoelastic waves (Rakhovskii [35]), and hydromagnetic flow of the molten material (Watson [36]) - it is believed that the experiments by Sultanov [16-21] strongly suggest the material is removed primarily by jet impact. For example, metal surfaces which were eroded by jet impact with and without current flow were virtually identical. (They also bore a remarkable similarity to the surfaces generated under unipolar pulse conditions at TTU). Thus, upon hitting the opposite electrode, high speed vapor jets melt the surface and remove the molten material as the jet is directed by the surface in the radial direction.

Erosion as a function pressure - Although experimental results for erosion as a function of pressure are quite varied [23, 34, 37, 40] generally the results can be grouped into two categories for pressures greater that 10^{-2} atm - the erosion either increases or does not change with increasing pressure. Most of the results which showed an increase involved reducing the gap spacing as the pressure was increased to keep the breakdown voltage and current the same. Interestingly, Gruber [37] found that there was a true distance effect (erosion decreasing with increasing distance) and when distance was fixed the erosion remained constant for

increasing pressure (keeping current and voltage the same by using an external trigger). His results explain the other observations in that the increased erosion with pressure was probably due to the corresponding decrease with distance although Gruber offered no physical explanation. Erosion by jet impact clearly would predict this trend, since at shorter gap distances the jet does not loose as much energy or become as diffuse.

To examine the effect of JIE several experiments are currently being designed. These experiments are scheduled for completion in May 1985. The experiments will make use of a special, ferrite isolated circuit designed to trigger the spark gap externally so as to allow for the decoupling of the variables which may affect erosion.

D. POWER DISSIPATED IN THE ARC PLASMA AND THE ELECTRODES

1. Measurement of tne Power Dissipated in the Arc

Information about the power dissipated in the arc plasma (including the attachment sites at the electrodes and its dependence on the relevant parameters (material and circuit data)) is important for the quantitative analysis of electrode erosion.

The general problem in determining arc voltage or resistance is the presence of inductive terms in the circuit equation

$$V_o = \frac{1}{C} \int i dt + \left(\frac{dL}{dt} + R\right) i + L \frac{di}{dt},$$

where $L = L_o + L_{arc}(t)$, $R = R_o + R_{arc}(t)$ with L_o, R_o are the circuit values which are determined by bulk material properties (major part is time independent) and surface properties (time dependent via skin effect).

The arc resistance $R_{arc}(t)$ has been determined with reasonable accuracy by measuring the arc radius vs time (using a streak camera registering the self luminance), and by estimating the circuit parameters, L_o, R_o, from a basic treatment of the time dependent skin effect [41]. These estimates have been checked by measurements of the anode and cathode voltage.

The measurements have been performed on an over-damped spark gap set up (Fig. 1) with a breakdown voltage of 35 kV and a maximum current of 30 kA. Figure 2 shows, as an example, the waveforms of current, arc resistance and resistive arc voltage drop for graphite electrodes and SF_6 filling gas at a pressure of 1 atm. The overall results can be summarized as follows:

1. Within the statistical error the resistance is independent of the electrode material.
2. The dependence of the minimum arc resistance on gap distance and pressure is

$$R_{min} = a \cdot pd$$

3. The constant a depends on the gas and has the values

$$a = 31 \pm 7 \text{ for air}$$
$$48 \pm 15 \text{ for } N_2$$
$$71 \pm 17 \text{ for } SF_6 \quad \text{in } \left(\frac{\Omega}{\text{cm bar}}\right)$$

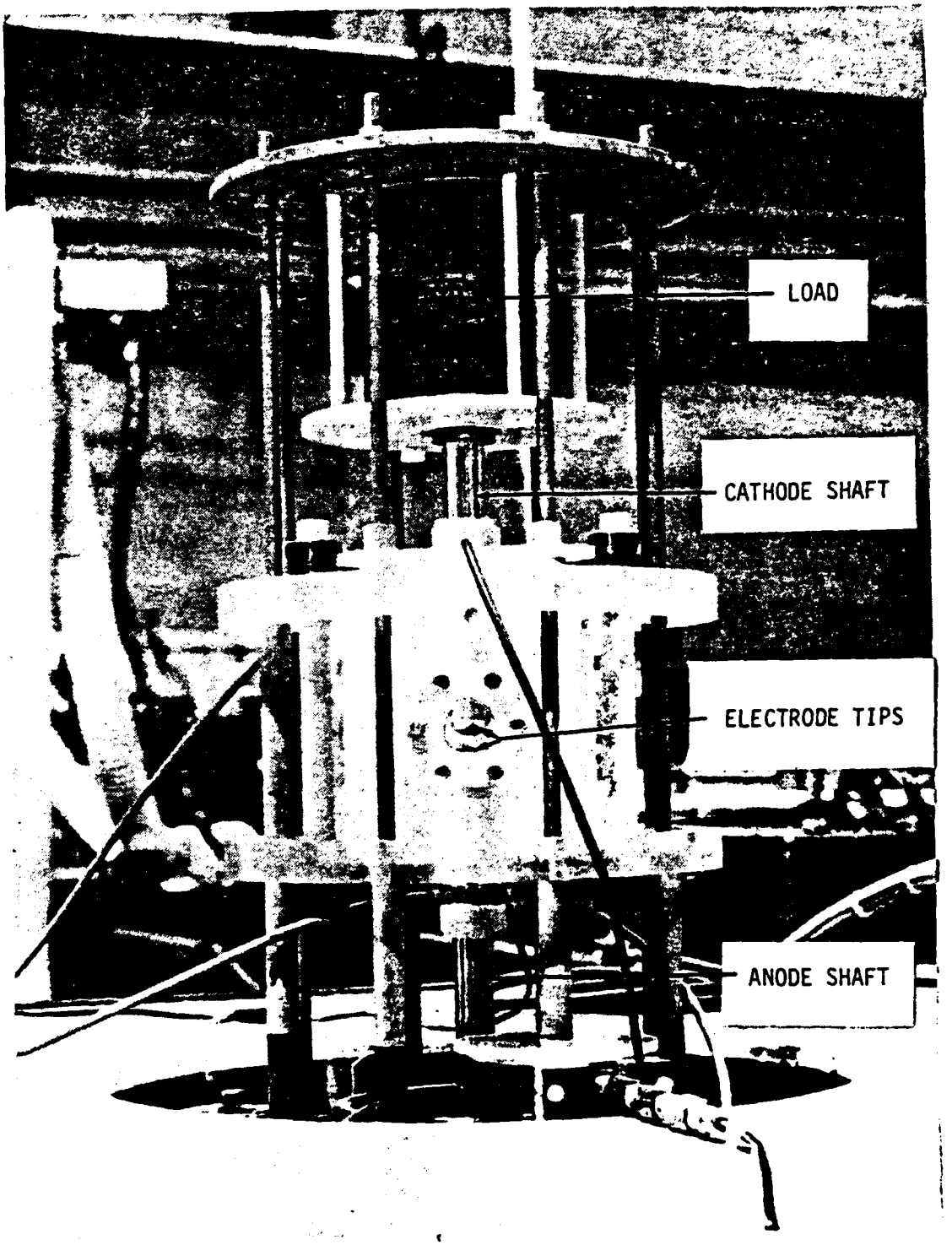

Figure 1 Mark IV Spark Gap.

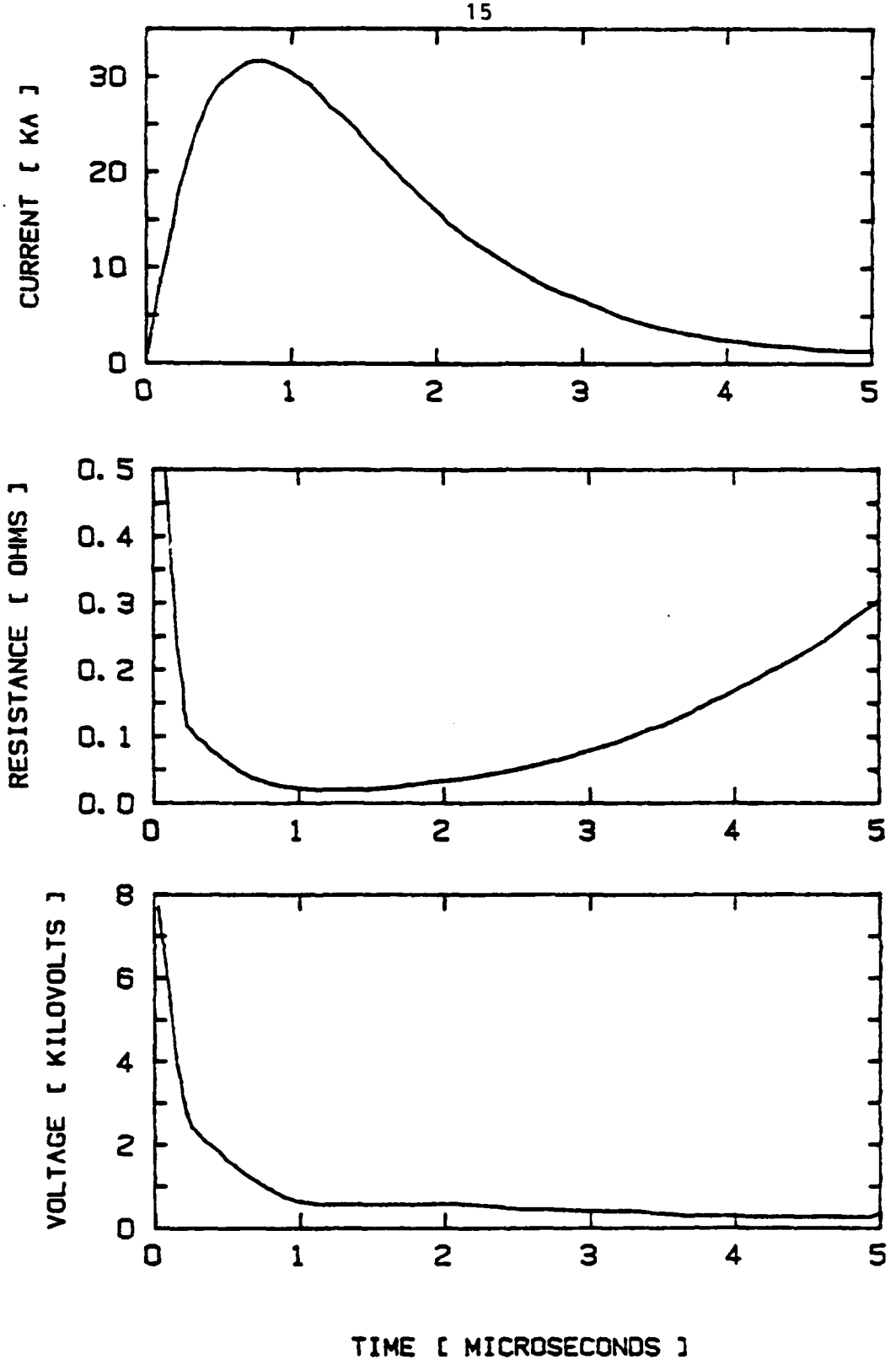

Fig. 2 Current, arc resistance and resistive arc voltage vs time for graphite-electrodes (gap distance 0.76 cm), filling gas SF_6 at a pressure of 1 atm.

4. The time dependence R(t) is in reasonable agreement with the description by Mesyats [42].

Table 1 gives an overview on some of the results (minimum arc resistance and total energy dissipated in the arc) for a variety of parameters.

TABLE I

Electrode Material	gas	pressure	R_{min}	R_{min}/pd	E_{diss}(J)
SS	air	1	41	32	70
		2	33	30	67
		3	29	30	62
Graphite	air	1	55	42	88
		2	42	33	73
		3	36	31	67
CuW	air	1	51	37	79
		2	35	28	69
		3	27	20	57
SS	N_2	1	76	72	110
		2	65	59	103
		3	45	43	83
Graphite	N_2	1	51	45	90
		2	48	43	78
		3	46	41	81
CuW	N_2	1	81	60	120
		2	50	31	75
		3	56	32	90
SS	SF_6	1	39	77	81
		2	40	68	77
		3	39	69	74
Graphite	SF_6	1	34	72	64
		2	34	68	60
		3	24	46	51
CuW	SF_6	1	42	90	76
		2	34	67	65
		3	40	79	73

Min. Resistance R_{min}, R_{min}/pd and Energy dissipated in the arc for different parameters. Total energy is 1.15 kJ.

2. Measurement of the energy deposited

To calculate the amount of energy deposited in the electrode and its origin an experiment is being performed similar to those done by Carder [43] and Foosnaes and Rondeel [44]. Figure 3 shows a typical heating and cooling curve for a thermally isolated electrode. Basically the experiment consists of measuring the temperature of the electrode during the cool-down cycle and calculating the effective temperature produced at the electrode during the firing cycle. From this information the energy delivered to the electrode per shot is calculated from $E = Mc\Delta T$, where m = mass and c = specific heat. A microprocessor controlled temperature acquisition device has been interfaced to our laboratory computer and the required thermocouples have been tested. In order to check the dependency of the energy on the resistive losses in the electrodes three different electrode materials are being used whose resistivities vary by almost three orders of magnitude (copper-tungsten; 3.4 μΩcm, stainless steel; 72 μΩcm, and graphite; 2700 μΩcm). To determine the effect of the gas the tests will be run in air and inert gases for pressures up to 3 atm. Both sets of experiments will be run with a ringing and a unipolar pulse and the results will be compared with the erosion rates obtained for these two pulse types in order to see if a correlation exists between the energy deposited in the electrode and the erosion rate.

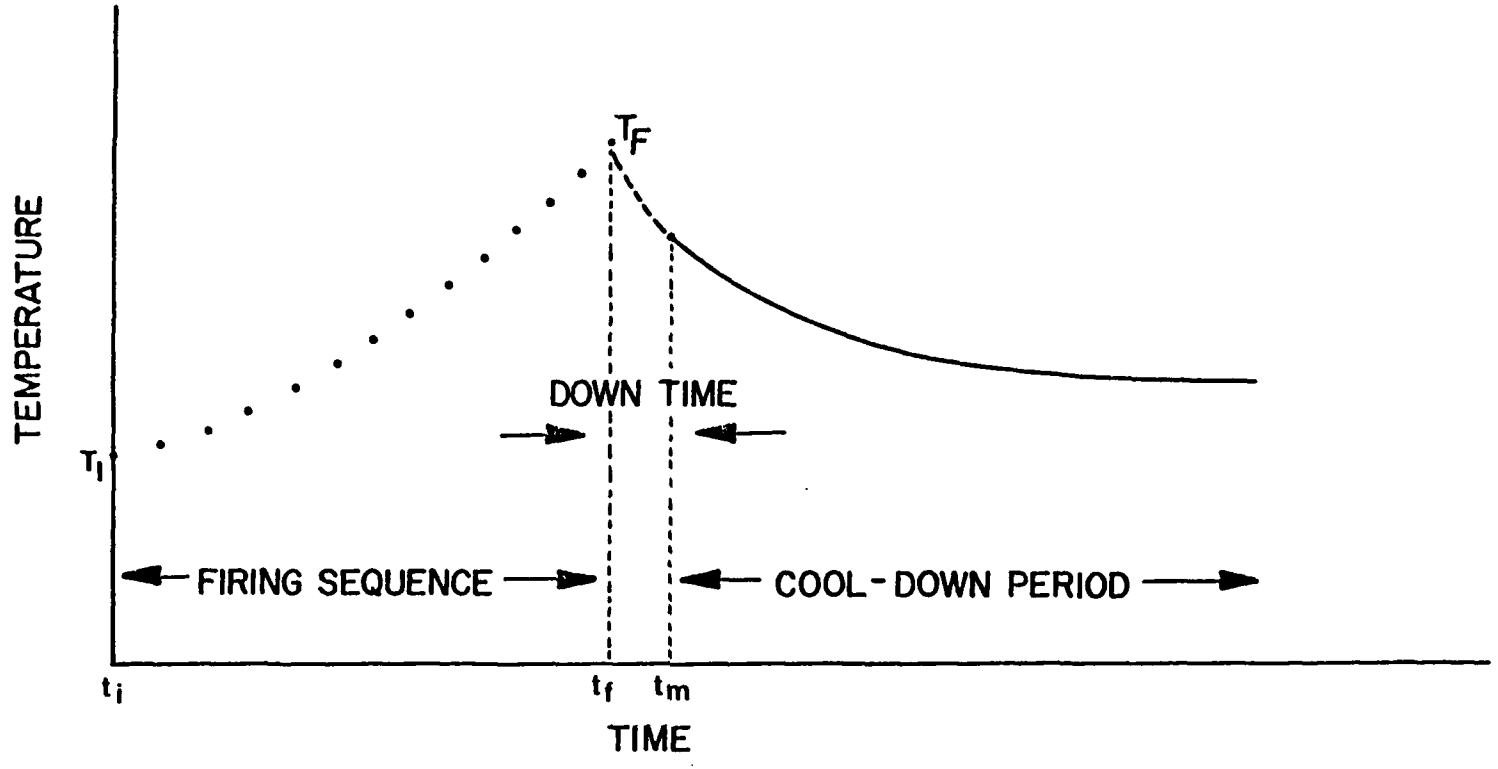

——— MEASURED (CONTINUOUS)

• • • • • • MEASURED (POINT BY POINT EXTRAPOLATION)

------- EXTRAPOLATED

$$\text{CALCULATION OF ENERGY PER SHOT} = \frac{MC\,\Delta T_{eff}}{\text{NO. SHOTS}}$$

Fig. 3 Typical Electrode Temperature vs Time for Energy Deposition Studies

E. Electrode Surface Analysis

Surface analysis work continued on the spark gap electrodes. This work, partially described in the Final Report [1] on AFOSR contract No. F49620-79-C-0191, is described in detail in Appendix II and is currently being revised in order to be submitted to the Journal of Applied Physics.

F. Voltage Recovery

Voltage recovery studies were concluded and resulted in a Ph.D. Dissertation [45]. Details of the diagnostic techniques and the results are discussed in a conference proceedings paper [46] reprinted in Appendix III.

F. REFERENCES

1. Final Report on Coordinated Research Program in Pulsed Power Physics, February 27, 1984, AFOSR Contract # F 49620-79-C-0191.
2. J. Haynes, Phys. Rev., 73, 891 (1948).
3. W. Finkelnburg, Phys. Rev., 74, 1475 (1948).
4. A.A. Plyutto, V.N. Ryzhkov, and A.T. Tapin, Soviet Phys. JETP, 20, 328 (1965).
5. H. Hugel, G. Kruelle, and T. Peters, AIAA Journ., 5, 551 (1967).
6. H. Minoo, 11th International Conference on Phenomena in Ionized Gases, Prague, Czechoslovakia, 74, (September 1973).
7. Electrical Breakdown of Gases, J.M. Meek and J.D. Craggs, ed, John Wiley and Sons, Chapter 11, p. 855 (1978).
8. M.P. Zekster and G.A. Lyubimov, Sov. Phys. Tech. Phys., 24, 1 (1979).
9. B. Ya Moizhes and V.A. Nemchinskii, Sov. Phys. Tech. Phys., 25, 43 (1980).
10. N.K. Sukhodrev and S.L. Mandel'shtam, Optics and Spectroscopy, 6, 473 (1959).
11. L.I. Grechikhin and L. Ya Min'ko, Sov. Phys. Tech. Phys., 7, 784 1963).
12. M.A. Sultanov and L.I. Kiselevskii, High Temperature, 4, 34 (1966).

13. L.I. Grechikhin and L. Ya Min'ko, Sov. Phys. Tech. Phys., 12, 846 (1967).

14. B.B. Davydov and L. Ya Min'ko Sov. Phys. Tech. Phys., 16, 53 (1971).

15. B.H. Zitka, Czech. Journ. of Phys., 3, 241 (1953).

16. M.A. Sultanov and L.I. Kiselevskii, High Temperature, 4, 375 (1966).

17. M.A. Sultanov, 9th International Conference on Phenomena in Ionized Gases, Bucharest, Romania, 669 (1969).

18. M.A. Sultanov, High Temperature, 8, 906 (1970).

19. M.A. Sultanov, Sov. Phys. Tech. Phys., 19, 478 (1974).

20. M.A. Sultanov and L.D. Senickin, Sov. Phys. Tech. Phys., 20, 1089 (1975).

21. M.A. Sultanov, Sov. Phys. Tech. Phys., 21, 815 (1976).

22. S.V. Gurov, T.A. Dzhafarov, A.A. Malinin, B.A. Osadin, and Yu. F. Tainov, Sov. Phys. Tech. Phys., 9, 665 (1964).

23. R. Dethlefsen, Aerospace Research Laboratories Report # ARL 68-0112, p. 48 (June 1968).

24. I.I. Kalyatskiy, V.I. Kurets, E. and E.N. Tarakanovskiy, translation from Elektromaya, Obrabotka Materialov, 76, 44-48.

25. G.S. Belkin and V.Ya. Kiselev, Sov. Phys. Tech. Phys., 12, 702 (1967).

26. V.E. Il'in and S.V. Lebedev, Sov. Phys. Tech. Phys., 7, 707 (1963).

27. J.E. Daalder, Physica, 104c, 91 (1981).

28. Y. Udris, Proc. 1st Int. Conf. on Gas Discharges, London, England, 108 (1970).

29. G.A. Farrall, F.G. Hudda, and J.C. Toney, IEEE Trans. on Plasma Science, PS-11, 132 (1983).

30. S. Shalev, I. Goldsmith, and R.L. Boxman, IEEE Trans. on Plasma Science, PS-11, 146 (1983).

31. A.L. Donaldson, M.O. Hagler, M. Kristiansen, G. Jackson, and L. Hatfield, IEEE Trans. on Plasma Science, PS-12, 28 (1984).

32. E.W. Gray and J.R. Pharney, J. Appl. Phys., 45, 667 (1974).

33. G.W. McClure, J. Appl. Phys. 45, 667 (1974).

34. G.S. Belkin and V.Ya. Kiselev, Sov. Phys. Tech. Phys., 23, 24 (1978).

35. V.I. Ratkhovskii and A.M. Yagudaev, Sov. Phys. Tech. Phys., 14, 227 (1969).

36. A. Watson, Proc. 2nd IEEE Int. Pulsed Power Conf., Lubbock, Tx, 471 (June 1979).

37. J.E. Gruber and R. Suess, Max Planck Inst. fur Plasmaphysik, Garching bei Munchen, IPP 4/72 (Dec. 1969).

38. R.A. Burden and T.E. James, Proc. 7th Symp. Fusion Technology, Grenoble, France, 24 (Oct. 1972).

39. C.W. Kimblin, J. Appl. Phys., 45, 5235 (1974).

40. C.W. Kimblin, IEEE Trans. on Plasma Science, PS-10 322 (1982).

41. J. Knoepfel, Pulsed High Magnetic Fields, North Holland Publishing Company, Amsterdam-London, pp. 46-72, (1970).

42. Mesyats, G.A., "Techniques of Shaping High Voltage Nanosecond Pulses", FTD-HC-23-643-70, Foreign Technology Division, Wright-Patterson Air Force Base, March 1971.

43. B. Carder, Physics Int. Report., PIIR 12-74 (Dec. 1974).

44. J.A. Foosnaes and W.G.J. Rondeel, J. Phys D: Appl. Phys. 12, 1867 (1979).

45. C.H. Yeh, Doctoral Dissertation, August 1984, Texas Tech University.

46. C.H. Yeh, M. Hagler, M. Kristiansen, and H. Krompholz, "Recovery Measurements in a Spark Gap", 16th Power Modulator Sym. Arlington, VA (1984.

Interactions

a. Papers

K. Schoenbach, G. Schaefer, M. Kristiansen, H. Krompholz, H.C. Harjes, and D. Skaggs, "Investigations of E-Beam Controlled Diffuse Discharges", IEEE International Conference on Plasma Science, St. Louis, MO, 1984.

K.H. Schoenbach, G. Schaefer, M. Kristiansen, H. Krompholz, H. Harjes, and D. Skaggs, "Investigations of E-Beam Controlled Diffuse Discharges', 4th Int. Symp. on Gaseous Dielectrics, Knoxville, TN, USA, 1984.

b. Consultative and Advisory Functions

1. Dr. M. Kristiansen served on the USAF Scientific Advisory Board (SAB).
2. Dr. Kristiansen served on the AF SAB committee to study Basic Research in the Air Force.
3. Dr. M. Kristiansen served on the Air Force SAB Ad Hoc committee on Effects of High Altitude EMP on Military C^3.
4. Dr. Kristiansen served as to Co-organizer (with Dr. A. Hyder of Auburn University) of the DoD workshop on "Foreign Switch Technology".

5. Dr. Kristiansen served as a Visiting Staff Member (Collaborator) at Los alamos National Laboratory and supervised a completed Ph.D. reseach project by one of their Staff Members.
6. Dr. Kristiansen directed the Foreign Applied Science Assessment Centers Study of Soviet Macroelectronics (Pulsed Power).

c. Other Interactions

1. Dr. Kristiansen gave an invited lecture series on pulsed power in Taiwan and Japan (together with Dr. F. Rose, NSWC).

Accepted for publication in
Journal of Applied Physics

Appendix F[27]

MODELING OF SELF-BREAKDOWN VOLTAGE STATISTICS IN HIGH ENERGY SPARK GAPS

A. L. Donaldson, M. O. Hagler, M. Kristiansen
Department of Electrical Engineering/Computer Science
Texas Tech University, Lubbock, Texas 79409

L. L. Hatfield
Department of Physics
Texas Tech University, Lubbock, Texas 79409

and

R. M. Ness
Maxwell Laboratories
8835 Balboa Avenue, San Diego, CA 92123

Abstract

A model which incorporates the influence of electrode surface conditions, gas pressure, and charging rate on the voltage stability of high energy spark gaps is discussed. Experimental results support several predictions of the model; namely, that increasing the pressure and the rate of voltage charging both produce a broadening of the self-breakdown voltage distribution, whereas a narrow voltage distribution can be produced by supplying a copious source of electrons at the cathode surface.

Experimental results also indicate that two different mechanisms can produce this broadening, both of which can be taken into account with the use of the model presented. Further implications of the model include changes in the width of the self-breakdown voltage probability density function as the primary emission characteristics of the cathode are modified by, for example, oxide or nitride coatings and/or deposits from the insulator. Overall, the model provides a useful and physically sound framework from which the properties of spark gaps under a wide variety of experimental conditions may be evaluated.

Introduction

Low-jitter, triggered spark gaps are needed for a wide variety of switching applications, including fusion machines[1], weapons systems, and high energy physics experiments. To achieve low jitter, the switch should be triggered as close to the self-breakdown voltage as possible. Thus, an ideal switch should have a delta function for the self-breakdown voltage probability density function. In actual operation the self-breakdown voltage will be somewhat erratic, and in most cases "prefires", or breakdown voltages which are significantly less than the mean, will occur. The self-breakdown voltage density functions and the respective distributions for these cases are shown in Fig. 1. This paper presents a model which incorporates the processes which can produce the voltage distribution shown in Fig. 1(b). The problem of prefires is not addressed here but is being considered for future work.

Numerous studies[2-6] have shown that the choice of gas, electrode, and insulator material can significantly influence the width and shape of the actual voltage density function. More specifically, several studies[7-9] have suggested a correlation of the statistical distribution in the self-breakdown voltage of a spark gap and the properties of the cathode surface, including its microstructure. The data have been interpreted in terms of models that consider:

1) the effect of the field enhancement, due to cathode microstructure, and the effect of lower surface work functions, resulting from surface coatings, on the generation rate of electrons at the cathode[7,10,11],
2) the effect of the field enhancement on Townsend's first ionization coefficient, α,[7,12,13], and
3) the effect of the surface coatings and the applied field on the secondary emission coefficient, γ, at the cathode[14].

These models usually include the concept of "waiting-for-an-electron," in that breakdown is assumed to occur when the first electron appears at the cathode after a breakdown condition (Townsend or Streamer condition) has been satisfied. The theoretical model presented here includes all of these mechanisms by which the cathode surface can affect the statistical distribution in the breakdown voltage, and includes the field enhancement effects on the cathode surface in a new way.

Hodges[15] et al. take into account the probability that no breakdown occurs even if the breakdown condition is satisfied. However, this probability goes from 0 to 1 quite rapidly near

self-breakdown and hence is ignored for simplicity in the present analysis.

Theoretical Model

General Case

Consider a spark gap subjected to a monotonically increasing applied voltage, v(t). Denote the breakdown voltage, a random variable, as V. The field enhancement factor, M, defined as the ratio of the enhanced electric field at the cathode with microstructure to the electric field without microstructure, is also considered to be a random variable (the underlying sample space is the geometrical surface of the cathode). The random variable M is characterized by a probability density function, $p_M(m)$. A basic assumption of the model is that the gap breaks down when an electron is born at a site on the cathode surface where M is as large as or larger than the value that satisfies the breakdown condition (perhaps Townsend or streamer) at the particular voltage applied. We denote this threshold value of the field enhancement as $m_t(v)$. Physically we expect that $m_t(v)$ is a monotonically decreasing function of v ($\partial m_t(v)/\partial v<0$), an increasing function of pressure ($\partial m_t(v)/\partial p>0$), and that $m_t(0) = \infty$ and $m_t(v_{max}) = 1$. Figure 2 shows an actual calculation of $m_t(v)$ using a model microstructure described in Appendix A. The trends for this model are listed in Table I.

We now calculate the probability, p_t, that the gap breaks down during the time between t and t + Δt and hence at a voltage between v and v + Δv. For Δt small, the probability (Δp_t) that an electron is born between t and t + Δt at a site where M takes a value between m and m + Δm is

$$\Delta p_t = \frac{i_e(m,v(t))}{e} \Delta t \; p_M(m)\Delta m \qquad (1)$$

The quantity e is the charge on an electron and i_e is the primary electron current generated at the cathode. In general, i_e could be generated naturally by:

a) cosmic rays ionizing the gas in front of the cathode surface[16],

b) Fowler-Nordheim field emission[17], and/or

c) Schottky field assisted thermal emission[10].

These emission processes could occur directly from the cathode material or from compounds existing on the cathode surface whose work function is usually lower than that of the metal and which can be effectively lowered even further by surface charging. Thus, in general, i_e could be a function of total cathode surface area, voltage, field enhancement, temperature, and work function. The last three are also functions of the position on the surface. For the following formulation, however, we will represent i_e as an explicit function of field enhancement and voltage only (see Appendix B).

If Δt is large compared with the time of avalanche formation (see Appendix C), then the probability that the gap breaks down between t and $t + \Delta t$ is

$$p_t(\Delta t) = \frac{\Delta t}{e} \int_{m_t(v)}^{\infty} i_e(m,v(t))p_M(m)dm \qquad (2)$$

Let the random variable T represent the time elapsed before breakdown of the gap. Then, from Eq. (2), the probability density function for T is readily seen to be[18]

$$p_T(t) = f(t) \exp\left(-\int_0^t f(\tau)d\tau\right) \tag{3}$$

where

$$f(t) = \frac{1}{e}\int_{m_t(v(t))}^{\infty} i_e(m,v(t))p_M(m)dm. \tag{4}$$

Since, by assumption, v(t) is a monotonic function of t, then the probability density function for the breakdown voltage, V, is[19]

$$p_V(v) = p_T(t(v)) \Big/ \left|dv/dt\right| \tag{5}$$

or[20]

$$p_V(v) = \frac{\lambda(v)}{v'} \exp\left(-\int_0^v \frac{\lambda(\eta)d\eta}{v'}\right), \tag{6}$$

where v' is the derivative of the charging voltage with respect to time (dv(t)/dt) and

$$\lambda(v) = \frac{1}{e}\int_{m_t(v)}^{\infty} i_e(m,v)p_M(m)dm. \tag{7}$$

It is easy to see that

$$F_V(v) = \int_0^v p_V(\xi)d\xi = 1 - \exp\left(-\int_0^v \frac{\lambda(\eta)d\eta}{v'(\eta)}\right), \tag{8}$$

where $F_V(v)$ is the cumulative probability distribution for the random variable, V. Equation (8) shows that the width of the self-breakdown voltage distribution: 1) decreases with increasing i_e, 2) increases with increasing m_t caused by, for example, an

increase in operating pressure, and 3) increases with increasing v', the charging rate. Note that v' is to be evaluated at v, and hence can be considered as a function of v, namely, $v' = v'(v)$. If v(t) is a ramp, then $v' = v_o'$, a constant. If v(t) is an RC charging waveform, then $v' = (v_o - v)/RC$ where v_o is the charging voltage. If $v(t) = A(1-\cos\omega t)$ for $0 \leq \omega t \leq \pi$, then $v' = \omega \sqrt{v(2A-v)}$.

From Equations (7) and (8), it is easy to show[20] that

$$\frac{1}{e}\int_{m_t(v)}^{\infty} i_e(m,v)p_M(m)dm = \frac{v'p_V(v)}{1-F_V(v)} \qquad (9)$$

Notice that all the terms on the right hand side of Eq. (9) can be measured experimentally. This will hold true for the special cases discussed below as well. This is an important result, for even when i_e depends on (implicit) variables other than m and v, the function $v'p_V(v)/(1-F_V(v))$ should still describe the results.

Special Cases

To proceed further, consider two special cases of the model. First, suppose that $i_e(m,v)$ is constant so that field enhancement distribution effects from the cathode surface microstructure and waiting-for-an-electron effects are the primary physical mechanisms included in the model. This circumstance is likely to hold, for example, when the cathode is illuminated with sufficiently intense ultraviolet radiation so that any field emission current is dwarfed by photoelectric current, which should be independent of M and V. If $i_e = i_{eo}$, a constant, then Eq. (9) gives

$$\frac{i_{eo}}{e}\,[1 - F_M(m_t(v))] = \frac{v' p_V(v)}{1-F_V(v)}\,, \qquad (10)$$

where $F_M(m)$ is the cumulative probability distribution for the random variable, M. If we know $m_t(v)$, we can determine $F_M(m)$ by plotting $F_M(m_t(v))$ versus $m_t(v)$. Therefore, for this special case it is possible, in principle, to deduce $F_M(m)$ from $p_V(v)$ (self-breakdown voltage histogram) under a given set of conditions and thus predict $p_V(v)$ (or $F_V(v)$) for a different v' or gas pressure (which affects $m_t(v)$), for example. For this special case, Eq. (8) becomes

$$F_V(v) = 1-\exp\left(-\frac{i_{eo}}{e}\int_0^v \frac{[1-F_M(m_t(n))]dn}{v'}\right) \qquad (11)$$

Consider now a second special case in which $p_M(m) = \delta(m - m_o)$, where $\delta(\cdot)$ is the Dirac delta function and m_o is a constant. In this case the field enhancement is assumed to be uniform (that is, sufficiently characterized by its mean value rather than its distribution) so that the primary effects included are the voltage dependence of the primary electron current, i_e, and waiting-for-an-electron. In this case Eq. (8) becomes

$$F_V(v) = 1-\exp\left(-\frac{1}{e}\int_{v_t}^{v} \frac{i_e(m_o,n)dn}{v'}\right)\,, \qquad (12)$$

where v_t is the threshold voltage, and $m_t(v_t) = m_o$, while Eq. (9) becomes

$$i_e(m_o,v) = \frac{v' p_V(v)}{1-F_V(v)}\,. \qquad (13)$$

Experimental Arrangement

The experimental arrangement and the system diagnostics used to test the theoretical results are shown in Fig's. 3 and 4. The construction of this facility and the development of the modeling software is described elsewhere[9,21]. The test circuit shown in Fig. 4 consists of a high energy (2 kJ) pulse forming network (PFN) and a low energy (<1 mJ) RC probing circuit. The PFN delivers a unipolar, 25 μsec pulse into a 0.6 Ω, matched load in order to generate an electrode surface which is characteristic of a high energy switch. The RC probing circuit is used to generate the voltage distributions with a low energy, low current pulse so that the equilibrium temperature is reached prior to each shot. This low energy circuit is also used so that the surface microstructure produced by the high energy shots will not be altered significantly from shot to shot. The criteria for determining that no alteration in surface features had occurred was the comparison of the voltage distributions before and after a given experiment. The pressure in the spark gap could be raised to 3.5 atmospheres and the voltage ramp rate could be varied from 3 to 60 kV/s by changing R_C. A 5 Watt UV lamp was used to generate additional electrons at the cathode surface when needed.

A testing sequence consisted of firing 2000 - 7000 shots at high energy, waiting approximately one hour for the electrode to cool, and proceeding with several series of 500 low energy shots with different i_e, v', and pressure. The Kolmogorov - Smirnoff[22] test indicates that this number of shots should determine $F_V(v)$,

within a confidence level of 99%, to an accuracy of 7%. Figure 5 shows a typical electrode surface generated by the high energy pulses for the case of 304 stainless steel run in one atmosphere of nitrogen gas at a gap separation of 5 mm. Examination of the electrode surface after application of the low energy pulses indicates that no significant changes had occurred which might alter the breakdown statistics.

Experimental Results

Several experiments were performed to verify the model's predictions for the effect of i_e, v', and pressure on the probability density function $p_V(v)$. In the first experiment, an UV source was used to generate a continuous supply of photoelectrons at the surface of a stainless steel electrode in air. Figure 6 shows that, without UV, the density function is very broad; indicating that the cathode surface is a very poor emitter of electrons. However, with the UV source on, the density function is reduced and shifts to the lowest value of breakdown voltage. Nitta, et al.[23], observed the same effect in SF_6 at pressures up to 2 atm. This result is significant for at least two reasons. First, it supports the waiting-for-an-electron concept as one mechanism responsible for statistical variation in the self-breakdown voltage; and second, it provides an externally controllable experimental "switch" where the effect of waiting-for-an-electron can be turned on or off. The behavior observed is consistent with Eq. (8).

A second experiment consisted of varying the voltage ramp

rate v' from 3 kV/s ("slow" ramp) to 30 kV/s ("fast" ramp). According to the model (Eq. (8)), if you are waiting for an electron to appear, then the faster the ramp rate, the higher the breakdown voltage will be when the electron appears and thus the greater the scatter in the density function, $p_V(v)$. Figure 7 shows that this effect was indeed observed. Also, from Eq. (8), the density function for the slower ramp rate could be theoretically calculated from the data for the fast ramp rate. Figure 7 shows this result for the assumption $i_e = i_{eo}$, a constant. The result is fair, indicating that for better agreement a more realistic expression for i_e, perhaps $i_e(m,v)$, would have to be used. Hodges[10,11] has modeled this effect using $i_e(m,V,\phi,T)$ and was able to achieve good agreement between experimental and theoretical values.

Previous work[13,24-26] has shown that with the presence of cathode microstructure, an increase in pressure can lead to significant deviations from the Paschen curve breakdown voltage if the product of the protrusion height and the pressure is greater than a gas dependent threshold. For example, Berger[13] calculated that pressure-height products of 30 μm·atm for SF_6 and 200 μm·atm for air would be required for the onset of breakdown voltage modifications due to enhanced ionization occurring near the microprotrusions. Avrutskii[8] stated that an increase in pressure should lead to an increase in scatter in the breakdown voltage, but no data were given. Thus, in order to understand the effect of pressure on the breakdown voltage statistics for a surface with large protrusions, the brass sample shown in Fig. 8 was

generated and the breakdown voltages were recorded for pressures up to 3.5 atmospheres. (Earlier work in electrode erosion showed that brass electrodes in high energy operation can form protrusions up to 500 μm[21].) Figure 9 clearly shows an increase in scatter, especially at the low end, in the density function $p_V(v)$ for higher pressures. If the effect is due to field enhancements, then the calculated range of m's at any pressure should be the same since the distribution of surface field enhancements is not changing from shot to shot. For p = 1.7 atm, the range of m's, calculated using the model in Appendix A, was 1 - 2.93; for p = 2.5 atm, the range was 1 - 3.63.

Increased scatter with increased pressure has also been observed for electrode surfaces with microstructures much smaller than the size required to affect the breakdown voltage. Figure 10 shows the breakdown voltage distribution as a function of pressure for graphite electrodes in air. The entire electrode surface was examined with a high power optical microscope and no protrusions greater than 10 μm were discovered. Although the pressure-height product is an order of magnitude less than the amount required to affect the breakdown voltage by enhanced ionization[13], there is still a significant spreading of the distribution at higher pressures. Unlike the results for the brass electrodes, the spreading occurs at the high end of the distributions, i.e., for voltages larger than those calculated from the Townsend breakdown criteria for a gap without protrusions, and M = 1. Whereas the results for brass indicated a lowering of the Townsend breakdown criteria due to enhanced

ionization, the results for graphite indicate that a different mechanism is producing the scatter at high pressures; seemingly, by altering the effective generation rate of electrons. Levinson and Kunhardt[27] have reported a reduction in the effective electron generation rate at the cathode for higher pressures, although no specific mechanism was described.

The pressure data were also found to be of importance for analyzing the different i_e cases which were studied theoretically. Figure 11 shows theoretical plots of the quantity $v'p_V(v)/(1-F_V(v))$ for the three physical cases discussed earlier: a) $i_e = i_e(m_o,v)$, m_o is a constant over the entire surface (Eq. (13)); b) $i_e = i_{eo}$ is a constant (Eq. (10)); and c) the most general case, $i_e = i_e(m,v)$ which assumes a distribution of surface field enhancements (Eq. (9)). A Gaussian distribution in field enhancements was used for cases b) and c). The function $m_t(v)$ was calculated using the model described in Appendix A and a Schottky emission current was used for $i_e(m,v)$. Case a) illustrates that if there is no spread in the distribution for M (Eq. (13)), then an increase in pressure will correspond simply to a higher emission current because of the higher breakdown voltage occurring at that pressure, which is typical for a field dependent Schottky or Fowler-Nordheim emission mechanism[10]. A higher emission current at higher pressure would imply narrower statistics, but experimental results indicate just the opposite; namely, broader statistics at higher pressures. However, in case b) for a fixed voltage, the increase in pressure has the effect of raising the threshold, m_t, required for breakdown,

which raises $F_M(m_t(v))$, and thus the function $v'p_V(v)/(1-F_V(v))$ is multivalued and decreases with increasing pressure (Eq. (10)). For case c) $v'p_V(v)/(1-F_V(v))$ is also multivalued and decreases with increasing pressure, but in a different way (Eq. (9)). For a fixed voltage, and assuming that the surface features do not change with pressure, the integrand is constant with increasing pressure. However, the lower limit on the integral, namely $m_t(v)$, increases with increasing pressure which has the effect of reducing the value of the function.

Figure 12 is a plot of the function $v'p_V(v)/(1-F_V(v))$ from experimental data for the pressure data of Figure 9. From this plot it is clearly seen that the experimental data are inconsistent with the theoretical results for case a) (a constant M surface). Thus, the effect of a distribution in field enhancements should be considered in the analysis of the breakdown statistics. In addition, the function $v'p_V(v)/((1-F_V(v))$ increases very rapidly with voltage and only very extreme values for the work function, $\Phi < 0.5$ eV, and field enhancement, $M > 50$, could give reasonable agreement between the experimental data and the Fowler-Nordheim or Schottky field emission mechanisms.

Conclusion

A model has been described which correctly accounts for the influence of pressure, v', i_e, and surface microstructure on the self-breakdown voltage statistics. The model's importance in the area of pulse-charged and triggered switches stems from the fact that the statistics for these systems have been recently shown[28]

to be heavily dependent on the self-breakdown statistics discussed in this paper.

Using this model, theoretical and experimental results show:

1) The spread in self-breakdown voltages in a spark gap is a function of the charging rate (v') and the cathode surface properties which determine the electron emission current i_e and the distribution of field enhancement sites $F_M(m)$.

2) Increasing i_e provides a practical method for reducing the width of the self-breakdown voltage density function. This can be accomplished with an external UV source, by sandblasting the electrodes to supply a large number of low work function emitting sites[28], or perhaps with an electron emission agent introduced into the cathode material[29].

3) The spread in self-breakdown voltages increases with increasing pressure, and/or increasing charging rate.

4) Increasing pressure had two distinctive effects on the breakdown voltage distributions. For large microstructures (>200 μm) on brass electrodes, increasing pressure led to increased scatter at the lower end of the distributions as a result of enhanced ionization near the microprotrusions. For small microstructures (<10 μm) on graphite electrodes, an increase in pressure led to increased scatter at the high end of the distributions which presumably was due to a lowering of the effective electron emission current, i_e.

5) The function $v'p_V(v)/(1-F_V(v))$, which can be computed directly from self-breakdown voltage data, is useful for determining the nature of i_e for a given set of conditions.

Acknowledgments

The authors are indebted to B. Conover, P. Krothapalli, K. Rathbun and A. Shaukat for their work on the construction of the experiment and the implementation of the data acquisition system. In addition, a special thanks goes to M. Byrd, J. Clare, R. Davis, L. Heck, R. Higgenbotham, M. Katsaras, and M. C. McNeil for their work on the manuscript.

This work was supported by the Air Force Office of Scientific Research.

Appendix A

The Townsend breakdown criterion for a spark gap with microstructure is given by

$$\int_h^d \bar{\alpha}\, dz = K \qquad \text{(A-1)}$$

where $\bar{\alpha}$ is the effective ionization coefficient of the gas which is equal to $\alpha-\eta$; where α is the Townsend first ionization coefficient, η is the attachment coefficient, h is the protrusion height, d is the gap spacing, and K is a function of E/p which is obtained from empirical data. The microstructure modifies the voltage which satisfies Eq. (A-1) by altering the electric field and thus $\bar{\alpha}$ in the region near the protrusion. One can model the protrusion several ways[12,30], but the semi-ellipsoidal model shown in Fig. A1 was chosen because the electric field along the z axis was known analytically and could be expressed in terms of the field enhancement M. The axial field for this configuration is given by[12]

$$E(z) = E_o \left(1+(M-1)\,\frac{h^3}{z^3}\right) \qquad \text{(A-2)}$$

where E_o is the electric field with no protrusions.

The field enhancement factor M is related to b, the radius of the base of the protrusion, and h, the protrusion height, by the equation

$$M = \frac{c^2}{1-c^2}\left(\frac{1}{2c}\ln\frac{1+c}{1-c} - 1\right)^{-1}, \qquad \text{(A-3)}$$

where

$$c = 1 - b^2/h^2.$$

The coefficients $\bar{\alpha}$ and K were obtained from the literature[13,31]. Thus, Eq. (A-1) was solved for a variety of conditions and plotted in Fig's. A2-A4. It should be remembered that these graphs are useful only for showing trends since actual surface structure effects are not as simple as a single ellipsoid. Also, it was assumed that $\bar{\alpha}$ takes on its equilibrium value instantly, when in reality it would gradually approach its equilibrium value within a few collision paths[32]. This effect is depicted in Fig. A5 and the calculated results in Fig. A6 show that if one takes this into account the effect would be to smooth the surface out or to reduce protrusion effects. The actual transition was calculated using an α which reached equilibrium in a linear manner. Any monotonic transition function, however, would have a similar effect.

Thus, the values obtained for the breakdown voltage using equilibrium values of $\bar{\alpha}$ are lower limits for a given set of conditions.

APPENDIX B

Suppose that the primary electron current, $\tilde{i}_e$, depends on the random variables, θ, the temperature over the cathode surface, and ϕ, the work function over the cathode surface, in addition to the random variable M and the applied voltage, v(t). Then Eq. (2) becomes

$$p_t(\Delta t) = \frac{\Delta t}{e} \int_0^\infty d\phi \int_0^\infty d\theta \int_{m_t(v)}^\infty \tilde{i}_e(\phi,\theta,m,v(t)) p_{\phi\theta M}(\phi,\theta,m)dm$$

where $P_{\phi\theta M}(\phi,\theta,m)$ is the joint probability density function for ϕ, θ, and M. Since[33]

$$p_{\phi\theta M}(\phi,\theta,m) = p_M(m)p_\phi(\phi|m)p_\theta(\theta|m,\phi)$$

where $p_\phi(\phi|m)$ and $p_\theta(\theta|m,\phi)$ are conditional probability densities, then

$$p_t(\Delta t) = \frac{\Delta t}{e} \int_{m_t(v)}^\infty i_e(m,v(t)) p_M(m)dm$$

where

$$i_e(m,v(t)) = \int_0^\infty d\phi \int_0^\infty d\theta\, \tilde{i}_e(\phi,\theta,m,v(t)) p_\phi(\phi|m) p_\theta(\theta|m,\phi)$$

Clearly, the form of $p_t(\Delta t)$ does not change when the dependence of the current on the additional random variables, ϕ and θ, is included. The dependence of the current on the random variable, M, is important, on the otherhand, because the limits of the integral over m are not fixed, but depend on $m_t(v)$, a

quantity that depends on the breakdown criterion, Townsend or streamer. The work function over the surface, ϕ, and the temperature over the surface, θ, do not enter into the breakdown criterion, however, and hence are important only in an average sense in this formulation.

Note that the various probability densities are assumed constant in time. This assumption seems implausible for the temperature, θ, until we realize that it is the temperature probability density at the time of breakdown that matters, and that the time between breakdowns is nearly constant so that the temperature probability density should be essentially the same for each shot.

It is instructive to consider M, ϕ, and θ, as random processes[34], not in time, but in the spatial variables that describe the cathode surface. The sample functions of these processes are the spatial distributions of field enhancement, surface work function, and surface temperature after each shot, just before the next breakdown. Particularly for other than planar electrodes, we expect each process to be spatially non-stationary[35]. In that case, the probability densities, the primary current density, j_e, and the field enhancement threshold, m_t, become functions of the spatial variables, σ, that describe the cathode surface. Let the primary electron current density be $\tilde{j}_e(\phi,\theta,m,v(t);\sigma)$ where we set off the spatial dependence with a semicolon; then Eq. (2) becomes

$$p_t(\Delta t) = \frac{\Delta t}{e} \int_{\Sigma} d\sigma \int_{m_t(v;\sigma)}^{\infty} dm \int_{o}^{\infty} d\phi \; \tilde{j}_e(\phi,\theta,m,v(t);\sigma) p_{\phi\theta M}(\phi,\theta,m;\sigma)$$

where Σ is the cathode surface. Or,

$$p_t(\Delta t) = \frac{\Delta t}{e} \int_{\Sigma} d\sigma \int_{m_t(v;\sigma)}^{\infty} j_e(m,v(t);\sigma) p_M(m;\sigma) dm$$

where

$$j_e(m,v(t);\sigma) = \int_0^{\infty} d\phi \int_0^{\infty} d\theta \, \bar{j}_e(\phi,\theta,m,v(t);\sigma) p_\phi(\phi|m;\sigma) p_\theta(\theta|m,\phi;\sigma)$$

The corresponding value of $\lambda(v)$ is

$$\lambda(v) = \frac{1}{e} \int_{\Sigma} d\sigma \int_{m_t(v;\sigma)}^{\infty} j_e(m,v;\sigma) p_M(m;\sigma) dm$$

Consider, as an example, a spark gap with hemispherical electrodes and let $\sigma = \sigma_o$ correspond to the point on the surface at the center of the gap where the distance between the electrodes is a minimum. As we move further away from the center of the cathode, j_e tends to remain constant (if it results from photoemission) or decrease (if it results from Schottky or Fowler-Nordheim emission) because the electric field at the cathode surface decreases as we move away from the electrode center. For a given relatively high value of m, $p_M(m;\sigma)$ should decrease sufficiently far away from electrode center as the cathode surface becomes smoother. The threshold field enhancement, $m_t(v;\sigma)$, on the other hand, will increase rapidly as we move away from cathode center because m_t increases rapidly with the increasing distance between electrodes. Thus, the integral

over m decreases rapidly as we move away from σ_o. That is, the contributions to $\lambda(v)$ come primarily from a small area, δA, near the electrode center, σ_o. Thus,

$$\lambda(v) = \int_{m_t(v;\sigma_o)}^{\infty} i_e(m,v;\sigma_o) p_M(m;\sigma_o)\, dm$$

where

$$i_e(m,v;\sigma_o) = j_e(m,v;\sigma_o)\delta A.$$

This result is the same as Eq. (7) if we, in Eq. (7), use i_e, p_M and m_t corresponding to conditions near the cathode center. The use of these quantities appropriate to the central region is consistent with empirical observations that almost all breakdowns occur in this region.

Appendix C

In the main body of the paper, it was assumed that the time for avalanche formation (formative time) is sufficiently short so that the applied voltage changes only negligibly (<100 V) during this time. For SF_6 and air at 1 atm, the maximum formative times are approximately 100 μs[36,37] and thus, for charging rates less than 1000 kV/s, this assumption is valid.

If the formative time is not negligible, then it is considered to be a random variable, T†, with a probability density $p_{T\dagger}(t)$. The increase in applied voltage during T† is a random variable, V†. Because the voltage and time are monotonically related[18]

$$p_{V\dagger}(v) = p_{T\dagger}(t) \Big/ \left| dv \Big/ dt \right| \qquad \text{(C-1)}$$

Under these circumstances, the gap breakdown voltage is not simply V, the applied voltage when the first electron is born at a site at the cathode surface where $M > m_t$, but rather the sum of V and V†, which will be called U.

$$U = V + V\dagger \qquad \text{(C-2)}$$

Thus, U is the sum of two random variables. Its probability density is therefore given by[38]

$$p_U(v) = \int_{-\infty}^{\infty} p_{V,V\dagger}(v-u,u)\,du \qquad \text{(C-3)}$$

where $p_{V,V\dagger}(\cdot,\cdot)$ is the joint probability density for V and V†.

If V and V† are statistically independent, then this result simplifies to[39]

$$p_U(v) = p_V(v) * p_{V\dagger}(v) \qquad \text{(C-4)}$$

where the asterisk denotes convolution in v, $p_V(v)$ is given by Eq. (6) and $p_{V\dagger}(v)$ is found using Eq. (C-1). The random variables V and V† are simply transformations of T and T†. Therefore[40], V and V† will be statistically independent if the formative time, T†, does not depend on the time, T, required for an electron to be born at a site on the cathode surface where $M > m_t$.

Notice that if the formative time is negligible, then $p_{V\dagger}(v)$ becomes $\delta(v)$, a Dirac delta function, so that

$$p_U(v) = p_V(v) * \delta(v) = p_V(v) \qquad \text{(C-5)}$$

This case is the one assumed in the body of the paper.

References

1) R. A. White, Proc. of 3rd IEEE International Pulsed Power Conf., Albuquerque, N.M., 359, (June 1981).

2) L. B. Gordon, M. Kristiansen, M. O. Hagler, H. C. Kirbie, R. M. Ness, L. L. Hatfield, and J. N. Marx , IEEE Trans. on Plasma Science, PS-10, 286 (1982).

3) E. I. Zolotarev, V. Mukhin, L. E. Polyanskii, and V. N. Trapeznikov, Sov. Phys. Tech. Phys., 21, 340 (1978).

4) Physics International Report PISR-127-4, Physics International Co., 2700 Merced Street, San Leandro CA 94577 (July 1969).

5) M. T. Buttram, Sandia National Lab Report, Sand 81-1552 (1981).

6) T. H. Martin, Air Force Pulsed Power Lecture Note #11, Plasma and Switching Laboratory, Department of Elec. Eng. Texas Tech University (1983).

7) V. A. Avrutskii, Sov. Phys. Tech. Phys., 18, 389 (1973).

8) V. A. Avrutskii, G. M. Goncharenko, and E. N. Prokharov, Sov. Phys. Tech. Phys., 18, 386 (1973).

9) R. M. Ness, Masters Thesis, Texas Tech University, (August 1983).

10) R. V. Hodges, R. C. McCalley, and J. F. Riley, Lockheed Missiles and Space Company Report, LMSC-0811978 (1982).

11) R. V. Hodges and J. F. Riley, Lockheed Missiles and Space Company Report, LMSC-0877208 (1983).

12) A. Pedersen, IEEE Trans. on Power Apparatus and Systems, PAS-94, 1749 (1975).

13) S. Berger, IEEE Trans. on Power Apparatus and Systems, PAS-95, 1073 (1976).

14) W. S. Boyle and P. Kisliuk, Phys. Rev. 97, 255 (1955).

15) F. V. Hodges, R. N. Varney, and J. F. Riley, "The Probability of Electrical Breakdown: Evidence for a Transition Between the Townsend and Streamer Breakdown Mechanisms," to be published.

This paper calculates P*, the probability of electrical breakdown as a function of the applied voltage, v, to the probability of an infinite avalanche sequence plus the probability of a finite sequence that achieves a critical size. This result can be incorporated into the present paper by letting $\lambda(v) \rightarrow \lambda(v) = P^*(v)\lambda(v)$ beginning with Eq. (8) below.

16) M. W. Watts, 5th Int. Conf. on Gas Discharge, University of Liverpool, 11-14 Sept. 1978, 297, (IEE London 1978).

17) R. H. Fowler and L. Nordheim, Proc. Roy. Soc. 199, 173-181 (1928).

18) W. B. Davenport, Jr. and W. L. Root, An Introduction to the Theory of Random Signals and Noise (McGraw-Hill, New York, 1958) 113-117.

19) W. B. Davenport, Jr. and W. L. Root, An Introduction to the Theory of Random Signals and Noise (McGraw-Hill, New York, 1958) 32-34.

20) agler, A. L. Donaldson, and R. M. Ness, Texas Tech
ity Pulsed Power Lab Notes, TTU-EEPP-83-1 (1983).

21) onaldson, M. O. Hagler, M. Kristiansen, G. Jackson,
Hatfield, IEEE Trans. on Plasma Science, PS-12, 28

22) faffenberger and J. H. Patterson, Statistical Methods
iness and Economics, R. D. Irwin, Inc., Homewood, IL,
685.

23) a, N. Yamada, and Y. Fujiwara, IEEE Trans. on Power
us and Systems, PAS-93, 623 (1974).

24) er, IEEE Trans. on Power Apparatus and Systems,
1179 (1977).

25) ooke, IEEE Trans. on Power Apparatus and Systems,
1518 (1975).

26) cAllister, Elektrotechnische Zeitschrift-A, 99, 283

27) evinson and E. E. Kunhardt, IEEE Trans. on Plasma
, PS-10, 266 (1982).

28) in, Sandia National Labs, private communication,
1983.

29) rizhanovskii, A. I. Kuz'michev, G. V. Levchenko,
uban, and A. I. Shendakov, Sov. Phys. Tech. Phys.,
4 (1981).

30) ewis, J. of Appl. Phys., 26 1405 (1955).

31) s, J. Phys. D., 1, 769 (1968).

32) Y. Tzeng and E. E. Kunhardt, 36th Gaseous Electronics Converence (Abstracts), State University of New York, 11-14 Oct. 1983, 42.

33) J. M. Wozencraft and I. M. Jacobs, Principles of Communication Engineering, Wiley, New York, (1965), 76.

34) J. M. Wozencraft and I. M. Jacobs, Principles of Communication Engineering, Wiley, New York, (1965), 129-132.

35) J. M. Wozencraft and I. M. Jacobs, Principles of Communication Engineering, Wiley, New York, (1965), 135-143.

36) L. H. Fisher, Phys. Rev. 72, 423 (1947).

37) P. Narbut, E. Berg, C.N. Workes, and T. W. Dakin, AIEE Trans., 78, 545 (1959).

38) J. M. Wozencraft and I. M. Jacobs, Principles of Communication Engineering, Wiley, New York, (1965), 68-69.

39) R. C. Pfaffenberger and J. H. Patterson, Statistical Methods for Business and Economics, R. D. Irwin, Inc., Homewood, IL, (1977), 72.

40) R. C. Pfaffenberger and J. H. Patterson, Statistical Methods for Business and Economics, R. D. Irwin, Inc., Homewood, IL, (1977), 77.

TABLE I

General trends for the threshold field enhancement $m_t(v)$ calculated for an ellipsoidal protrusion in a uniform field using the Townsend breakdown criteria in N_2 and the streamer criteria in SF_6.

TREND	IMPLICATION
T-1: $\frac{\partial V}{\partial m_t} > 0$	The greater the spread in field enhancements, the greater the possible range in breakdown voltages.
T-2: $\frac{\partial m_t}{\partial p} > 0$	The higher the pressure, the higher the required threshold field enhancement for a fixed voltage.
T-3: $\frac{\partial}{\partial p}\left(\frac{\partial V}{\partial m_t}\right) > 0$	For a fixed distribution of field enhancements, the higher the pressure, the greater the possible spread in breakdown voltages.
T-4: $\frac{\partial}{\partial d}\left(\frac{\partial V}{\partial m_t}\right) < 0$	The larger the gap spacing, the smaller the effect of surface microstructure.
T-5: $\frac{\partial}{\partial h}\left(\frac{\partial V}{\partial m_t}\right) > 0$	The larger the microstructure, the greater the spread in breakdown voltage for a fixed distribution of field enhancements.

NOTE: All trends for SF_6 are greater than and in the same direction as the trends for nitrogen.

List of Figures

Fig. 1. The Self-Breakdown Voltage Probability Density Function, $p_V(v)$, and its Distribution Function, $F_V(v)$ for: a) Ideal Spark Gap; b) Actual Spark Gap, c) Actual Spark Gap with Prefires.

Fig. 2. $m_t(v)$ vs. V for Two Different Pressures in Nitrogen.

Fig. 3. Experimental Arrangement and System Diagnostics.

Fig. 4. Test Circuits.

Fig. 5. Stainless Steel Electrode After 2200 High Energy Discharges in Nitrogen: a) Cathode Surface-Top View (Marker is 4 mm); b) Cathode Surface-Side View (Marker is 1 mm).

Fig. 6. Self-Breakdown Voltage Probability Density Function for Stainless Steel in Air, With and Without UV.

Fig. 7. Self-Breakdown Voltage Probability Density Function for Different Charging Rates.

Fig. 8. Surface of Brass Cathode used for Pressure Studies (Marker is 4 mm).

Fig. 9. Self-Breakdown Voltage Probability Density Function for Brass Electrodes in Air at Different Pressures.

Fig. 10. Self-Breakdown Voltage Probability Density Function for Graphite Electrodes in Air at Different Pressures.

Fig. 11. Theoretical Plots of $v'p_V(v)/(1-F_V(v))$ for: a) $i_e = i_e(m_o,v)$; b) $i_e = i_{eo}$; and c) $i_e = i_e(m,v)$.

Fig. 12. Experimental Plots of $v'p_V(v)/(1-F_V(v))$.

Fig. A1 Elipsoidal Surface Protrusion Model.

Fig. A2 $m_t(v)$ vs. V as a Function of Pressure in Nitrogen.

Fig. A3 $m_t(v)$ vs. V as a Function of Pressure in SF_6.

Fig. A4 $m_t(v)$ vs. V as a Function of Protrusion Height for two Different Pressures in Nitrogen.

Fig. A5 a) Electric Field Across the Gap; b) α With and Without Correction Factor for Nonequilibrium Values Over a Distance S.

Fig. A6 $m_t(v)$ vs. V With and Without Equilibrium α Correction in Nitrogen.

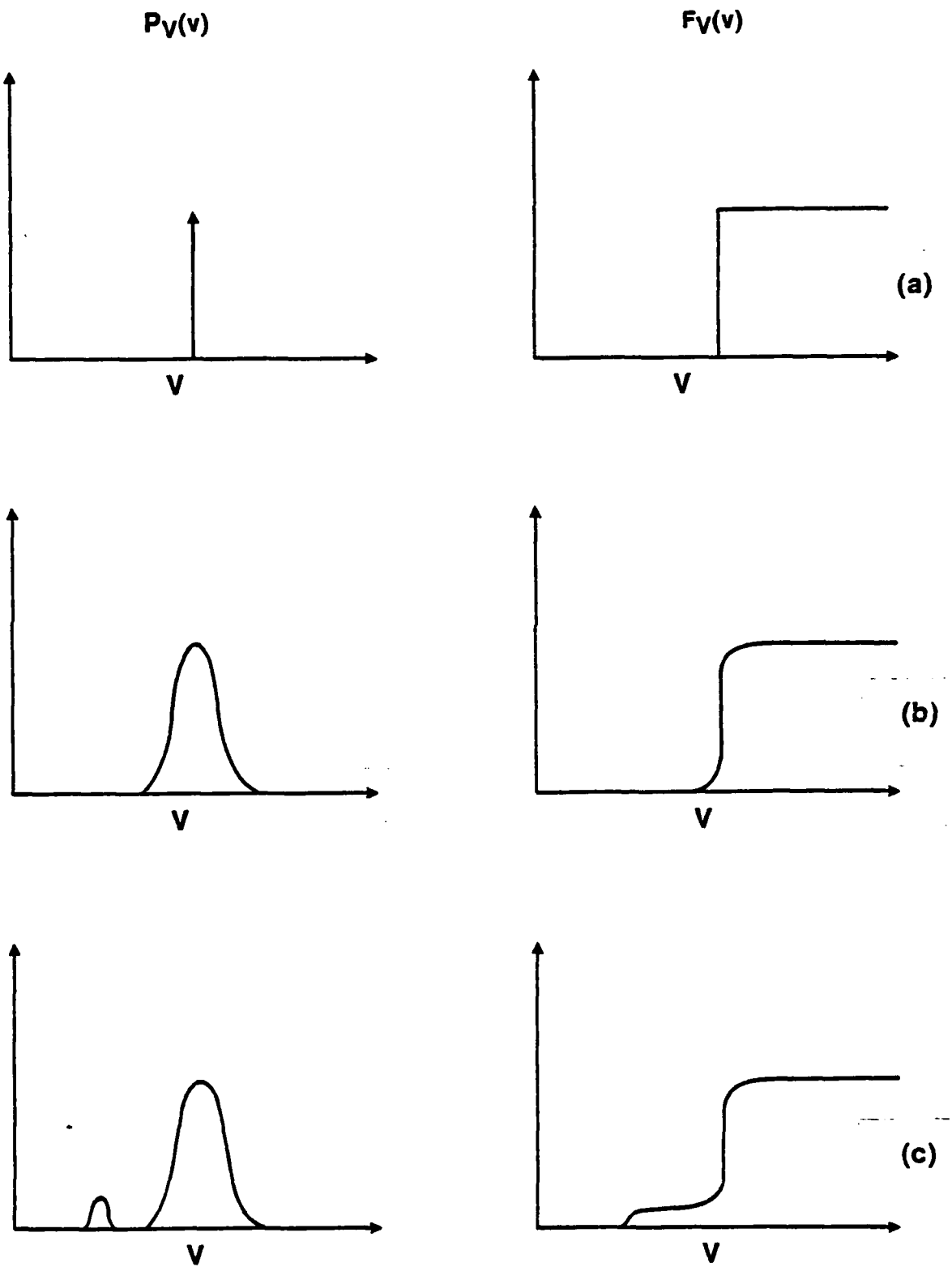
$P_V(v)$
$F_V(v)$
V
V
(a)
V
V
(b)
V
V
(c)

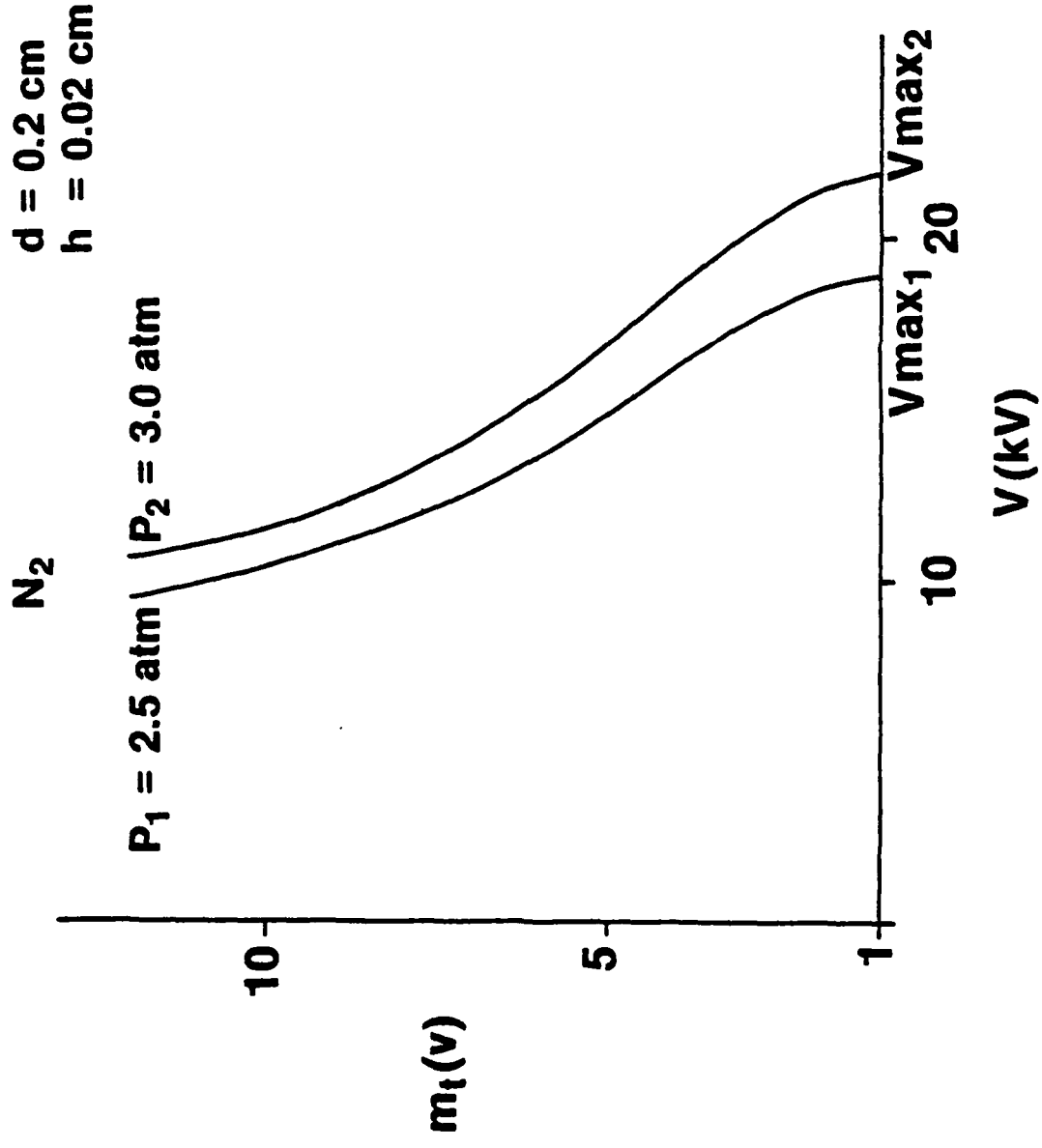
d = 0.2 cm
h = 0.02 cm
N2
P2 = 3.0 atm
P1 = 2.5 atm
Vmax2
Vmax1
10
20
V(kV)
10
5
1
mt(v)

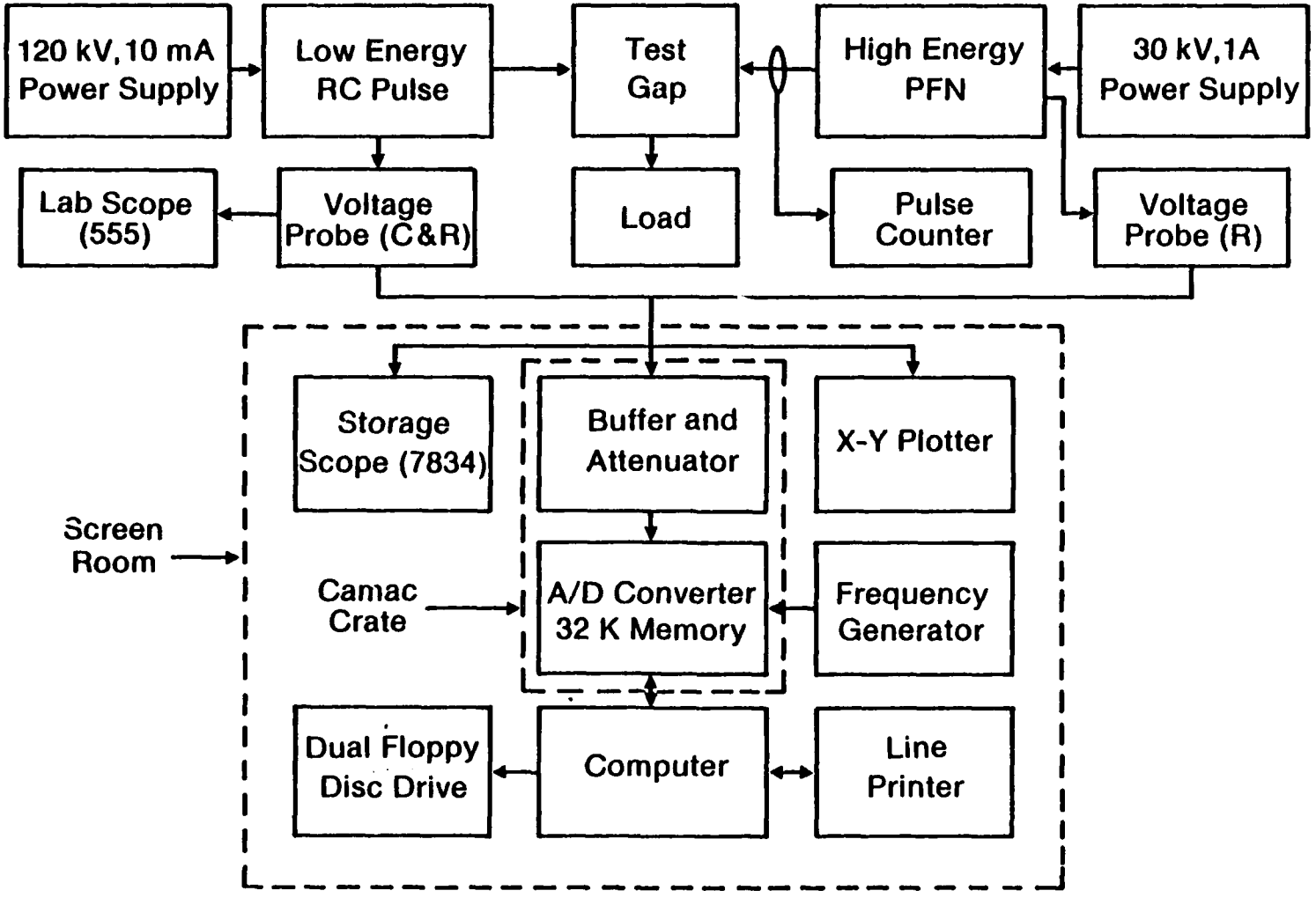
120 kV, 10 mA Power Supply
Low Energy RC Pulse
Test Gap
High Energy PFN
30 kV, 1A Power Supply
Lab Scope (555)
Voltage Probe (C&R)
Load
Pulse Counter
Voltage Probe (R)
Storage Scope (7834)
Buffer and Attenuator
X-Y Plotter
Screen Room
Camac Crate
A/D Converter 32 K Memory
Frequency Generator
Dual Floppy Disc Drive
Computer
Line Printer

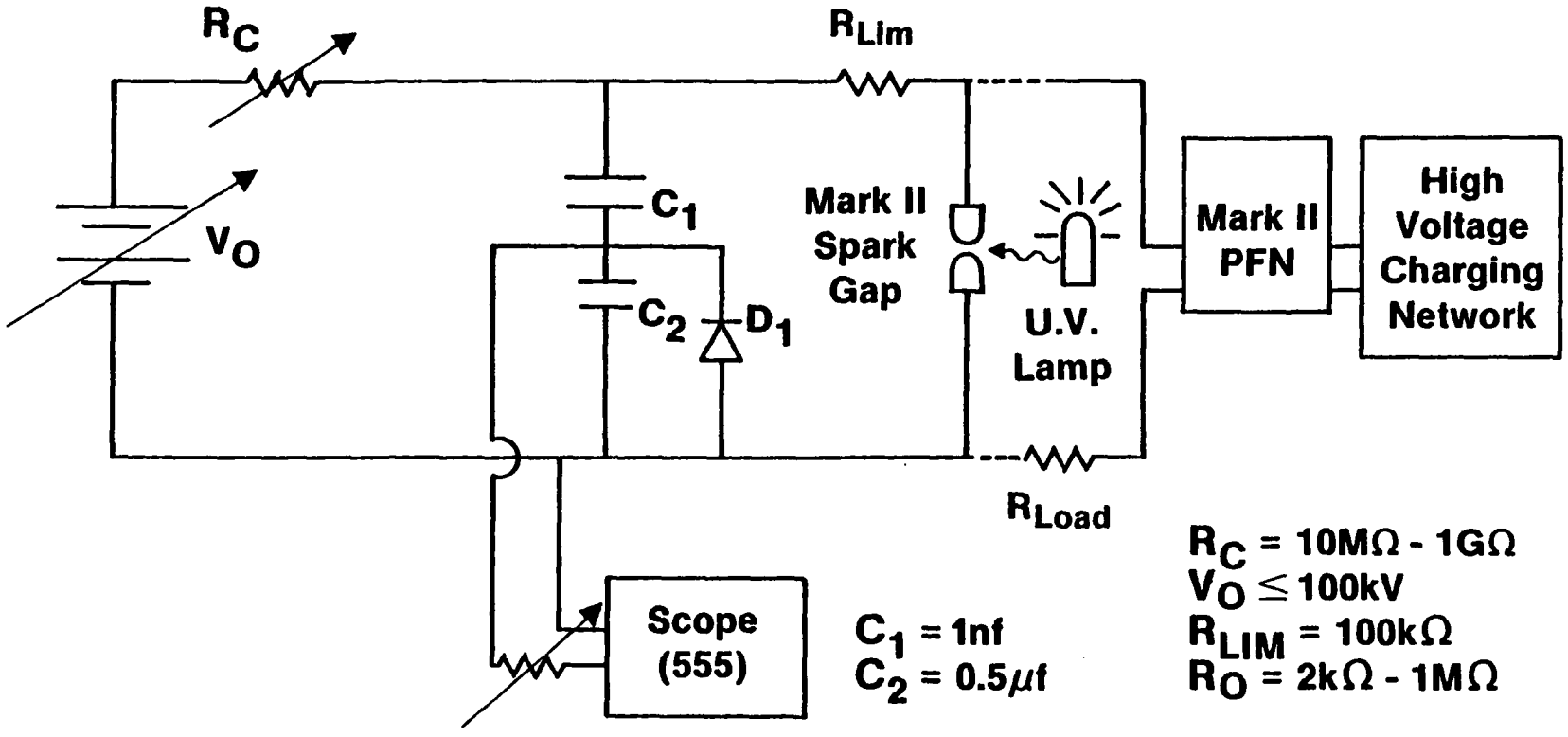
R_C
R_{Lim}
V_O
C_1
C_2
D_1
Mark II Spark Gap
U.V. Lamp
Mark II PFN
High Voltage Charging Network
R_{Load}
Scope (555)
C_1 = 1nf
C_2 = 0.5μf
R_C = 10MΩ - 1GΩ
$V_O \leq$ 100kV
R_{LIM} = 100kΩ
R_O = 2kΩ - 1MΩ

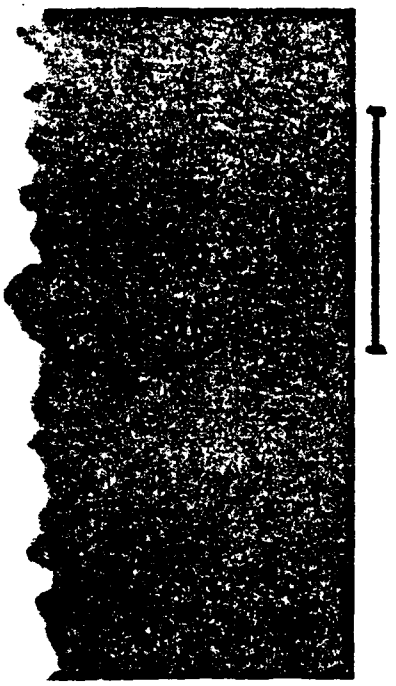

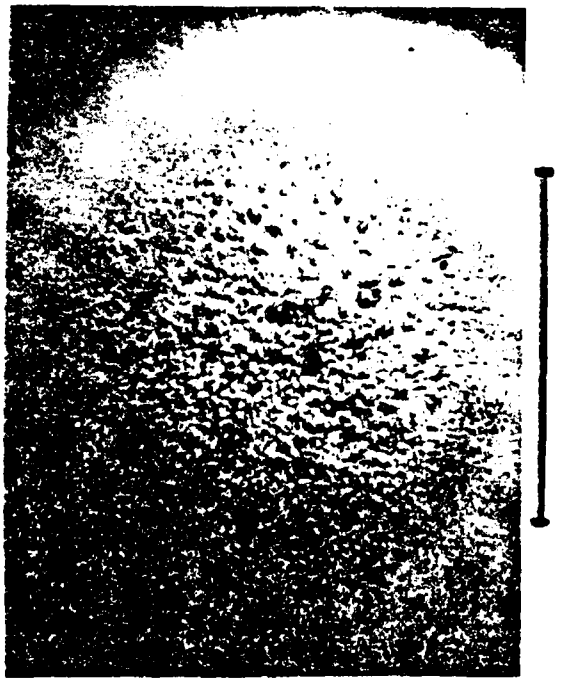

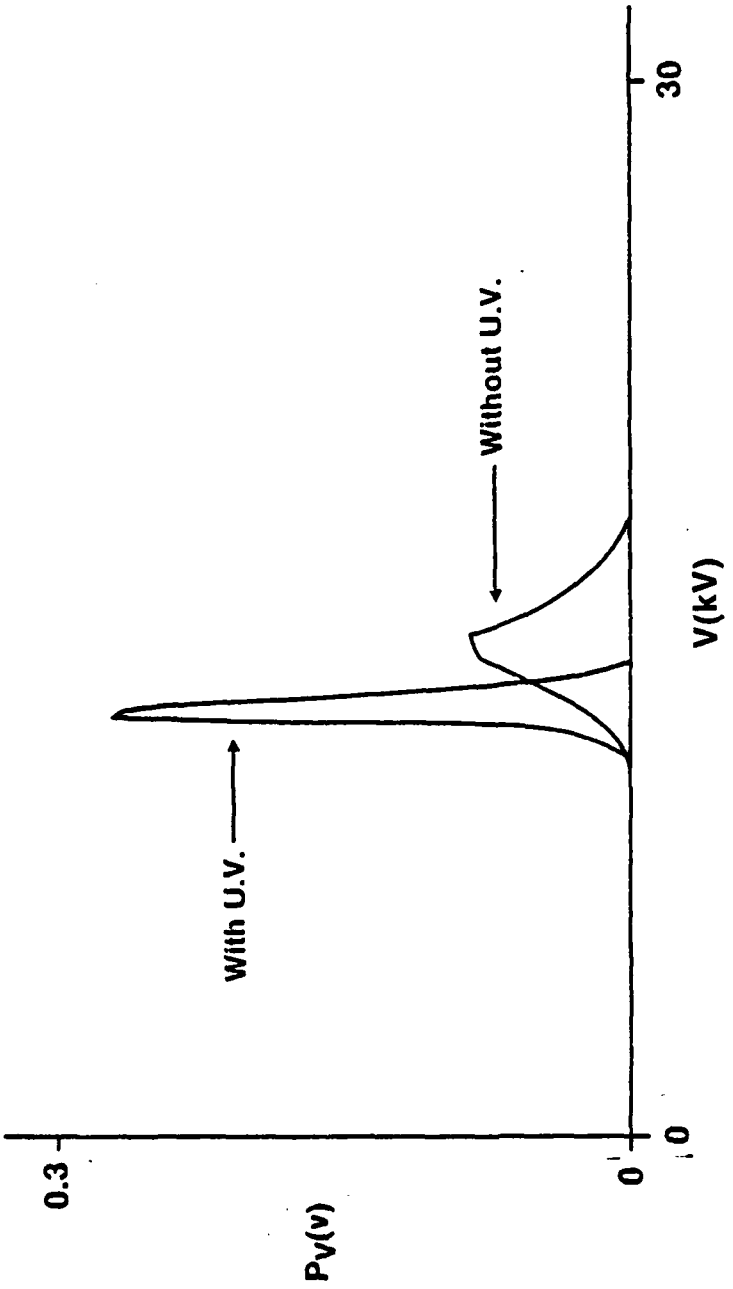
0.3
$P_V(v)$
0
0
30
V(kV)
With U.V.
Without U.V.

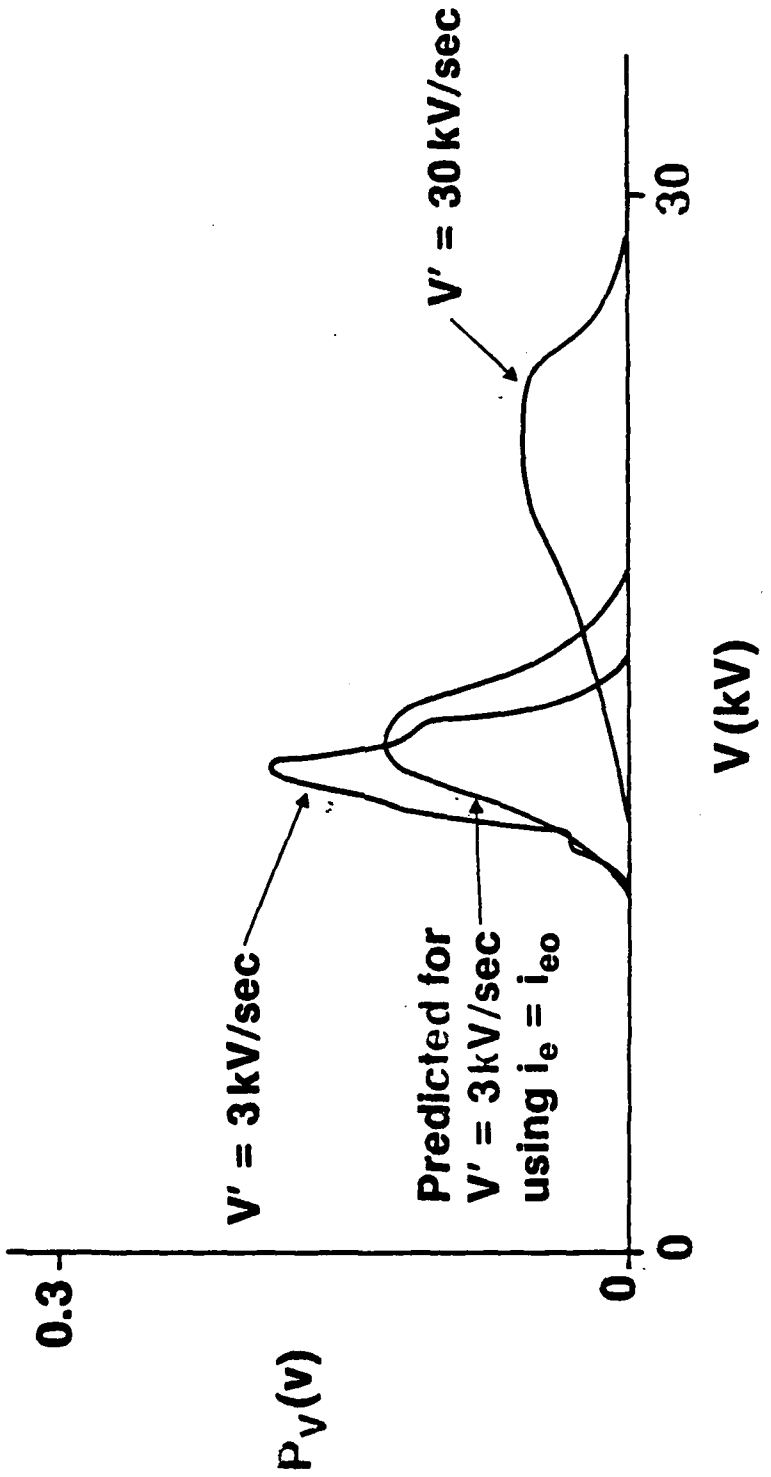
0.3
$P_V(v)$
0
0
30
V(kV)
V' = 3 kV/sec
Predicted for
V' = 3kV/sec
using $i_e = i_{eo}$
V' = 30 kV/sec

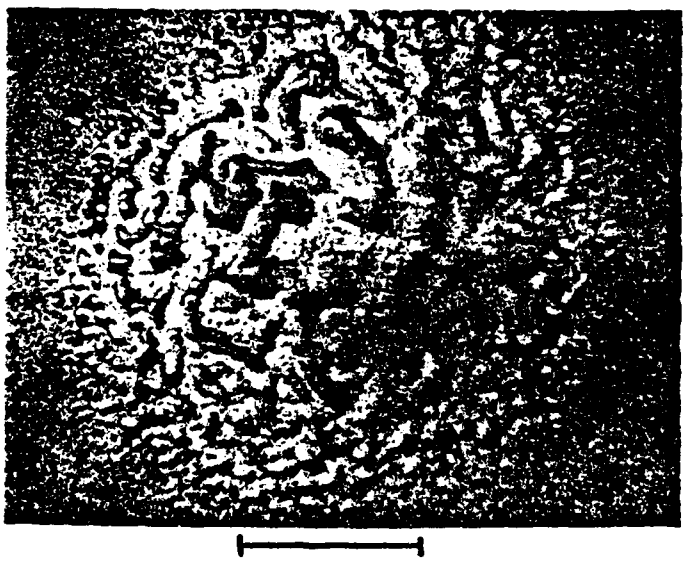

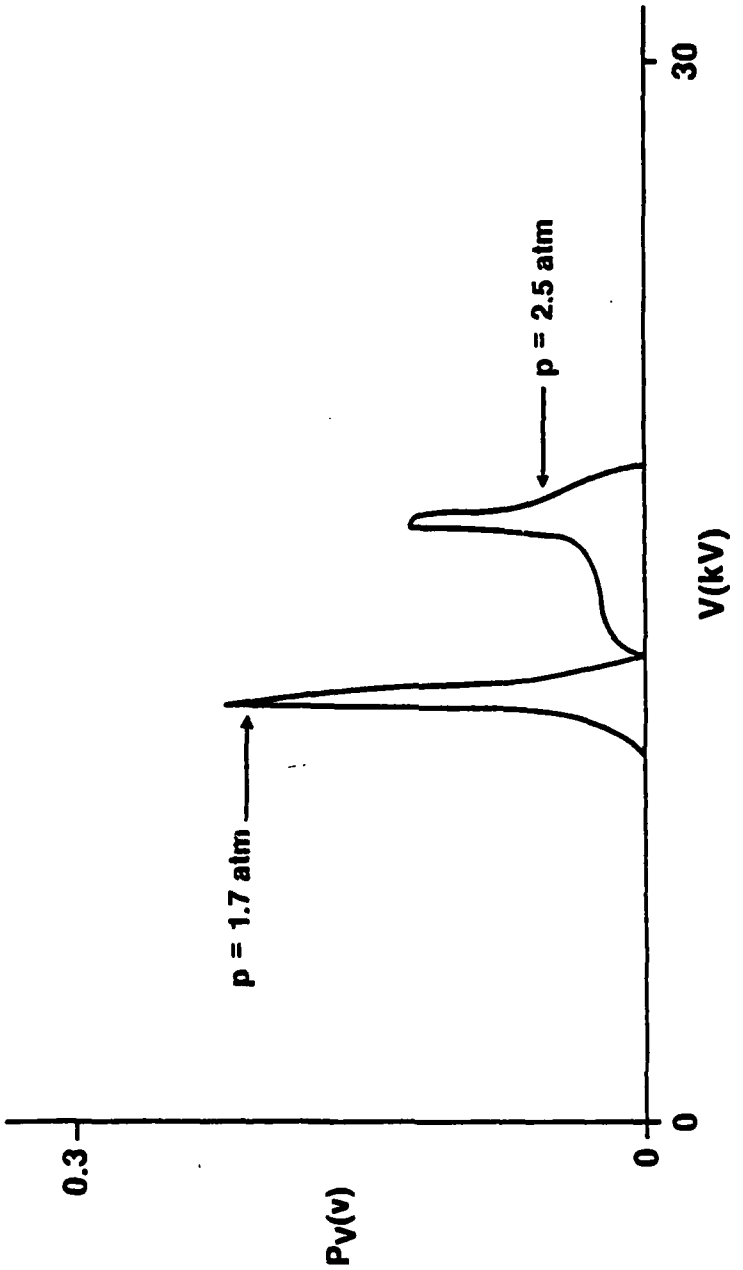
0.3
0
$P_V(v)$
0
30
V(kV)
p = 1.7 atm
p = 2.5 atm

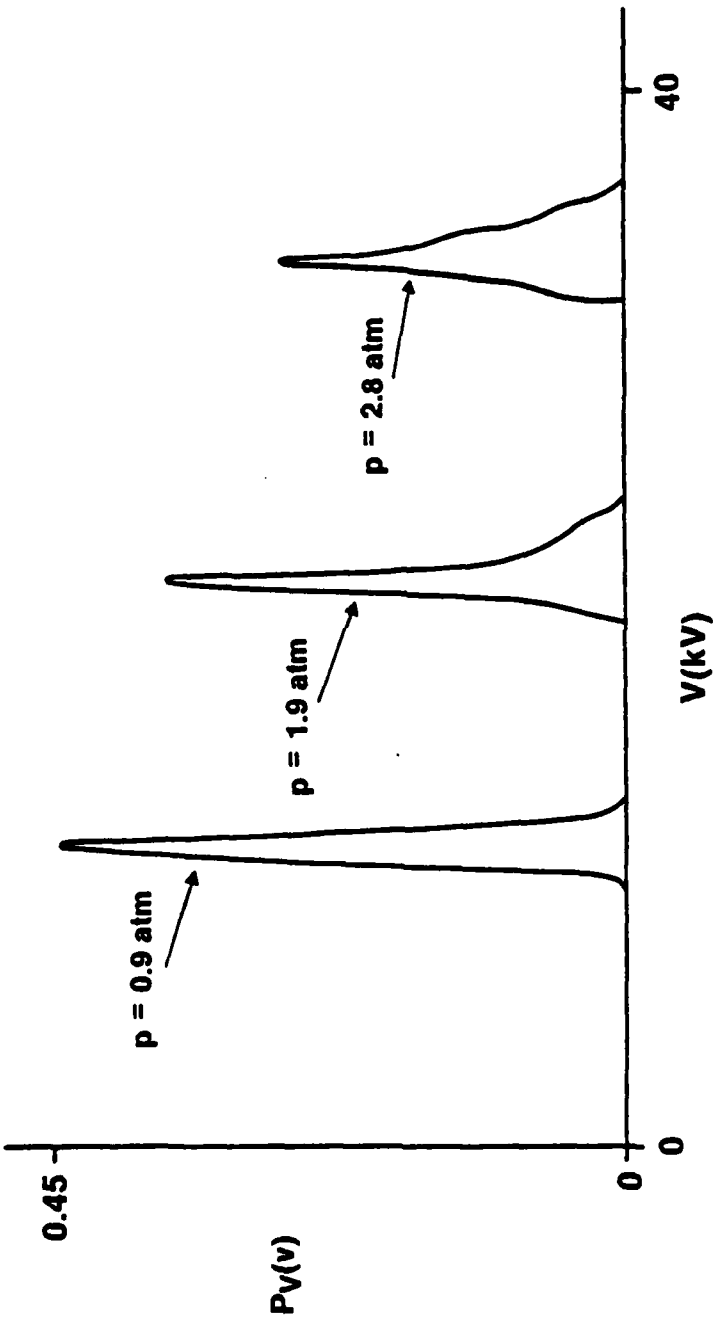
0.45
0
$P_V(v)$
0
40
V(kV)
p = 0.9 atm
p = 1.9 atm
p = 2.8 atm

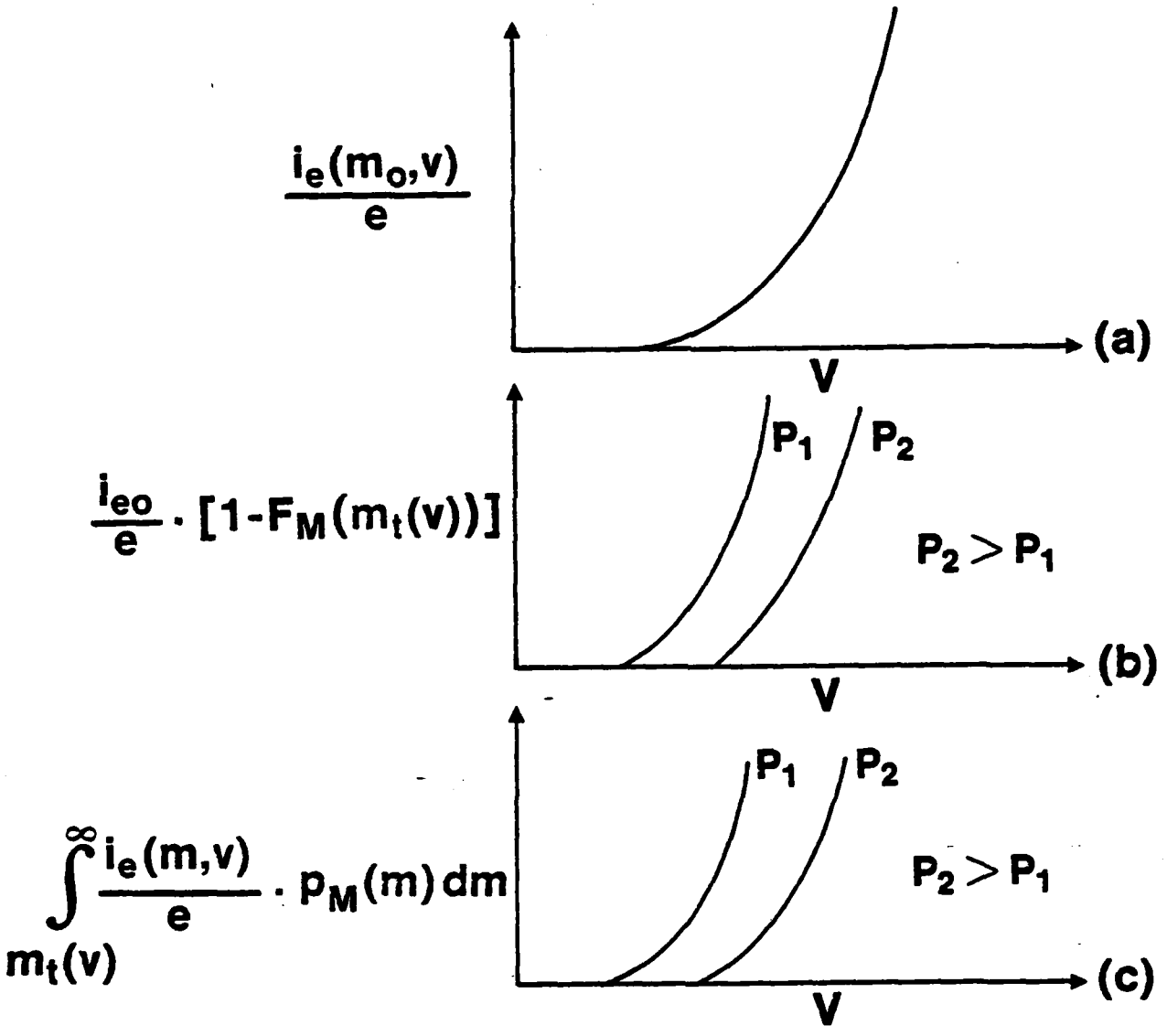
$\frac{i_e(m_o,v)}{e}$
V
(a)
$\frac{i_{eo}}{e} \cdot [1-F_M(m_t(v))]$
P_1
P_2
$P_2 > P_1$
V
(b)
$\int_{m_t(v)}^{\infty} \frac{i_e(m,v)}{e} \cdot p_M(m)\,dm$
P_1
P_2
$P_2 > P_1$
V
(c)

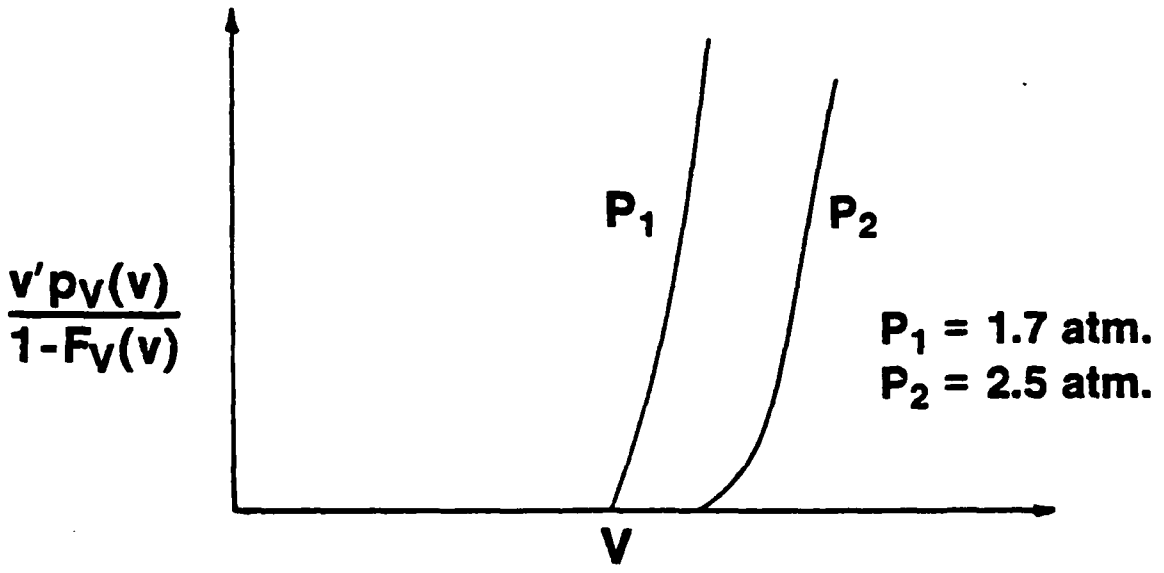
$\frac{v' p_V(v)}{1-F_V(v)}$
P_1
P_2
P_1 = 1.7 atm.
P_2 = 2.5 atm.
V

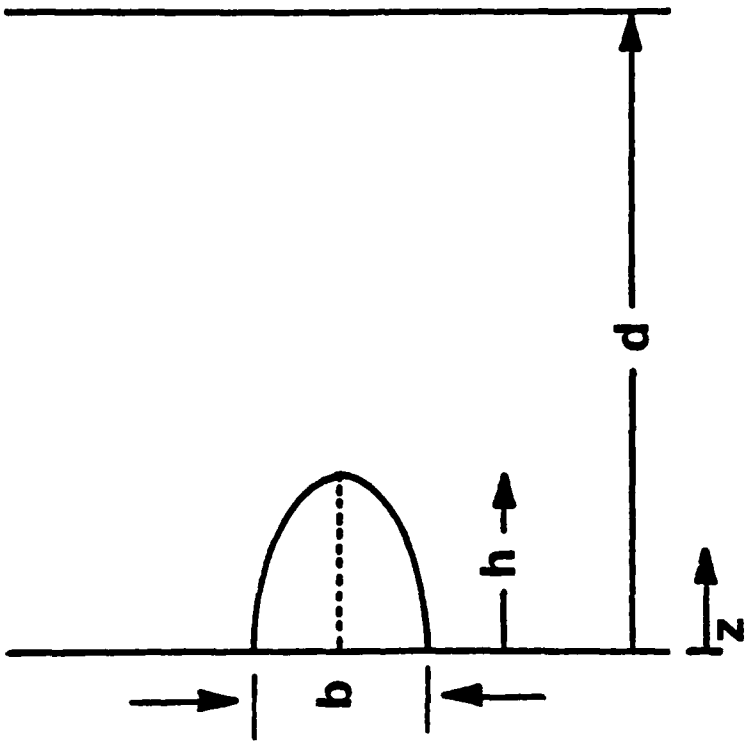
d
h
z
b

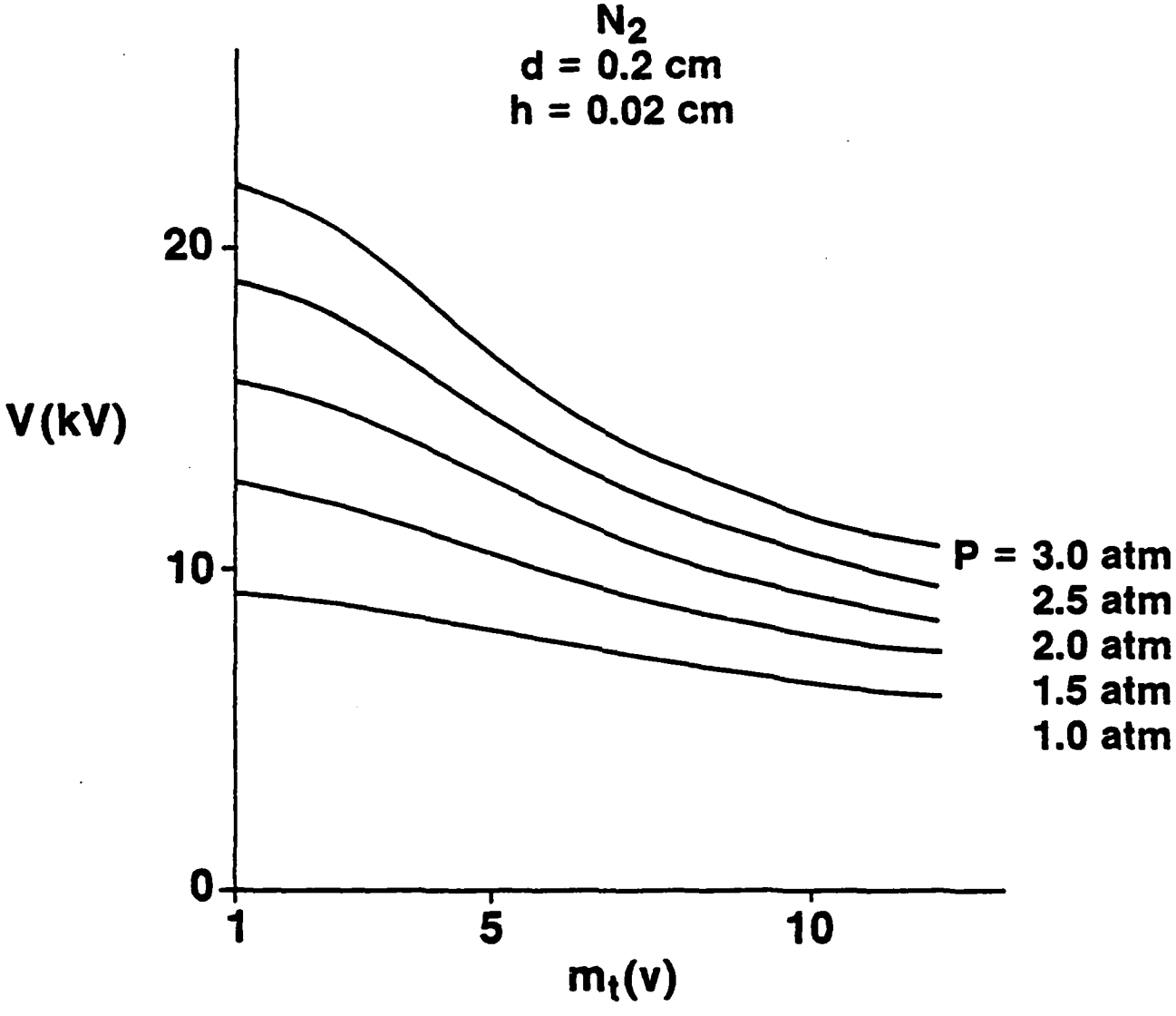
N_2
d = 0.2 cm
h = 0.02 cm
V(kV)
20
10
0
1
5
10
$m_t(v)$
P = 3.0 atm
2.5 atm
2.0 atm
1.5 atm
1.0 atm

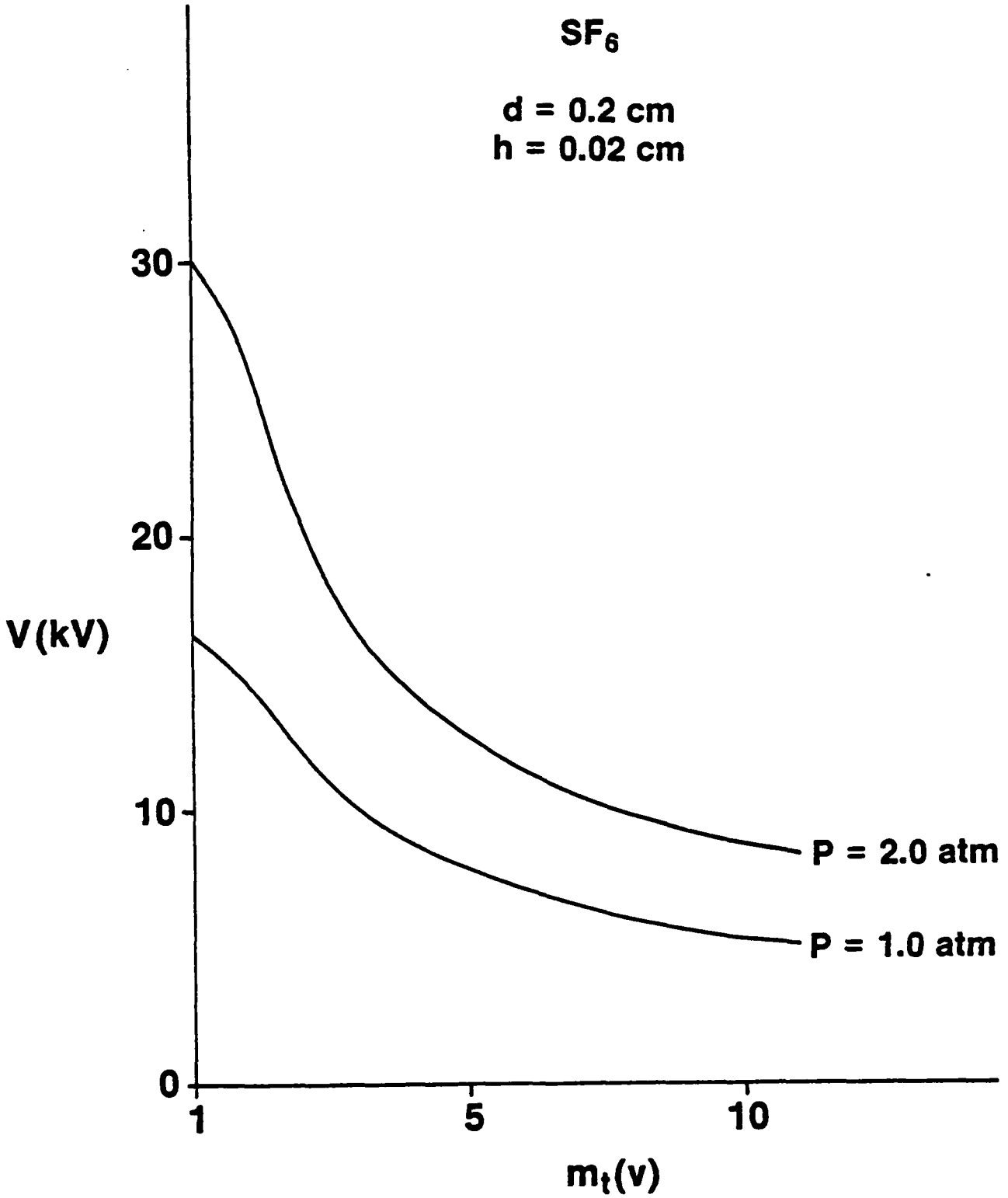
SF6
d = 0.2 cm
h = 0.02 cm
30
20
10
0
V(kV)
P = 2.0 atm
P = 1.0 atm
1
5
10
mt(v)

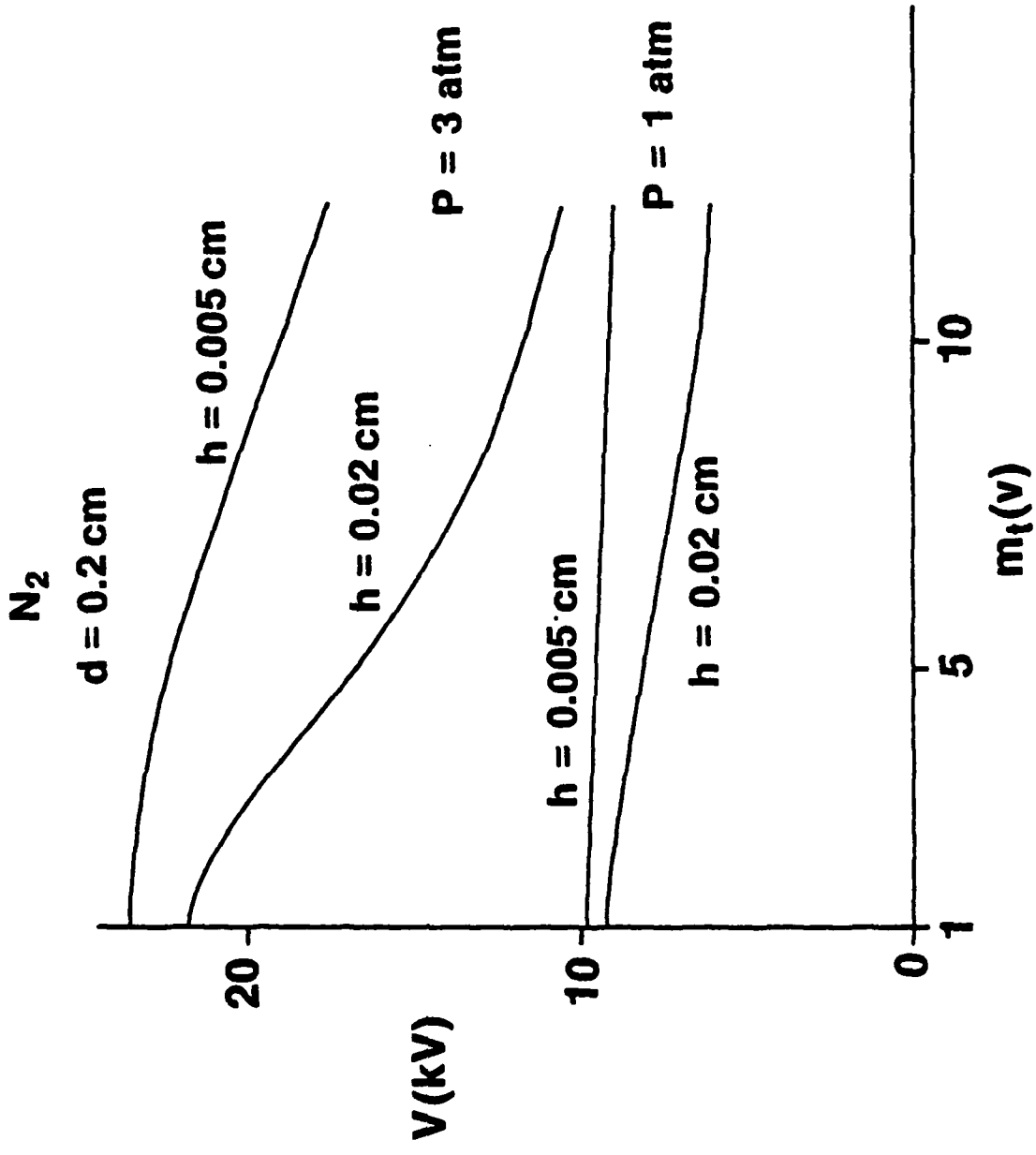
N_2
d = 0.2 cm
h = 0.005 cm
h = 0.02 cm
P = 3 atm
h = 0.005 cm
h = 0.02 cm
P = 1 atm
20
10
0
V(kV)
1
5
10
$m_t(v)$

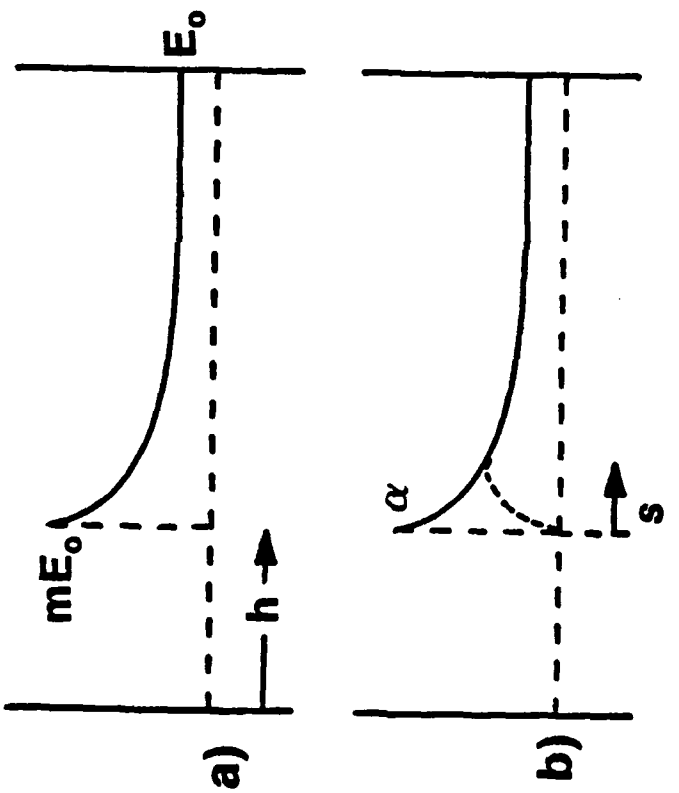
E_o
mE_o
h
a)
α
s
b)

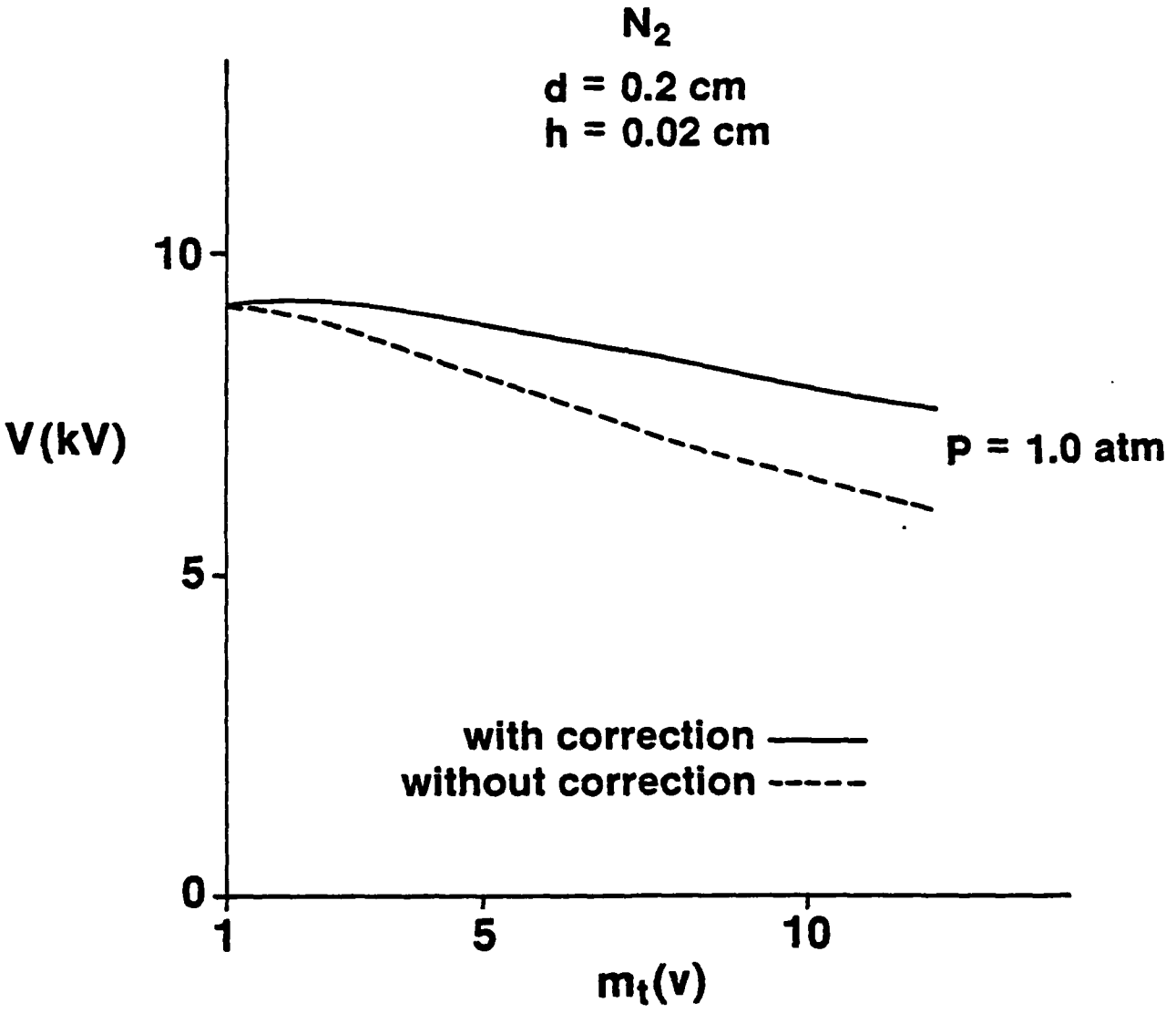
N_2
d = 0.2 cm
h = 0.02 cm
10
5
0
V(kV)
P = 1.0 atm
with correction
without correction
1
5
10
$m_t(v)$

Appendix II

Surface Analysis of Gas Filled Spark Gap Electrodes

Authors:

G.L. Jackson
The BDM Corporation
Huntsville, AL 35805

L.L. Hatfield and G.R. Leiker
Dept. of Physics & Engr. Physics

A. Donaldson, M.O. Hagler, M. Kristiansen & R.M. Ness
Dept. of Electrical Engineering

J. Marx
Dept. of Chemistry
Texas Tech University
Lubbock, TX 79409

Paul K. Predecki
University of Denver
Denver, CO 80208

Abstract

The surfaces of electrodes used in a gas filled spark gap have been analyzed using Auger Electron Spectroscopy (AES) and Scanning Electron Microscopy (SEM). The electrodes were machined from stainless steel, a copper-tungsten composite, and brass. They were analyzed after operation for 2000 shots in a spark gap filled to one atmosphere with air or nitrogen gas. The spark gap switched a 25 μs long, unipolar pulse, delivering 0.1 to 0.6 Coul/shot to a resistive load at a repetition rate of up to 5 pps. The SEM was used to determine the density and size of protrusions formed on the electrodes. Energy Dispersive Spectroscopy (EDS) and AES were used to determine surface composition and bulk composition using cross sections. The results of this analysis are applied to produce qualitative explanations of previously reported self-breakdown voltage distributions for the spark gap operated with these electrodes.

INTRODUCTION

The surface structure and composition of electrodes used in high energy, gas filled spark gaps changes during operation of the gap.[1] Chemical and physical processes enhanced by high temperatures and large electromagnetic forces produce craters, protrusions, and coatings of various compounds on the surface. Protrusions on the surfaces of electrodes lead to local field enhancements on the surface, which may lower the self-breakdown voltage of the spark gap. The size, shape, and distribution of these protrusions will determine the distribution of local field enhancements, and the chemical composition of these protrusions will influence field emission and thermionic emission which produce the initial electrons in the gap.[2,3] If these initial electrons are born in a region of large local field enhancement the self-breakdown voltage of the gap may be very low.[4,5]

Stainless steel, copper-tungsten, and brass electrodes were used in the course of a study of the performance of a gas filled spark gap.[6] The surface topography and composition of these electrodes were studied with a Scanning Electron Microscope (SEM), an Auger Electron Spectrometer (AES), and an optical microscope. Stereo pair pictures of the protrusions were taken with the SEM and examined with a stereo viewer in order to obtain information about their heights and base diameters. The AES was used to determine the composition of these protrusions and the composition of the substrate material on which these protrusions are located.

EXPERIMENTAL SETUP

The spark gap shown schematically in Figure 1 was used to test the electrode materials in different gases. The electrode materials tested were 304 stainless steel, brass, and a tungsten-copper composite (K-33). Air and nitrogen were the two gases used in these studies. This spark gap is designed for frequent electrode and insulator replacement and to allow for accurate control of the electrode alignment and gap spacing. The electrodes are 2.5 cm diameter hemispherical inserts in a brass holder. The Lucite inserts provide protection for the main gap housing and studies of the surfaces of these insulator inserts give information about the debris deposited on them as well as information about the effects of the byproducts of the discharges on the insulators.[7]

A detailed description of the spark gap assembly and diagnostic system has been published elsewhere.[8] The operating parameters of the gap, pertinent to this study, are summarized in Table I.

4

TABLE I

Operating Conditions

Gap spacing	<.75 cm
Voltage	<30 kV
Current	<25 kA
Total Capacitance	21 μF
Charge/shot	<.6 Coul
Energy/shot	<9 kJ
Pulse width	25 μs
Rep-rate	<5 pps
Pressure	1 atm (absolute)
Flow rate	1 gap vol. every 5 sec.

5

RESULTS

Virgin electrodes (machined, polished, and cleaned in ethyl alcohol) of 304 stainless steel, K-33, and brass were analyzed using AES in order to make a comparison between unused electrodes and electrodes used in this gap. Initial analysis of all these electrodes showed that they were covered with a thin layer of carbon and oxygen. Figure 2 is an SEM micrograph of a virgin, stainless steel electrode at a magnification of 200. The surface was composed of carbon (67%), oxygen (22%), and iron (11%). Figure 3 is an SEM micrograph of a virgin K-33 electrode at a magnification of 200. This sample exhibited a surface composed of carbon (30%), oxygen (7%), copper (13%), and tungsten (50%). A virgin brass sample was composed of carbon (22.9%), oxygen (34.9%), copper (36.4%) and tin (2.1%). These samples were then etched with a 5 kV Argon ion beam in order to remove the top surface layer. After sputtering for 120 seconds the surface of the stainless steel electrode changed to carbon (2%), oxygen (2%), iron (67%), chromium (21%), and nickel (7%). The known bulk concentration of this alloy is iron (70.2%), chromuim (22%), and nickel (9.3%). After sputtering the K-33 electrode for 30 seconds the surface composition was copper (28%) and tungsten (72%), compared with the known bulk concentration of copper (33%) and tungsten (66%). After sputtering the brass electrode for 30 seconds the surface composition was copper (83%), tin (7%) and trace amounts of carbon, oxygen and zinc, whereas the specified bulk composition of this alloy is copper (86%), tin (6%), and zinc (6%).

The surface layer of carbon and oxygen which was removed by the Argon ion beam etching is typical and is assumed to be the result of exposure of the electrode, after it has been machined, polished and cleaned, to the ambient laboratory atmosphere. Hydrocarbons, which produce such a layer, are always present in the air.

Figure 4 is an optical micrograph (10x) of a stainless steel cathode used for 2000 shots in this spark gap, with 1 atmosphere absolute pressure of flowing air. There are three distinct, circular regions on this electrode. The middle region (region 1) is about 10 mm in diameter, the first ring (region 2) is about 6 mm in width and the outer ring (region 3) is about 3 mm in width. SEM micrographs of region 1 indicate that there is approximately 1 large particle per mm^2 imbedded in the surface. The sizes of these particles range from 30 μm to 40 μm in height and 70 μm to 80 μm in base diameter. Figure 5 is an SEM micrograph, at a magnification of 240, which shows a typical particle imbedded in the surface. This micrograph also shows that the surface is considerably different from the virgin surface, having a matrix structure on the surface, which resembles a dried-up river bed. AES analysis of this region after 60 seconds of etching shows the surface to be composed of oxygen (57%), iron (32%), chromium (6%) and nickel (4%). The relative percentages of iron, chromium and nickel to oxygen indicate that these metals may all be present on the surface as oxides. If they are all oxidized the surface is composed of 62% Fe_2O_3, 23% CrO, and 15% NiO, however, this is only a speculation based on the measured relative elemental composition.

7

Figure 6 is an SEM micrograph at a magnification of 300 of a cross section of this same electrode after it was electrolyticly etched with a solution of oxalic acid and distilled water until the grain structure was exposed. The view shown here is a cross section perpendicular to the electrode surface. The electrode surface is at the top of the micrograph and the three dark regions extending down into the material are the cracks forming the "river bed" effect in Figure 5. This micrograph shows that the grains are approximately 20 μm in size and that there are a large number of inclusions in the stainless steel. Using x-ray fluorescence it was determined that the inclusions are magnesium sulfide stringers. The cracks occur by connecting pits formed in places where stringers are located. These cracks are formed as the result of biaxial tensile stresses in the material during the arcing process. The temperature of the surface cycles vary rapidly between shots, leading to thermal expansion and contraction of the surface. Calculations of the temperature differential between the heating and cooling cycles necessary to cause this type of structural change indicate that only about a 200°C change in temperature is required.

Figure 7 shows the upper edge of this same cross-section at a magnification of 2500. Four distinct layers can be seen in this micrograph. Analysis of these layers with an energy dispersive x-ray attachment showed that the top layer (layer 1) contains a substantial amount of carbon and oxygen and is greatly enriched in chromium compared to virgin stainless steel. The presence of oxygen in this layer confirms the results obtained with AES. The amount of carbon in this

layer is too large to be the result of contamination by exposure to air after removal from the spark gap. However, the insulator used in this spark gap is Lucite and during operation of the spark gap it is exposed to the byproducts of the discharge, which leads to deterioration of the insulator and the subsequent release of large amounts of carbon and oxygen into the spark gap. Therefore, the carbon seen in layer 1 probably results from the deterioration of the insulator. The second layer (layer 2) is composed of only the three metals: iron, chromium and nickel. However, there is an enrichment of nickel and a depletion of chromium in this layer compared to a virgin stainless steel sample. The relative vapor pressures of these three metals from highest to lowest is chromium, iron and nickel, respectively.[9] Consequently, the depletion of chromium in this layer and the enrichment of nickel can be the result of the higher evaporation rate of chromium compared to nickel. Once the chromium has evaporated from layer 2 it could be retained in layer 1 and oxidized during the arcing process. The third and fourth layers have essentially the same composition as the virgin material.

Figure 8 is an optical micrograph of a stainless steel cathode at a magnification of 10, used for 2000 shots in the spark gap, with 1 atmosphere absolute pressure of flowing nitrogen gas. There are three distinct circular regions on the surface of the electrode, which are similar in appearance and shape to the areas seen on the stainless steel electrode used in air.

Figure 9 is an SEM micrograph of the central region of this electrode at a magnification of 400. Analysis of the two areas in this

micrograph (marked 7 and 8) were performed using AES. The area marked 7 is composed of oxygen (30%), nitrogen (17%), chromium (26%), nickel (5%) and iron (22%). The presence of large amounts of oxygen and nitrogen on the surface after sputtering indicates that these elements are probably chemically bonded to the surface; however, with AES it is usually not possible to determine the chemical bonds. The oxygen probably comes from the disassociation of water in the system. The Lucite insulator will absorb 4% by volume of water in a humid environment. The spark gap is not baked out before the experiments are performed and during the experiment the temperature of the insulator increases so that water absorbed by the insulator could be released and available to react chemically with the electrodes.

The area marked 8 in this micrograph is a protrusion on the surface with a height of about 62 μm and a base diameter of about 100 μm. The composition of this protrusion, after etching, is carbon (7%), oxygen (21%), nitrogen (12%), chromium (20%), nickel (6%) and iron (35%). It is difficult to determine how this protrusion formed; one possibility is that the material surrounding the protrusion was eroded away by the discharge, leaving the protrusion on the surface.

Figure 10 is an SEM micrograph of region 2 at a magnification of 1000. This region appears to be very smooth in comparison to region 1; however, there are a large number of cracks in the surface and many small holes. Analysis of this region, using AES, shows the surface to be composed of carbon (34%), oxygen (43%), nitrogen (2%), and iron (21%). After sputtering for 30 seconds the composition changed to carbon (6%), oxygen (46%), nitrogen (9%), iron (31%), chromium (4%),

and nickel (5%). The relative percentages of oxygen to iron (3 to 2) indicates that the oxygen is chemically bonded with the iron to form the compound Fe_2O_3; however, since AES does not give chemical bonding information this is only a speculation.

Region 3 of this electrode was impossible to analyze with AES because of surface charging. Surface charging occurs in AES when the surface being analyzed is highly insulating. Probably the surface is coated with an insulating layer of hydrocarbon material. This material could be the result of contamination by exposure of the electrode to the laboratory atmosphere after the experiment although such material is usually removed by the Argon ion beam or it could be the result of deterioration of the Lucite insulator insert in the spark gap. Microparticles from the electrodes cause a considerable amount of damage to this insulator resulting in the ejection of insulator material in either solid or vapor form, which can then be deposited onto the electrodes.[7] Region 3 does not actively participate in the discharge, consequently this insulator material can build up in this region. In regions 1 and 2 this material would be vaporized by the discharge and not remain on the surface.

Figure 11 is an SEM micrograph at a magnification of 300 of a cross-section of this electrode. This electrode exhibits the same type of structural damage as the stainless steel electrode used in air; however, the damage is much less severe. Obviously, the combined effects of thermal stresses and oxidation promote propagation of the cracks in the stainless steel electrode when used in air. Using energy dispersive analysis it was not possible to find evidence of metal

nitrides or oxides on the surface of the electrode used in pure nitrogen, however, AES analysis definitely indicated large amounts of both elements present on the surface. The analysis depth of AES is approximately 50 Å and the analysis depth of EDS is approximately 5 μm. Therefore, the analysis of this electrode, using AES, is more indicative of the surface layer on the electrode than the analysis using EDS.

Examination with an optical microscope at a magnification of 10 of a K-33, tungsten-copper, electrode used for 2000 shots with 1 atmosphere absolute pressure of flowing nitrogen showed that the surface of this electrode is very smooth and similar in appearance to the polished virgin electrode. There is only a very small region on this electrode where damage can be seen. Figure 12 is an SEM micrograph of the damaged region at a magnification of 200. The surface is pitted and cracked in some areas, however, stereoscopic analysis of this electrode with the SEM indicates that there are no protrusions on the surface greater than 10 μm in height. Analysis of the electrode with AES shows that this region is mainly composed of carbon (23%), oxygen (15%), nitrogen (5%), copper (34%), and tungsten (23%). After sputtering the surface for 30 seconds, the composition changes to tungsten (62%) and copper (38%), which is very nearly the known bulk concentration of the virgin K-33. The copper on the top of the electrode before sputtering is probably copper that has redeposited onto the electrode from the vapor state, leaving a very thin layer of copper on the surface. The melting point of copper is 1339 K and the boiling point is 2823 K, whereas tungsten melts at 3660 K and boils at 6186 K. Thus,

copper boils at a temperature which is 1000 K less than the melting point of tungsten. It is likely that the cathode spot temperature exceeds the boiling point of copper but not that of tungsten and therefore the copper may be selectively boiled out of the electrode and then recondense on the electrode between arcs. Analysis of areas of this electrode outside of this damaged area shows a surface composed of carbon (13%), oxygen (11%), copper (42%), tungsten (29%), and nitrogen (6%). After sputtering for 30 seconds the composition changes to that of the virgin K-33 electrode. The large amount of copper compared to tungsten in this area therefore supports the hypothesis presented above.

Figure 13 is an optical micrograph at a magnification of 10 of a K-33 electrode used for 2000 shots, with 1 atmosphere absolute pressure of flowing air. There are 3 distinct circular regions visible on this electrode. The inner region (region 1) is approximately 12 mm in diameter and very smooth in appearance. The first ring (region 2) is about 3 mm in width and very pitted and rough. The second ring (region 3) is approximately 5 mm in width and appears to be very smooth.

Figure 14 is an SEM micrograph of region 1 of this electrode at a magnification of 200. On this scale the surface is rough and pitted with some cracks that are as wide as 5 μm (this surface is similar in appearance to the damaged area of the K-33 electrode in nitrogen gas). Analysis of region 1, with AES, shows the surface to be composed of carbon (40%), oxygen (19%), copper (36%), with trace amounts of nitrogen and chlorine. The chlorine is probably an impurity in the gas used. After this region was sputtered for 60 seconds the composition

changed to oxygen (31%), copper (23%), and tungsten (46%). Probably the tungsten and copper are present on the surface as oxides as well as pure metal particles. Again the presence of copper in a large ratio to tungsten on the surface supports the hypothesis that the copper has been selectively boiled out of the matrix due to the discharge process and then redeposited on the electrode between arcs.

Figure 15 is an SEM micrograph at a magnification of 240 of region 2 of this electrode. This region is completely different in appearance to region 1. There is a large concentration of irregularly shaped "globs" resting on a relatively smooth surface. Figure 16 is an SEM micrograph at a magnification of 1000 of this same region. Analysis at the point marked 1 in this micrograph with AES shows carbon (49%), oxygen (16%) and copper (35%), and analysis of the square area marked 2 shows a similar composition. Sputtering this surface for 30 seconds shows that point 1 is composed of oxygen (44%) and tungsten (56%), whereas area 2 is composed of carbon (5%), oxygen (35%), copper (24%) and tungsten (36%). Apparently, this entire middle ring is covered with a very thin layer of copper and copper oxide, which may have condensed onto the surface from the vapor state. The "globs" appear to be tungsten and a tungsten oxide. These "globs" could be molten tungsten that has spilled over from the middle region of the electrode or has been physically ejected from the middle region and then resolidified onto region 2. This would imply that the

temperature of the cathode spot on a K-33 cathode is higher in an air environment, than in a nitrogen environment, since these "globs" were not seen on the K-33 electrode used in nitrogen.

Figure 17 is an SEM micrograph at a magnification of 1000 of region 3 of this electrode. The "globs" in this region are much larger than those in region 2 but they are similar in shape to the "globs" in region 2. Auger analysis of the area enclosed by the square shows the surface to be composed of copper (26%), oxygen (30%) and carbon (44%). Sputtering this surface for 30 seconds shows this "glob" to be composed of copper (24%), oxygen (24%) and tungsten (52%). Analysis of the material, on which these "globs" rest, was impossible to perform with AES because of surface charging.

A brass electrode used in this gap, with 1 atmosphere absolute pressure of flowing nitrogen gas, was removed after 2000 shots and visually inspected with the naked eye. The surface of this electrode was very rough and SEM micrographs of this surface show that the entire electrode surface is covered with very large irregularly shaped protrusions. The base diameters of these protrusions range in size from 100-500 μm, with heights of up to 200 μm. Analysis of this surface with AES is very difficult to perform because of this topography; however, analysis of the tips of some of the protrusions shows that they are composed of carbon (23%), oxygen (35%), tin (2.1%), and copper (36%). Sputtering for 5 minutes produces very little change in the composition readout which implies that this is a thick layer, perhaps 50 Å or more deep. No further analysis of the brass was attempted.

15

Conclusions

The results on all the virgin electrodes show that hydrocarbons accumulate on the surfaces due to exposure to the atmosphere. However, these are merely adsorbed on the surface and are removed almost immediately by sputtering in the AES machine. This implies they are also removed during the first few arcs in a spark gap. These hydrocarbon layers are, therefore, of no consequence in spark gap operation. The virgin electrode studies also show that, after sputtering, the surface composition is the specified bulk composition of the material except for the brass in which the specified amount of zinc was not seen.

The studies on stainless steel used in air and pure nitrogen gas show that the oxygen promotes corrosion which occurs most efficiently along the magnesium sulfide stringers. The use of nitrogen gas retards the corrosion and surface cracking and, therefore, probably also retards the rate of erosion of the electrode. The implication is that higher purity of the stainless steel would also lead to less surface damage during spark gap operation.

The K-33 electrode used in air also exhibited more visible surface damage than the one used in nitrogen. In addition, the globs of material thrown out from the center region of the electrode used in air appear to be pure tungsten covered by a thin layer of copper oxide. The copper oxide coating is no surprise because the copper layer deposited from vapor is seen on all K-33 electrodes after arcing. The question is, why are pure tungsten particles ejected from

the arc region when air is used and not when nitrogen is used? Perhaps, when air is used, the temperature at the arc attachment point on the cathode is higher, boiling out a larger fraction of the copper, leaving the sintered tungsten structure behind. This structure would have a lower thermal conductivity and thermal capacity than the original composite and therefore be more vulnerable to melting or fracturing during the next arc.

The brass electrode studies show that this particular brass is unsuitable in this operating regime. The large protrusions formed cause large fluctuations in the self-breakdown voltage of the gap. In fact, the self-breakdown voltage dropped to such a low value after a few shots that data collection was discontinued on the basis that such low energy shots would not be comparable to the tests on other materials. AES data on the tips of the large protrusions indicated very thick layers of carbon and oxygen which were not removed by argon ion sputtering. Such thick layers were not observed on the stainless steel or K-33 electrodes.

Figures 18 and 19 show the self-breakdown voltage distributions for the stainless steel and K-33 electrodes from which the samples reported on here were taken. (These figures are reproduced from reference 10.) Figure 18 b shows a much broader distribution occurs for the stainless steel-air combination which, as we have shown, results in more electrode surface damage than the stainless steel N_2 combination. The self-breakdown voltage distribution has been modelled in terms of the electric field enhancement due to protrusions on the cathode surface and the electron emissivity of the cathode surface.[1]

At one atmosphere gas pressure with a one centimeter gap (the conditions of these experiments) the model predicts no effects due to protrusions less than 500 microns in height. No protrusions greater than 70 microns have been observed on the stainless steel electrodes. However, the electrode used in N_2 exhibits nitrogen on the surface which is not removed by argon ion etching and may, therefore, be chemically bonded to the iron. If this nitrogen compound has a higher electron emissivity than the oxides found on the surface of the electrode used in air, then the model would predict a narrower self-breakdown voltage distribution for the electrode used in N_2.

Figure 19 shows no significant difference in the width of the self-breakdown voltage distribution for K-33 used in air and N_2. Our surface analysis showed no nitrides on the K-33 surfaces, and both exhibited oxides. In other words, the surface analysis gives no reason to expect a difference in the self-breakdown voltage distributions, in agreement with the data in Figure 19.

Acknowledgments

We thank the Center for Research in Surface Science and Submicron Analysis (CRISS) at Montana State University for the use of their facilities and for their technical assistance. This work was supported by the Air Force Office of Scientific Research.

References

1. V.A. Avrutskii, Sov. Phys. Tech. Phys., 18, 389 (1973).

2. R.V. Hodges, R.C. McCalley, and J.F. Riley, Lockheed Missiles and Space Company Report, LMSC-0811978 (1982).

3. R.V. Hodges and J.F. Riley, Lockheed Missiles and Space Company Report, LMSC-0877208 (1983).

4. A. Pedersen, IEEE Trans. on Power Apparatus and Systems, PAS-94, 1749 (1975).

5. S. Berger, IEEE Trans. on Power Apparatus and Systems, PAS-95, 1073 (1976).

6. A.L. Donaldson, M.O. Hagler, M. Kristiansen, G. Jackson, and L. Hatfield, IEEE Trans. Plasma Sci. PS-12, 28 (1984).

7. G. Jackson, L. Hatfield, G. Leiker, M. Kristiansen, M. Hagler, A. Donaldson, R. Curry, R. Ness, and J. Marx, Paper No. 31.3, Proc. 4th IEEE Pulsed Power Conf. Albuquerque, NM, June, 1983.

8. A.L. Donaldson, Masters Thesis, Texas Tech University (August, 1982).

9. Handbook of Chemistry and Physics 53rd Ed. R.C. Weast, Ed., The Chemical Rubber Co., Cleveland, Ohio, (1972) pp. D180.

10. G. Jackson, L. Hatfield, M. Kristiansen, M. Hagler, A.L. Donaldson, R. Ness, and J. Marx, paper No. 25.3, Proc. 4th IEEE Pulsed Power Conf. Albuquerque, NM (June, 1983).

Figure Captions

1. Cross sectional view of the spark gap in which the electrodes were subjected to high voltage sparks. Nitrogen gas or dry air were introduced through the air inlet.

2. Virgin, stainless steel electrode surface X200 (SEM). The grooves left by the polishing compound are about 5 μm wide.

3. Virgin, K-33 electrode surface X200 (SEM). In addition to the polishing marks, the surface is typical of a composite, in this case, copper-tungsten.

4. Axial view of the top of a stainless steel electrode used in air X10 (optical). The three regions discussed in the text are clearly visible.

5. Typical particle embedded in region 1 of the surface of the stainless steel electrode shown in Figure 4, X240 (SEM). This particle is about 70 μm in diameter at the base.

6. Cross sectional view taken from the central region of the stainless steel electrode of Figure 5, X300 (SEM). The electrode was sectioned perpendicular to the top surface, polished, and etched to expose the grain structure. The cracks extending downward into the surface are discussed in the text.

7. Magnified view of the cross section of Figure 6, X2500 (SEM). The viewing angle is such that the electrode top surface can be seen in the upper left quarter of the micrograph, while the bulk material is seen in the lower right quarter.

8. Axial view of the top of a stainless steel electrode used in nitrogen, X10 (optical). As in Figure 4, three distinct regions are visible.

9. A typical protrusion in the central region of the electrode shown in Figure 8, X400 (SEM). The regions marked 7 and 8 were analyzed using AES.

10. Magnified view of region 2 of the electrode shown in Figure 8, X1000 (SEM). There are a large number of small holes in the surface, but compared with Figure 9, this is a very smooth surface.

11. Cross section from the central region of the electrode shown in Figure 8, X300 (SEM). This cross section was prepared by the same procedure used to produce Figure 6. However, this electrode was operated in nitrogen gas instead of air. Note the lack of deep cracks in the surface.

12. Small damaged region in the center of the K-33 electrode used in nitrogen, X200 (SEM). There are no protrusions greater than 10 μm in height.

13. Axial view of the top of a K-33 electrode used in air, X10 (optical). In contrast to the K-33 electrode used in nitrogen, three distinct regions are visible.

14. Central region of the electrode shown in Figure 13, X200 (SEM). This surface is similar to that shown in Figure 12 even though the two electrodes were used in different gases.

15. Region 12 of the electrode shown in Figure 13, X240 (SEM). Comparison with Figure 14 shows that the central region and region 2 have quite different surface structures.

16. Magnified view of the surface shown in Figure 15, X1000 (SEM). AES was used to analyze the surface composition at the point marked 1 and the square area marked 2.

17. View of the surface in region 3 of the electrode shown in Figure 13, X1000 (SEM). The area marked with a square was analyzed using AES but the substrate on which this "glob" rests could not be analyzed due to surface charging.

18. a. Self-breakdown voltage distribution for a stainless steel electrode used in nitrogen gas. The mean breakdown voltage is 13 kV with a standard deviation of 0.5 kV.

    b. Self-breakdown voltage distribution for a stainless steel electrode used in air. The mean breakdown voltage is 18 kV with a standard deviation of 2 kV.

19. a. Self-breakdown voltage distribution for a K-33 electrode used in nitrogen gas. The mean breakdown voltage is 14 kV with a standard deviation of 2 kV.

    b. Self-breakdown voltage distribution for a K-33 electrode used in air. The mean breakdown voltage is 16 kV with a standard deviation of 2 kV.

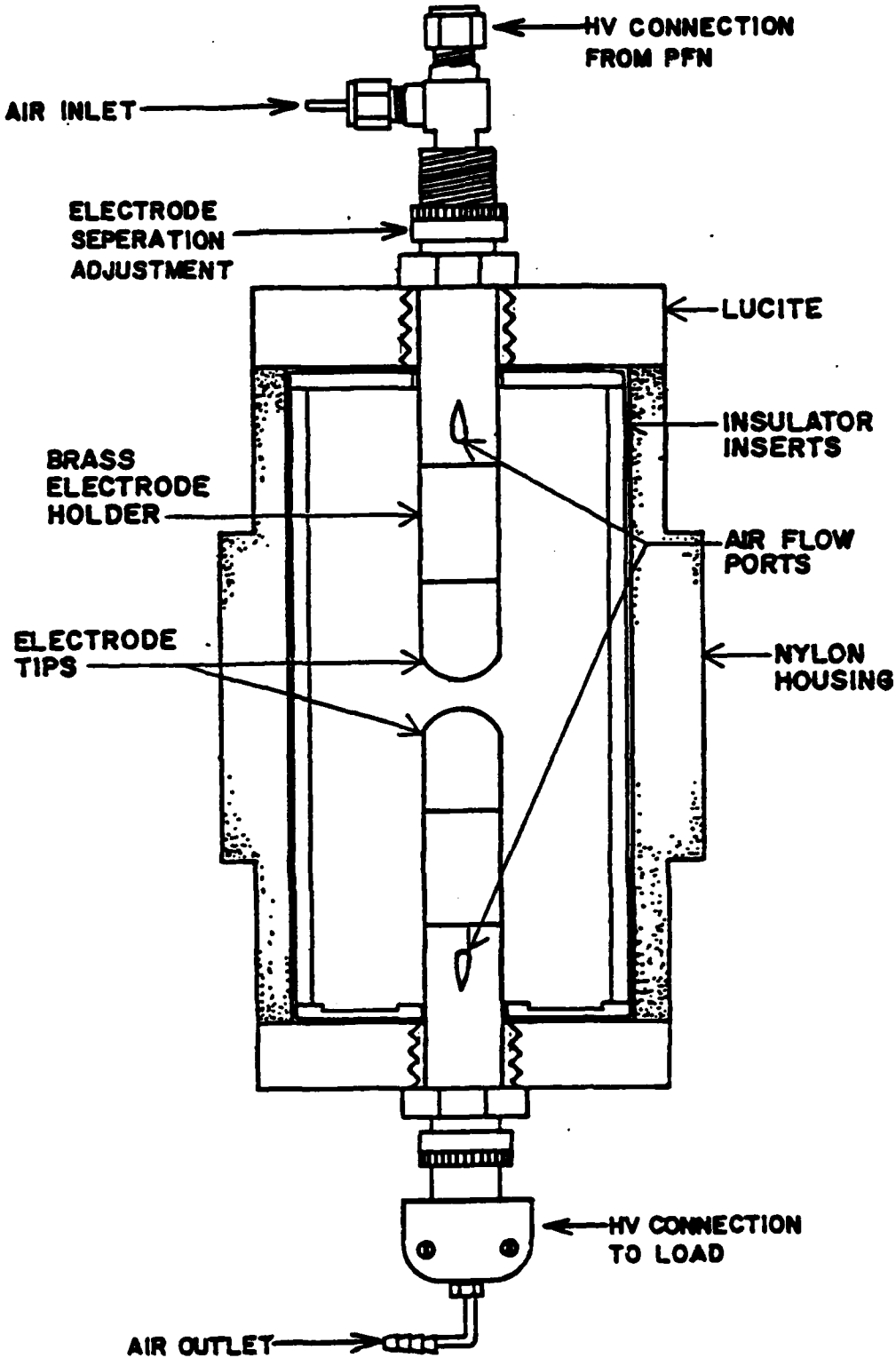
HV CONNECTION FROM PFN
AIR INLET
ELECTRODE SEPERATION ADJUSTMENT
LUCITE
INSULATOR INSERTS
BRASS ELECTRODE HOLDER
AIR FLOW PORTS
ELECTRODE TIPS
NYLON HOUSING
HV CONNECTION TO LOAD
AIR OUTLET

Fig. 1

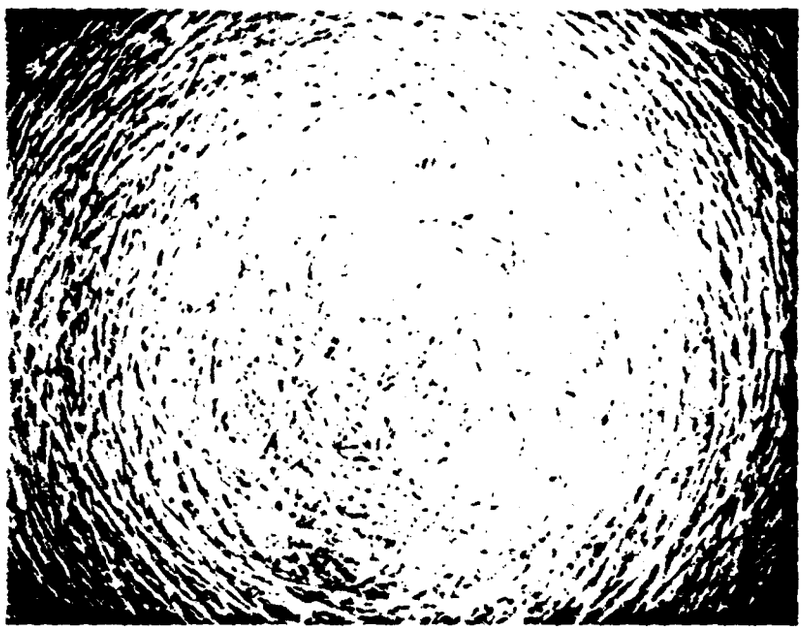

Fig. 2

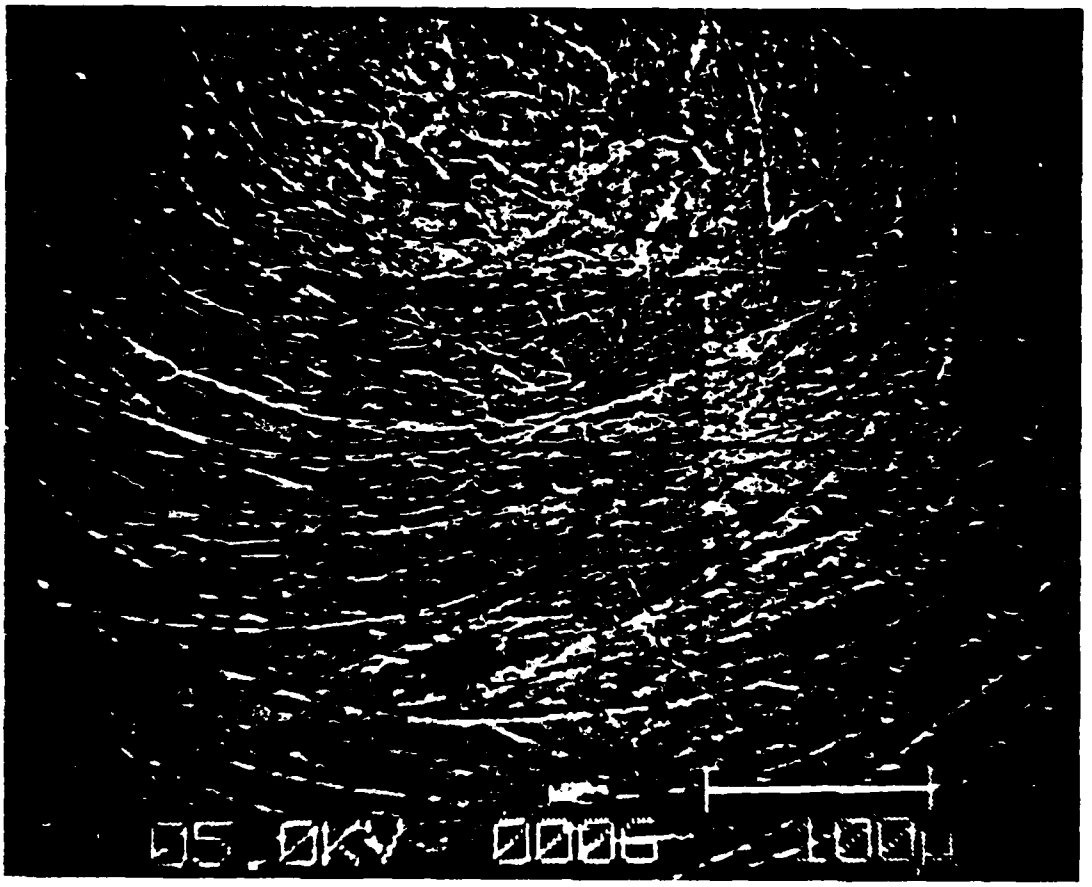

Fig. 3

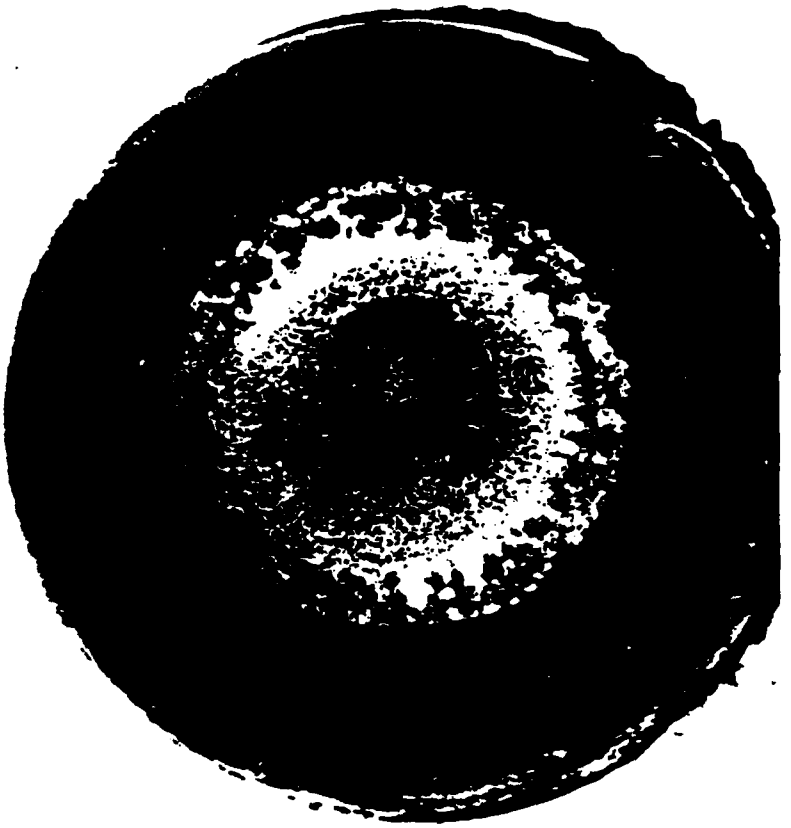

Fig. 4

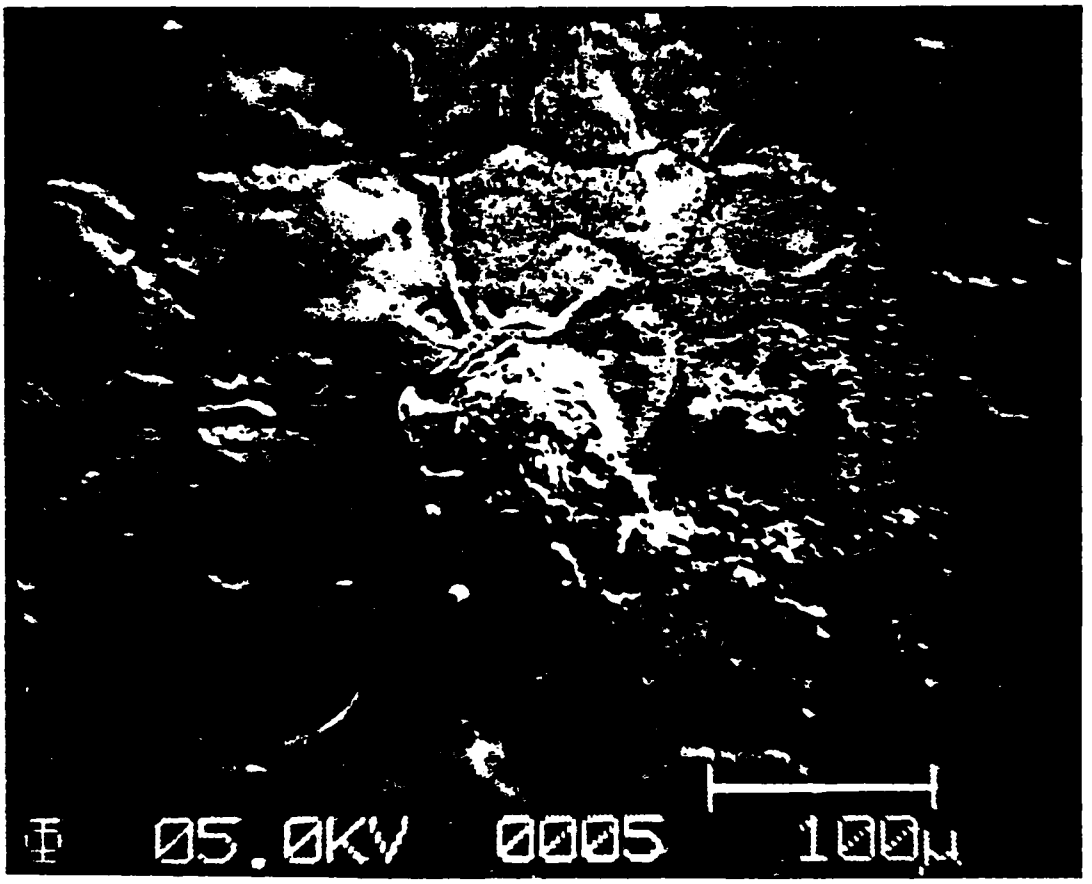

Fig. 5

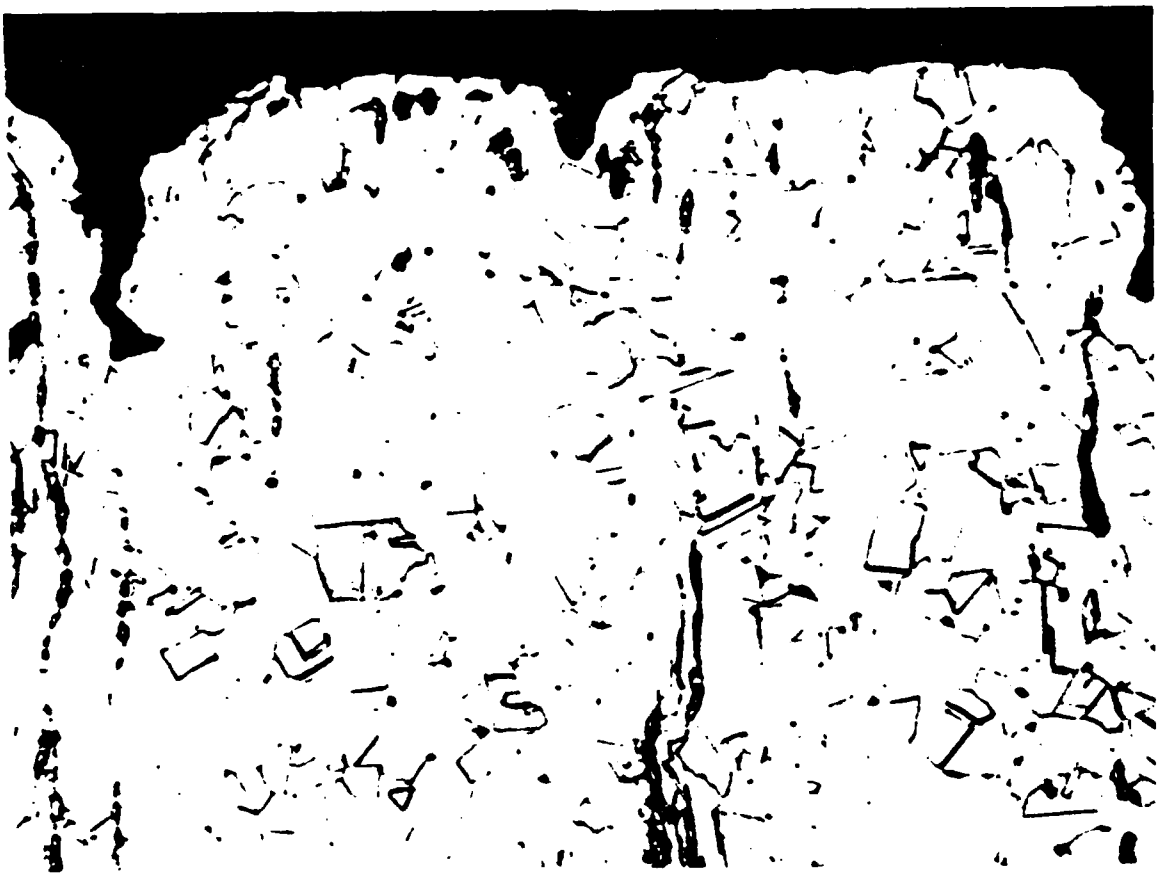

Fig 6

Fig. 7

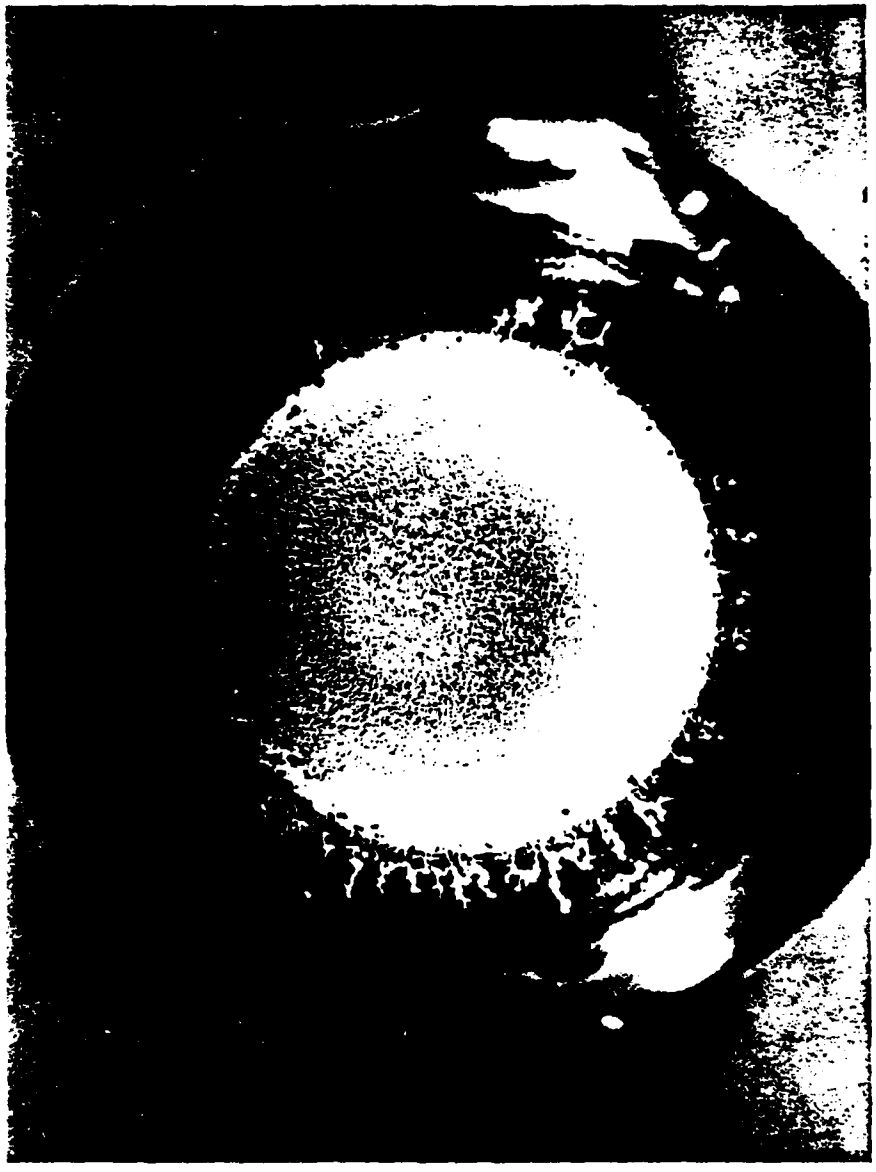

Fig 8

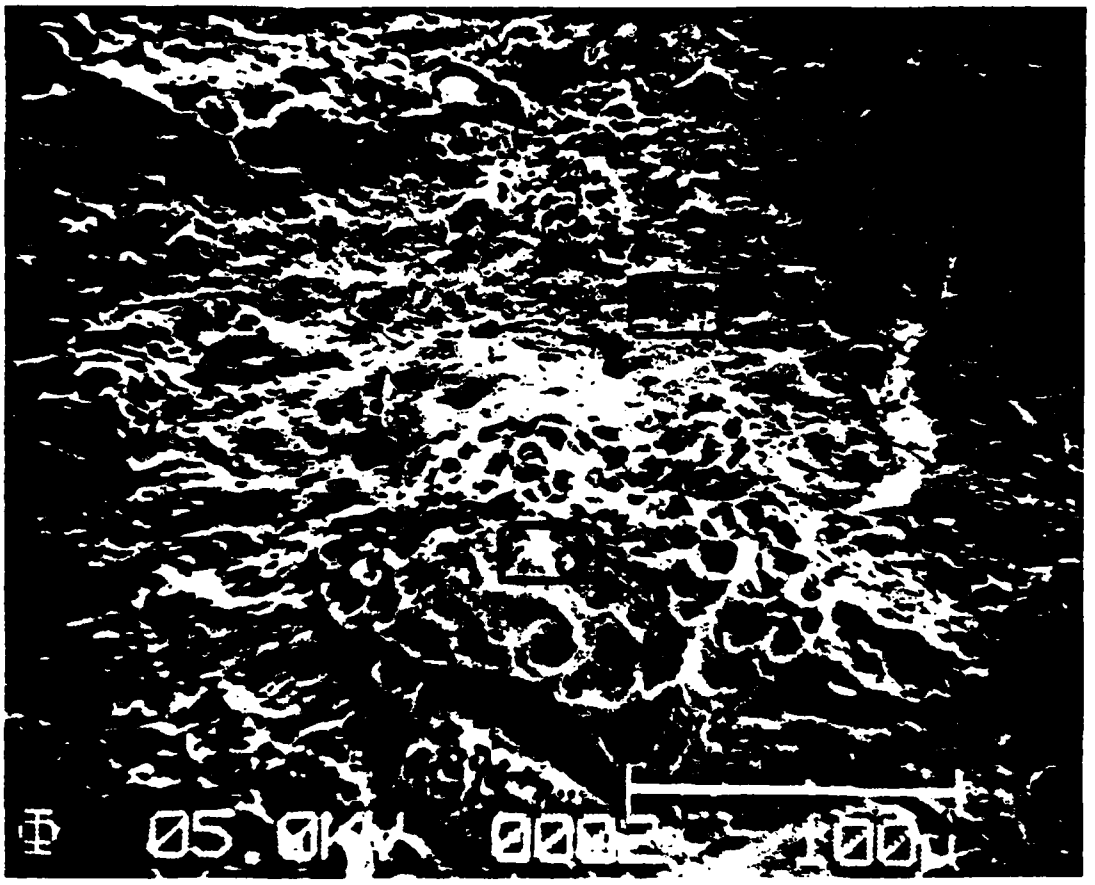

Fig 9

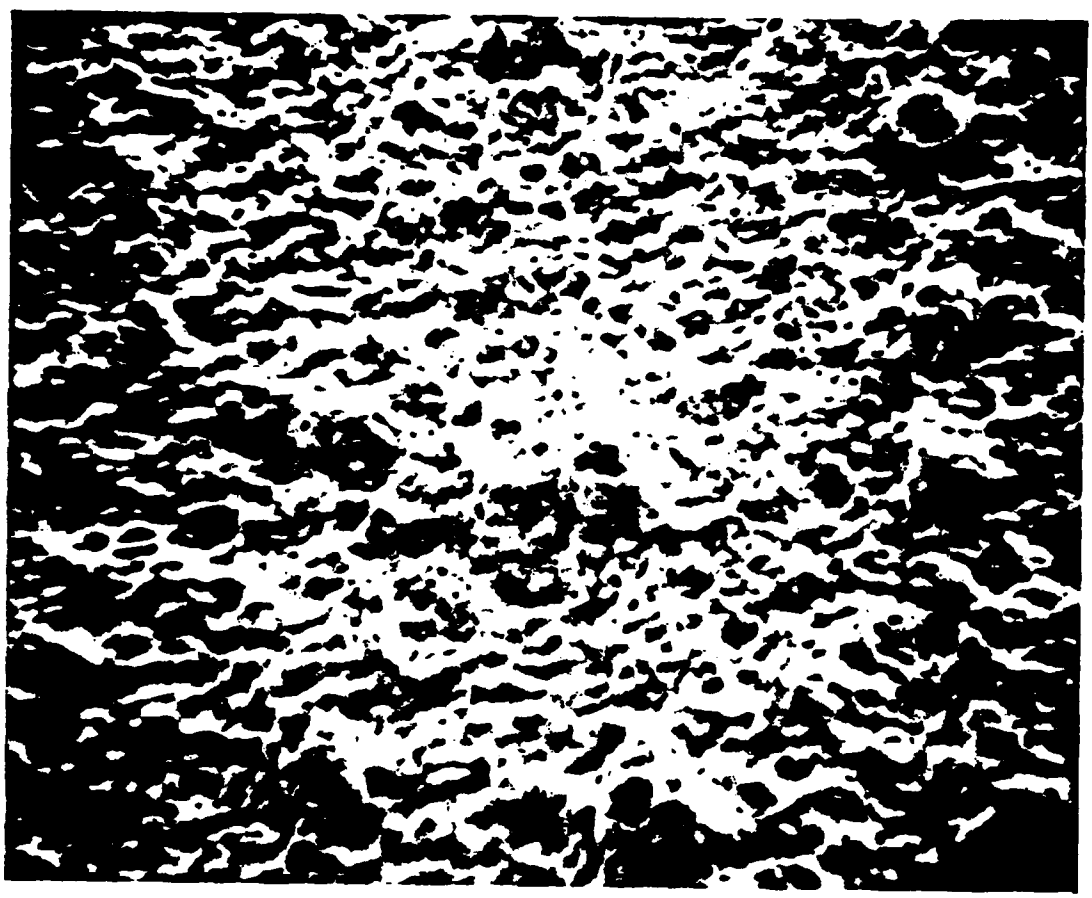

Fig. 10

Fig. 11

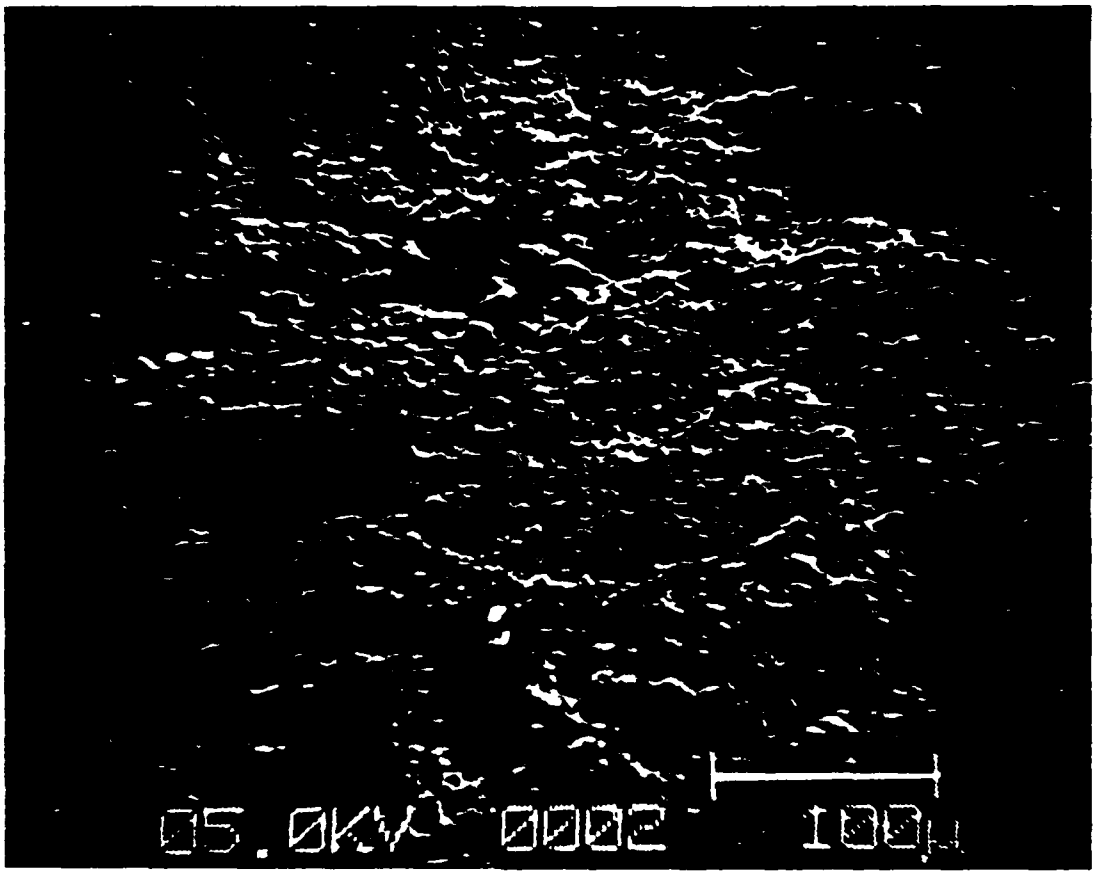

Fig. 12

Fig. 13

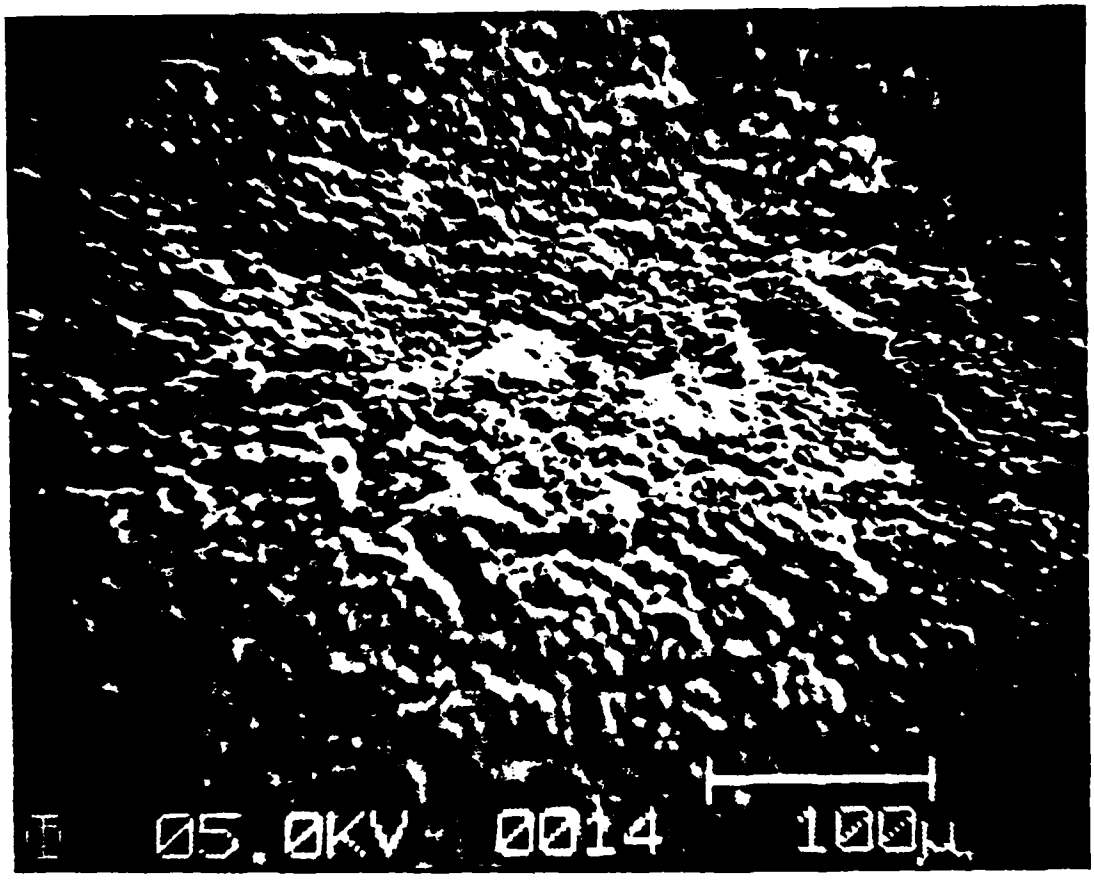

Fig. 14

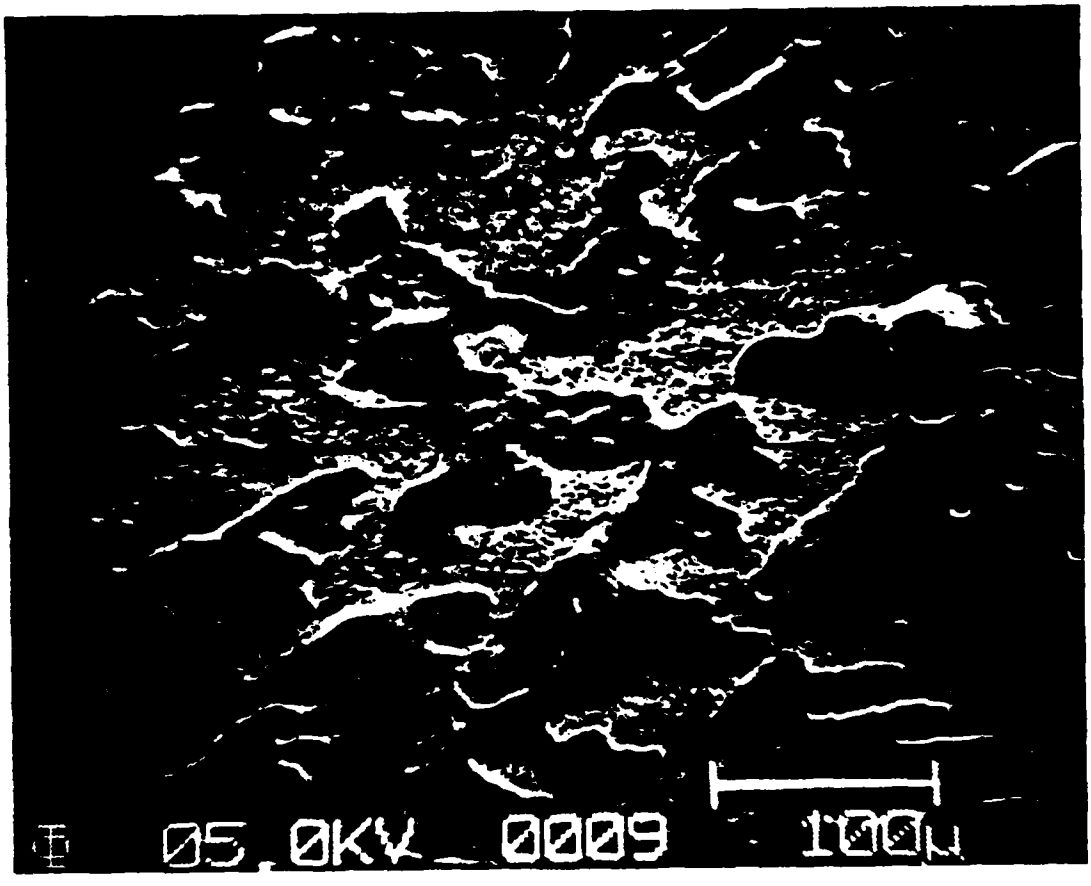

Fig. 15

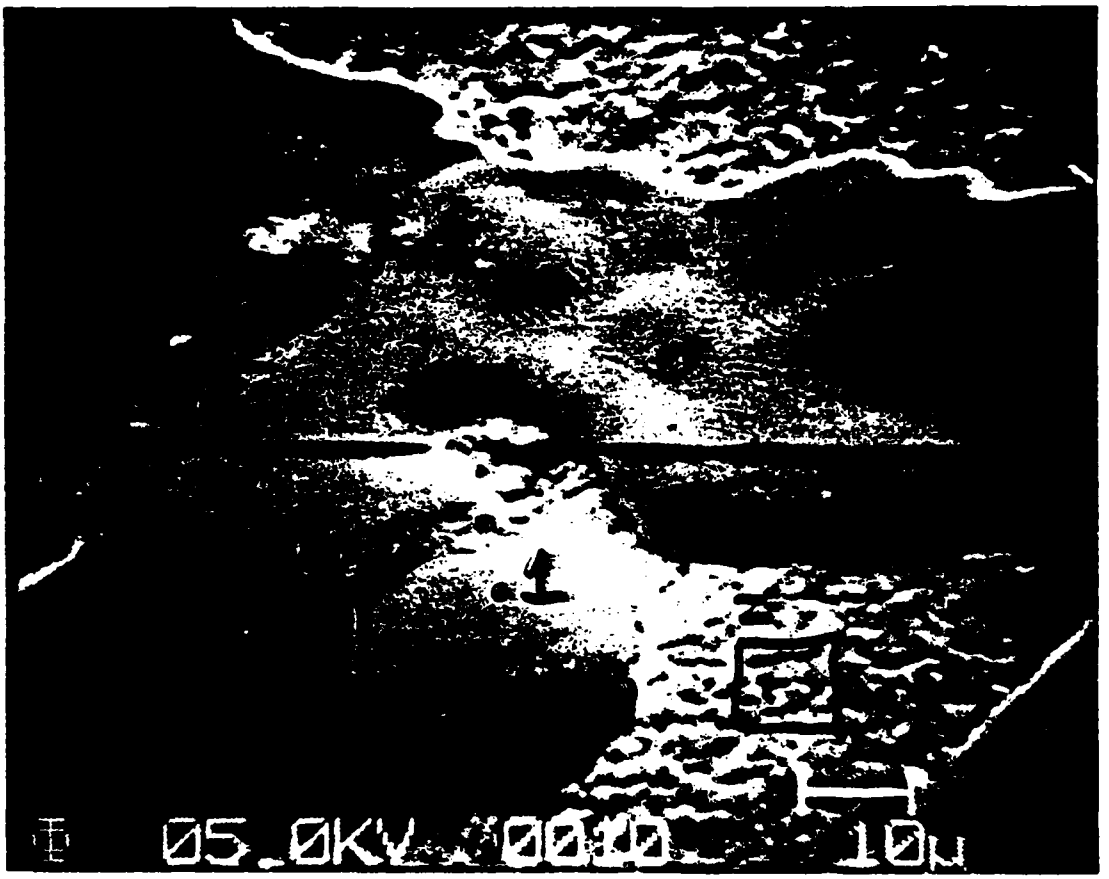

Fig. 16

Fig. 17

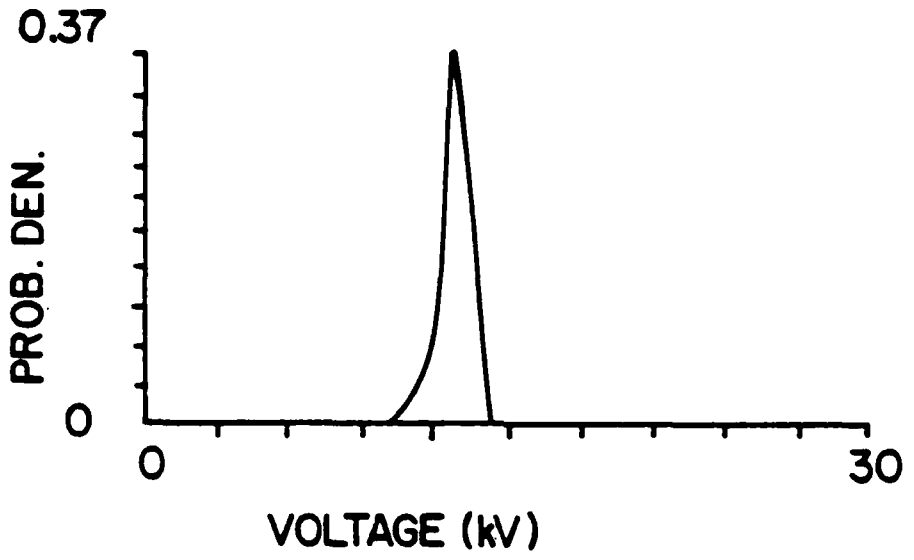

18a.

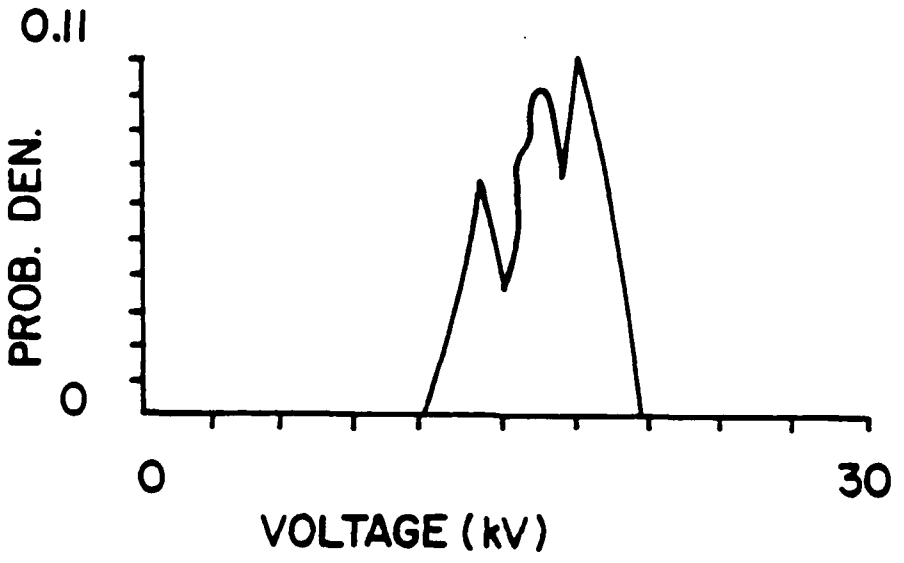

18b.

Fig 18 a. b.

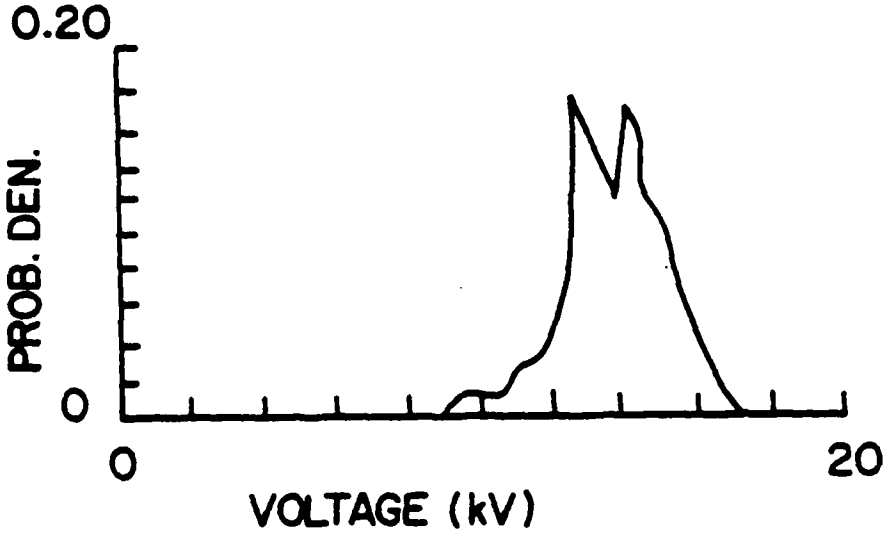

19 a.

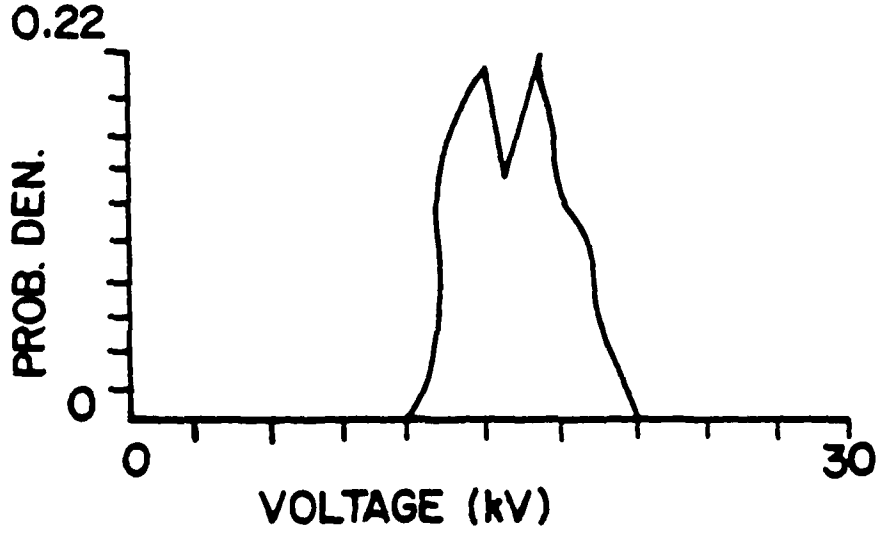

19 b.

Fig. 19 a.
b.

1984 IEEE 16th Power Modulator Sym.

Appendix III

RECOVERY MEASUREMENTS IN A SPARK GAP

C.H. Yeh, H. Krompholz, H. Hagler, and M. Kristiansen
Texas Tech University
Lubbock, Texas 79409 USA

Abstract

The voltage recovery for a high energy spark gap (up to 400 J/shot) has been measured in N_2, SF_6, and in a 20% SF_6/80% N_2 gas mixture by applying two identical pulses with a variable delay time between the pulses. Parameters determining the voltage recovery are charging rate, energy deposited in the spark gap, statistical delay time, and attachment coefficient of the gas. The most important influence on the recovery behavior is the temperature/density variations of the gas during recovery, which have been measured using a Mach-Zehnder interferometer.

Thermal expansion velocities of the gas heated by the initial spark and by subsequent heat transfer from the electrodes are in the range of 10^2 to 10^3 cm/s. The initial gas density 1 ms after breakdown is reduced by 50%. Restrike position and breakdown voltage for the second pulse are determined by these gas density variations and Paschen's law.

Introduction

The recovery behavior of spark gaps characterizes the properties which are relevant for rep-rated operation. The most important quantity characterizing the recovery behavior is the magnitude of the voltage which can be applied to the device after breakdown, without leading to a restrike, as a function of time. The usual method to determine this voltage magnitude is to apply a probing voltage pulse after the breakdown with a variable delay time. With respect to repetitive operation, it is essential that the pulse producing the initial breakdown and the probing pulse are identical in shape and amplitude. The aim of the present experiment was to find the recovery behavior for repetition rates in the kHz range, corresponding to delay times in the millisecond regime. It is expected that recovery in this time domain is mainly determined by thermal equilibrization processes, e.g. cooling of the gas by heat transfer to the electrodes and the surroundings. In order to obtain quantitative information on these processes, the breakdown voltage distribution and the gas density have been measured as a function of the time after the first breakdown.

Experimental Set-Up

The test gap assembly [1] with interchangeable electrodes and the pressure chamber is shown in Fig. 1a. The charging system consists of two overcritically damped C-L-C circuits providing identical current pulses with a duration of 2 μs and variable time delay between pulses (Fig. 1b). A low pressure mercury lamp is used for UV preionization in order to reduce statistical time lags. Breakdown voltage and current have been measured with standard methods. The gas density as a function of position and time has been determined using a Mach-Zehnder interferometer (Fig. 2). The light source was a 2 mW HeNe Laser. Temporal resolution is provided by using a rotating drum framing camera (Dynafax 326) with an exposure time of 4 μs and a time between frames of 0.5 ms. In addition, the breakdown positions have been registered.

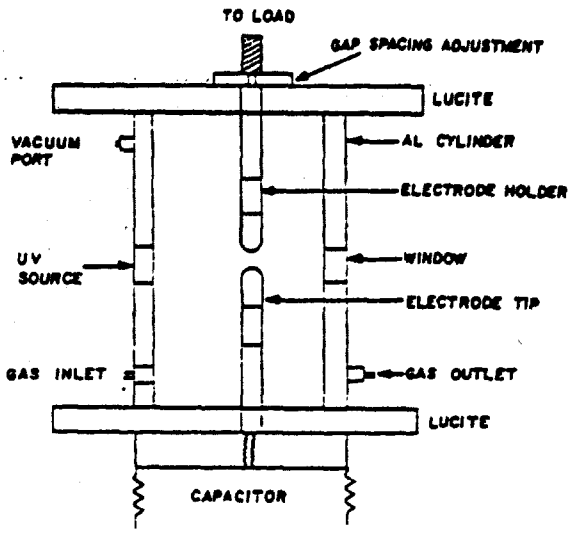

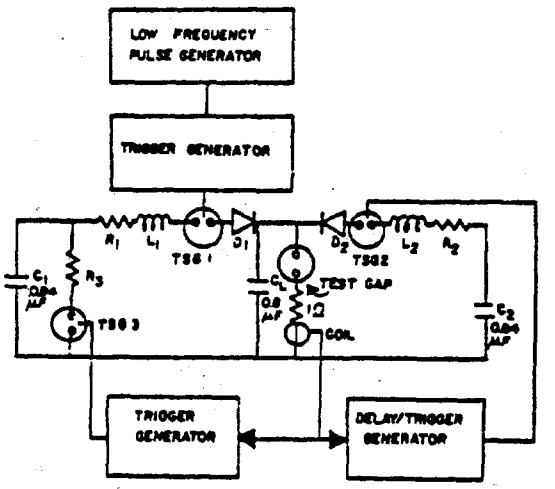

Fig. 1 Experimental set-up
a) spark gap assembly
b) double pulsed circuit

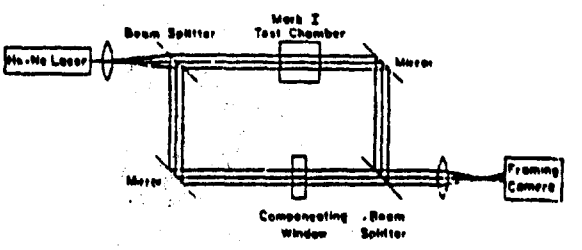

Fig. 2 Mach-Zehnder Interferometer Set-Up

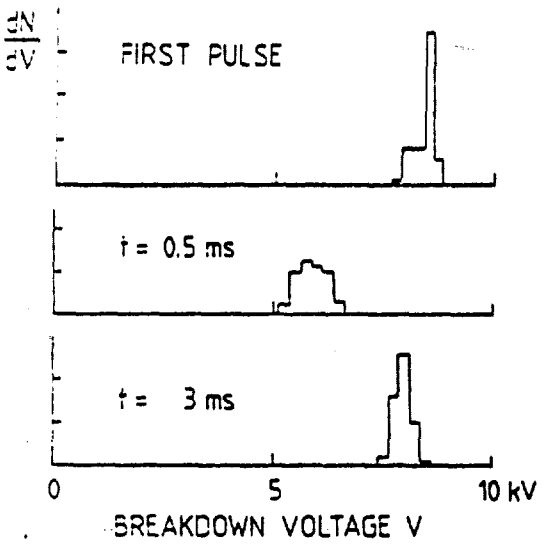

Fig. 3. Histogram for the breakdown voltage (probing pulse) in N_2 (pressure 1 atm, gap distance 1.2 mm)

Results

Figure 3 shows, as an example, the distribution of breakdown voltages for the probing pulse for different delay times in N_2. The broad distribution for short delay times and narrow distributions for longer delay times, approaching the original distribution, are characteristic for all investigated gases and electrode geometries. These breakdown voltage histograms formed the basis for determining the average values discussed in the following.

Average breakdown voltages as a function of time after the first breakdown, normalized to the initial breakdown voltage ("percentage voltage recovery"), are plotted in Fig. 4 for different gases and the data are given in Table 1. The gap distance was 1.2 mm and the gas pressure for all gases 1 atm.

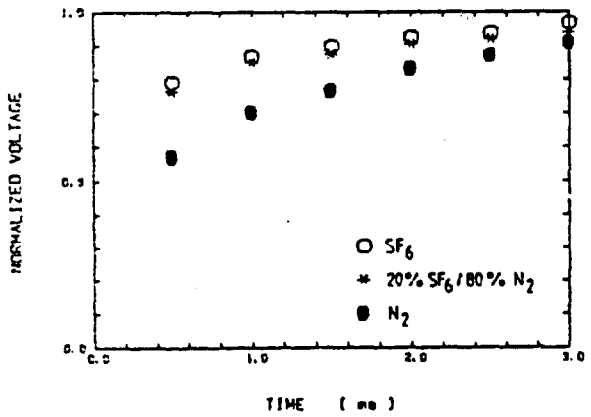

Fig. 4 Breakdown voltages (average values) as a function of delay time in different gases

Table 1

Gas	Voltage (kV)	Energy (J)	Charging Rate (kV/ms)
SF_6	19.4	359.4	503.0
20% SF_6/80% N_2	16.6	263.2	422.0
N_2	8.4	29.6	170.0

Faster recovery for SF_6 as compared to N_2, even for higher energy input is due to the higher charging rate and electron attachment in SF_6. Free electrons produced by UV preionization are attached in SF_6, and the breakdown voltage increases. Further influence on the faster recovery in SF_6 might be due to lower viscosity, which increases the convective heat transfer [2].

Results of interferometric measurements are given in Fig. 5. As indicated by the fringe shifts, a region of reduced gas density is moving with a velocity of 250 cm/s (after the first pulse) and 750 cm/s (after the second pulse) from the electrode center outward.

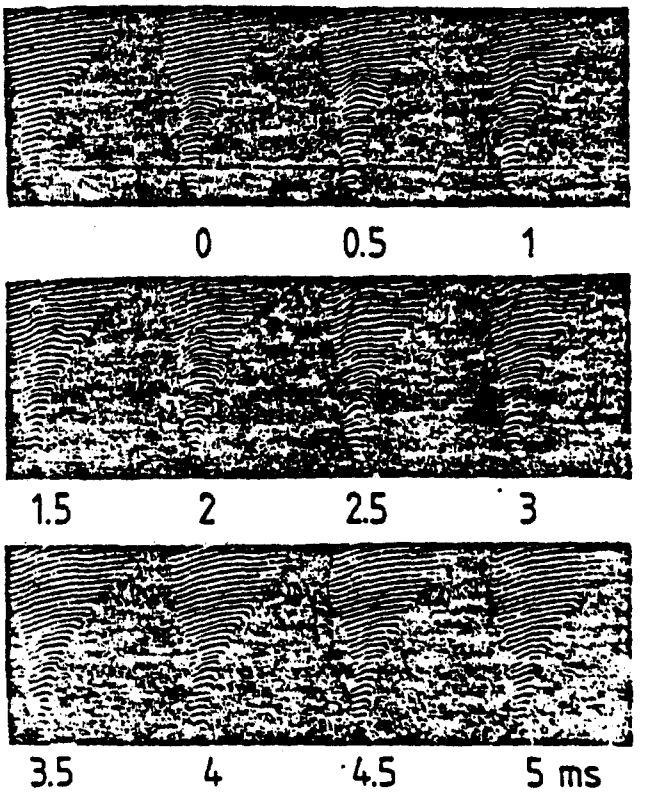

Fig. 5 Interferometer recordings (first pulse applied at t = o, second pulse at t= 2 ms)

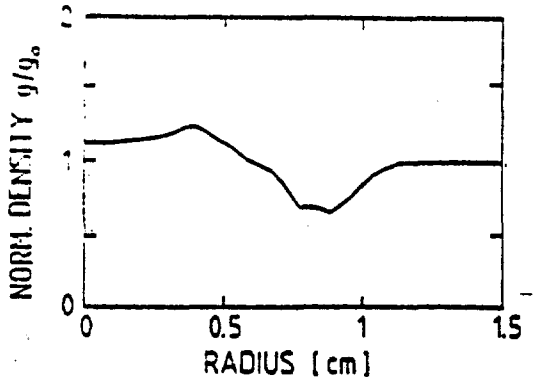

Fig. 6 Gas Density vs Radius for t = 1 ms

Metal vapor, which is assumed to move with similar velocities [3], has a density too low to produce this fringe shift. The gas density inferred from the interferogram by Abel inversion is shown in Fig. 6. The high density region in the center is probably caused by rapid cooling in the vicinity of the electrodes. For this case (hemispherical electrodes) the position of the second breakdown is at the electrode center, as predicted by Paschen's law, i.e. not influenced by the reduced gas density outside the center. In a plane electrode geometry, however, the position of the second breakdown is influenced by this time varying gas density, i.e. the average distance from second to first breakdown increases with time and is in quantitative agreement with Paschen's law applied to the measured gas density variation.

Heat Conduction Model

For a quantitative description of the voltage recovery for the central region of hemispherical electrodes, a one dimensional model [4] based on heat conduction and Paschen's law, was used. This model accounts for the simultaneous axial and radial heat transfer in the arc column, the electrode, the hot gas surrounding the arc and the cold ambient gas. The mutual heat transfer processes between these regions are imaged to a lumped parameter model. For large values of pd (pressure times distance), according to Paschen's law, a linear relationship between breakdown voltage and gas density is assumed.

Figure 7 shows the measured relative recovery voltage (dots) and three calculated model curves. The time constants for heat transfer have been calculated from the actual geometry and the initial arc temperature was assumed to be 12,000 K. The parameter in these model curves is the unknown initial electrode temperature, giving a closest fit to the experimental data for $T_{electrode}$ = 900 K.

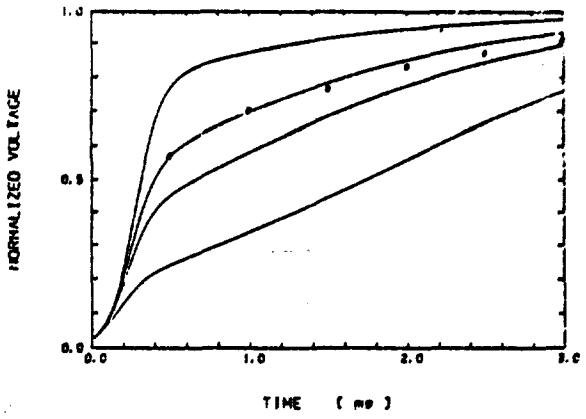

Fig. 7 Model curves and Experimental values (dots) for N_2. The parameter for these curves (from top to bottom) is the initial electrode temperature of 500, 900, 1300 and 3000 K.

Conclusions

Recovery times for the usual experimental situation of atmospheric pressure and voltages of several 10 kV are in the order of milliseconds and determined mainly by heat conduction. Scaling laws for the design of rep-rated spark gap switches can be formulated on this basis, requiring fast heat transfer from the gap region to the outside as the essential design criterion for rep-rated gaps operated in the kHz regime.

References

1. C.H. Yeh, et.al., "Voltage Recovery Measurements in a High Energy Spark Gap", Proc. of the 4th IEEE Pulsed Power Conference, Albuquerque, NM, June 1983, p. 159.

2. V.N. Maller, M.S. Naidu, "Advances in High Voltage Insulation and Arc Interruption", Pergamon Press, New York, NY, 1981, p. 9.

3. Y. Udris, "On the Emission of Cathode Material in Low Pressure Gas Discharges", Proc. Int. Conf. on Gas Discharges, London, England, 1970, p. 108.

4. H. Edels, et.al., "Experiments and Theory on Arc Reignition by Spark Breakdown", Proc. IEE, 112, 2343 (1965).

APPENDIX IV

Electrode Erosion Phenomena in a High-Energy Pulsed Discharge

A. L. DONALDSON, M. O. HAGLER, FELLOW, IEEE, M. KRISTIANSEN, FELLOW, IEEE, G. JACKSON, AND L. HATFIELD

Abstract—The erosion rates for hemispherical electrodes, 2.5 cm in diameter, made of graphite, copper-graphite, brass, two types of copper-tungsten, and three types of stainless steel, have been examined in a spark gap filled with air or nitrogen at one atmosphere. The electrodes were subjected to 50 000 unipolar pulses (25μs, 4-25 kA, 5-30 kV, 0.1-0.6 C/shot) at repetition rates ranging from 0.5 to 5 pulses per second (pps). Severe surface conditioning occurred, resulting in the formation of several spectacular surface patterns (craters up to 0.6 cm in diameter and nipples and dendrites up to 0.2 cm in height). Surface damage was limited to approximately 80 μm in depth and was considerably less in nitrogen gas than in air. Anode erosion rates varied from a slight gain (a negative erosion rate), for several materials in nitrogen, to 5 $\mu cm^3/C$ for graphite in air. Cathode erosion rates of 0.4 $\mu cm^3/C$ for copper-tungsten in nitrogen to 25 $\mu cm^3/C$ for graphite in air were also measured.

Introduction

HIGH-ENERGY spark gaps with lifetimes of 10^8 shots are seen as one of the critical components in pulsed power systems used for particle beam systems, lasers, nuclear isotope separation, electromagnetic pulse simulation, and thermonuclear fusion reactors. The performance of a pressurized spark gap as a high-energy rep-rated switching device is typically characterized by its hold-off voltage, recovery time, delay time, and jitter [1]. The switch lifetime is determined by the electrode erosion, gas decomposition and disassociation, and insulator damage that occur as energy is dissipated in the switch [2].

Manuscript received May 18, 1983; revised December 14, 1983. This work was supported by the Air Force Office of Scientific Research.

A. L. Donaldson, M. O. Hagler, and M. Kristiansen are with the Plasma and Switching Laboratory, Department of Electrical Engineering, Texas Tech University, Lubbock, TX 79409.

G. Jackson is with the BDM Corporation, Huntsville, AL 35803.

L. Hatfield is with the Department of Physics, Texas Tech University, Lubbock, TX 79409.

The purpose of this study was to measure the erosion rate of different electrode materials as a function of current in order to generate a data base from which theoretical models describing the complex erosion processes could be developed and verified. In addition, the electrode and insulator surfaces were examined in an effort to define the electrode erosion characteristics and to reduce the material parameter space used in further studies.

Experimental Apparatus

Spark Gap

The spark gap shown in Fig. 1 was designed to facilitate frequent electrode and insulator replacement and to allow for accurate control over electrode alignment and gap spacing. The electrodes are composed of three parts: the brass support (which also serves as a channel for gas flow), the brass adapter, and the electrode tip. The hemispherically shaped electrode tips are 2.5 cm in diameter and are made from the various materials studied. The Lucite inserts provide protection for the main gap housing and also provide a surface which gives a permanent history of the discharge debris which is deposited on the walls.

Test Circuit and Conditions

Numerous experimentors have measured erosion rates for high-current (10-800 kA) oscillatory discharges [3]-[7]. A few have studied erosion rates in high-current (<10 kA) unipolar discharges using brass and copper electrodes only [8], [9]. A test circuit capable of delivering a unipolar pulse was chosen for this study, both to simplify separate investigations of the erosion processes at the anode and the cathode and to simulate certain applications more closely. The circuit, shown in Fig. 2, consists of a six-section Rayleigh pulse forming net-

0093-3813/84 0300-0028$01.00

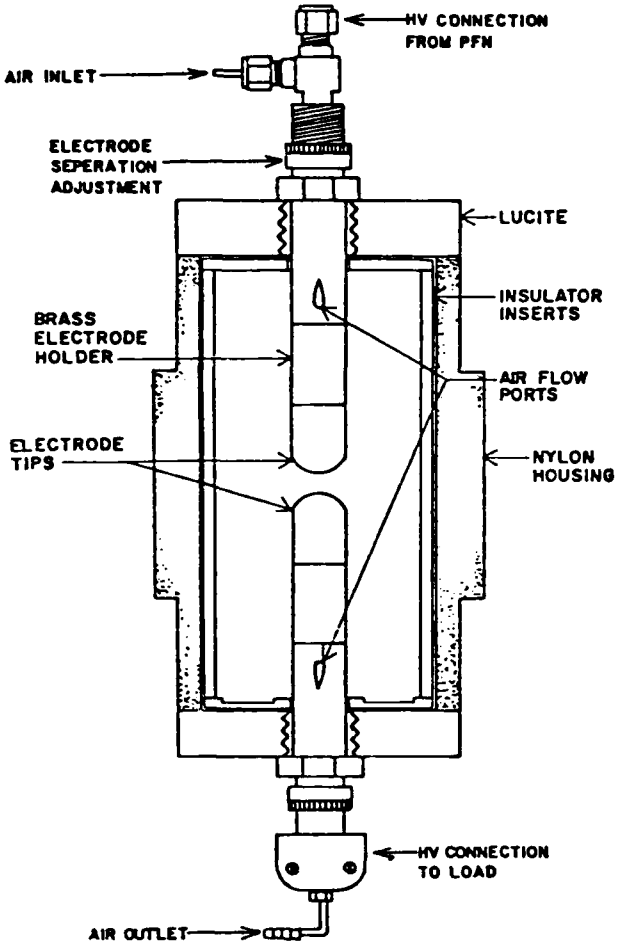

Fig. 1. Spark gap for erosion studies.

work (PFN) which is resistively charged to the self-breakdown voltage of the spark gap by a 30-kV 1-A constant voltage power supply. When the gap breaks down, the PFN is discharged into a matched 0.6-Ω high-power load. Further details of the test circuit and load design are discussed elsewhere [10]. The waveform of the discharge current is shown in Fig. 3. The test conditions are summarized below:

voltage	<30 kV
current	<25 kA
total capacitance	21 μF
charge/shot	<0.6 C
energy/shot	<9 kJ
pulse width	25 μs
rep-rate	0.5-5 pps
gas	air or N_2
pressure	1 atm (absolute)
flow rate	1 gap volume every 5 s
gap spacing	<0.8 cm.

Materials Tested

The electrode materials tested were: brass (SAE 660), stainless steel (304, 20Cb-3, 440-C) [11], copper-tungsten (K-33 [12], 3W3 [13], graphite (ACF-10Q), and copper-graphite

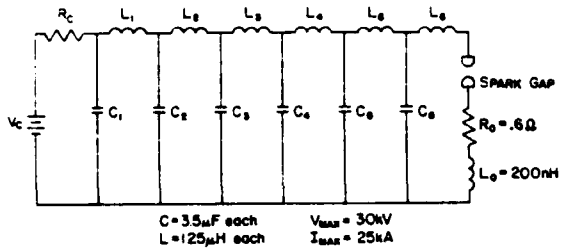

Fig. 2. Test circuit for erosion studies.

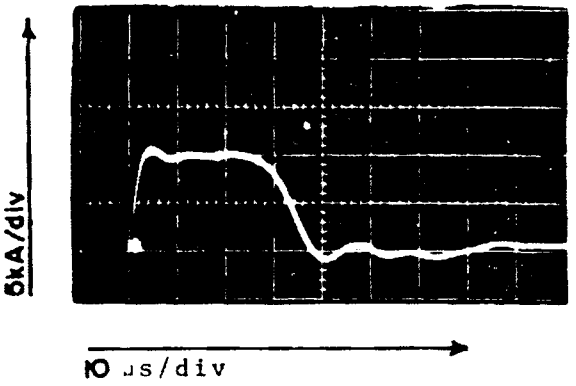

Fig. 3. Current pulse.

(DFP-1C) [14]. This combination of materials allowed for:

1) a comparision with existing data for brass and stainless steel [3], [4], [8], [15],
2) utilization of materials which experimentally have given good spark gap performance [3], [6], [16],
3) the testing of several new materials, namely copper-graphite, and the stainless steels 20Cb-3 (previously used in highly corrosive environments in MHD generators) and 440-C (a high strength stainless steel).

The thermophysical properties of these materials are given in Table I.

Experimental Results

Erosion Characteristics

The change in mass of the spark gap electrodes after 50 000 shots was measured with an analytical balance with a precision of ±5 mg. The individual test conditions and resulting erosion rates are given in Table II. Although many authors report erosion rates in micrograms per coulomb, the actual factor determining lifetime is the volume eroded, hence the units microcubic centimeters per coulomb ($\mu cm^3/C$). The results for brass are discussed later because of the failure of the electrodes due to gross material extraction.

Material: A ranking of the volume erosion rate for each material investigated, from smallest to largest, is:

Cathode: CT-3W3(N_2), CT-K-33(N_2), CT-3W3 (air), CT-K-33(air), SS-304(N2), SS-304(air), SS-440-C(air), SS-20Cb-3(air), CG(air), CG(N_2), G(N_2), G(air);

Anode: CT-3W3(air), CT-K-33(air), SS-440-C(air),CG(N2), SS-304(air), SS-20Cb-3(air), G(air). (The rest of the anodes showed no net erosion.)

TABLE I
ELECTRODE MATERIAL PROPERTIES

Material	Composition	T_{mp} (°C)	d (kg/m^3)	k (W/m °K)	c (kJ/kg °K)	ρ (10^{-8} Ω cm)
Brass	Cu 83%, Pb 7% Sn 7%, Zn 3%	980	8700	120	0.36	6.7
Stainless steel (SS) (304)	Fe 69%, Cr 19% Ni 9%, Mn 2%	1430	8000	16	0.56	72
Stainless steel (SS) (20Cb-3)	Fe 41%, Ni 33% Cr 19%, Cu 3%	1370	8100	13	0.50	108
Stainless steel (SS) (440-C)	Fe 79%, Cr 17% C 1%, Mn 1%	1370	7600	24	0.44	60
Copper-tungsten (CT) (K-33)	W 67%, Cu 33%	Cu 1080 W 3400	14000	270	0.25	3.4
Copper-tungsten (CT) (3W3)	W 68%, Cu 32%	"	"	230	NA	3.4
Graphite (ACF-10Q) (G)	C 100%	4200*	1830	87	0.80	2700
Copper-graphite (CG) (DFP-1C)	C 84%, Cu 16%	Cu 1080	2970	175	0.84	175

T_{mp}: melting temperature, d: density, k: thermal conductivity, c: specific heat ρ; resistivity, *: graphite sublimes.

TABLE II
ELECTRODE EROSION RATES

Electrode	Gas	V	Q	CE	AE
Stainless steel (304)	Air	10.3	0.21	1.8	1.2
Stainless steel "	Air	10.6	0.22	1.5	1.0
Stainless steel " [1]	Air	18.0	0.37	1.6	1.5
Stainless steel (440-C)	Air	12.4	0.26	1.8	0.5
Stainless steel (20Cb-3)	Air	10.0	0.21	2.5	0.9
Stainless steel (304) [2,3]	N_2	7.8	0.16	0.7	+ 0.0
Copper-tungsten (K-33)	Air	9.5	0.20	1.2	0.4
Copper-tungsten "	Air	11.5	0.24	1.2	0.3
Copper-tungsten "	Air	18.0	0.37	1.2	0.5
Copper-tungsten (3W3)	Air	15.8	0.32	0.8	0.2
Copper-tungsten (K-33) [3]	N_2	14.8	0.31	0.4	0.4
Copper-tungsten (3W3)	N_2	16.4	0.34	0.4	+ 0.0
Copper-graphite (DFP-1C)	Air	8.3	0.17	8.5	0.4
Copper-graphite "	Air	16.2	0.34	8.6	+ 0.0
Copper-graphite " [3]	Air	11.4	0.24	7.2	0.0
Copper-graphite " [3]	N_2	14.8	0.31	13.5	0.8
Graphite (ACF-10Q)	Air	9.2	0.19	24.1	3.5
Graphite "	Air	10.6	0.22	24.6	3.6
Graphite "	Air	16.0	0.33	23.5	5.0
Graphite " [3]	N_2	12.9	0.27	15.7	0.0

V: average voltage, kV; Q: charge/shot, coulombs; CE: cathode erosion, μcm^3/C; AE: anode erosion, μcm^3/C; [1] – 32 000 shots, [2] – 22 000 shots, [3] – experiment performed at approximately 85 percent of maximum power, + indicates that an increase in mass was measured.

As expected, the copper-tungsten composites gave the lowest volume erosion rate. Somewhat surprising, however, was the excellent performance of the stainless steels (304 and 440-C) and the poor performances of the graphite materials as cathodes. From the results obtained for stainless steel in a pulsed discharge, it is seen that the high erosion rate reported by Gruber and Suess [3], for an oscillatory discharge, was possibly a result of using a stainless steel which, according to the work reported here, is a poor anode material. Previous studies [6], [15], which indicated that graphite was highly resistant to erosion were done at a much slower repetition rate (0.03 pps) and, therefore, gave a significantly lower erosion rate (<1 μcm^3/C). More recent results by Bickford [16] at 1000 pps gave an erosion rate of 41 μcm^3/C which is reasonably close to the value of 25 μcm^3/C measured in this experiment. A summary of the erosion rates found by other investigators is given in Table III. If one takes into account the lower values of current used in this study, then the results obtained in this experiment are in generally good agreement with the measurements of other investigators.

Polarity: Unlike previous experiments, where oscillatory current conditions masked any polarity effect, a distinct difference in the cathode and anode erosion rate and, most likely, the erosion mechanisms themselves were observed using a unipolar pulse. The ratio of cathode to anode erosion, for those materials which had significant anode erosion, varied from 1.5 in stainless steel (304) to 16 in copper-graphite. Carder [8] reported ratios of 2.5 to 5 for brass under similar conditions. Previous experiments, which gave cathode to anode erosion ratios less than one, were done at much higher pulse repetition rates (10-1000 pps) [15]-[18]. In addition, the results obtained by Petr [18] were done with smaller anode diameters and gap spacings (both <2.5 mm).

In general, anode erosion rates were somewhat scattered, and thus general trends were hard to obtain, given the limited data base. However, some agreement with an anode erosion rate proportional to $Q^{1.5}$ was observed for graphite. A similar dependence has been found experimentally and derived theoretically by numerous other investigators [19]-[21].

Some anodes actually gained mass, which indicated that material was being transferred from the cathode to the anode and/or chemical reactions were forming compounds on the anode. The material transfer was demonstrated experimentally when a stainless steel cathode was found to deposit molten material on a graphite anode. Gray and Pharney [22]

TABLE III
SUMMARY OF COMPARABLE EROSION RESULTS

Investigator	Erosion Rate (μcm^3/coul)	Material	Gas	Current (kA)	Waveform
Affinito [15]	1	Graphite	N_2 (2 atm)	100	Oscillatory (0.03 pps)
Belkin [17]	0.7-1.4	Brass	Helium (1 atm)	40	Oscillatory
Bickford [16]	5	Copper-tungsten	CO (1 atm)	1.5	Unipolar (1000 pps)
	6	Stainless-steel	"	"	"
	41	Graphite	"	"	"
Burden and James [4]	5	Brass	Air (1.25 atm)	400	Oscillatory
Carder [8]	3-5	Brass	N_2 (2 atm)	10-22	Unipolar (1 pps)
Gruber and Suess [3]	2-10	Copper-tungsten	Air (1 atm)	40-170	Oscillatory
	5-40	Brass	"	"	"
	20-40	Stainless-steel	"	"	"
Kawakita [7]	80	Copper-tungsten	SF_6 (4 atm)	100	"

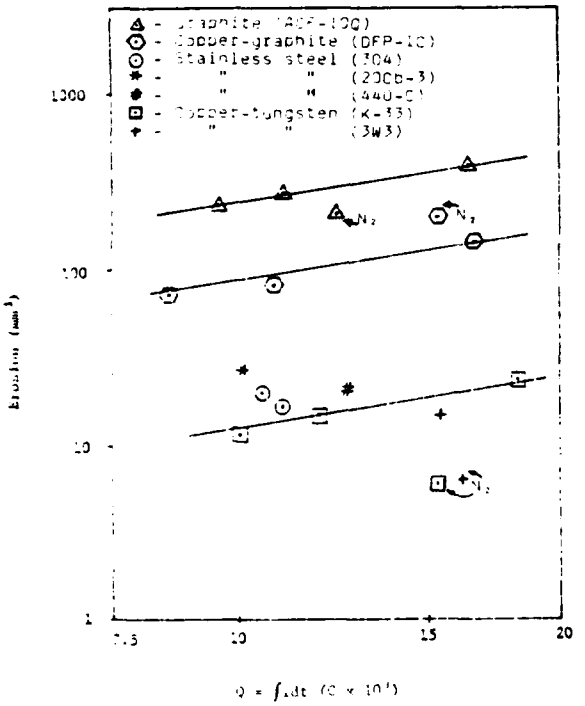

Fig. 4. Total cathode erosion versus total charge transfer for different electrode materials in air.

proposed a reasonable model for this effect at low currents, which is based upon the reduction of the ion bombardment force on the molten cathode material during the fall of the current pulse.

Cathode erosion rates are plotted in Fig. 4 as a function of the total charge transferred in 50 000 shots ($\int i\,dt$)[1]. The actual experimental variable used to change the current was the gap spacing. Thus, from these data, there is no way to isolate the effect of increasing gap spacing and increasing current.

[1]Note that the constant slope shown implies constant erosion rate per Coulomb.

For a given cathode material these results indicate a linear dependence of the erosion rate on the quantity $Q = \int i\,dt$ over the entire range of currents. Since the energy in the arc is equal to $\int V_{arc}\, i\,dt$, this seemed to indicate that the main source of energy producing molten material and subsequent vaporization and droplet ejection is in the cathode fall region of the arc (ion impact heating) and not the localized i^2R losses (Joule heating) in the material. (A similar statement by Belkin [5] touched off a heated debate in the literature [23], [24].) Although both experimental [25] and theoretical results [26] exist which support this conclusion it will be shown that you can obtain erosion rates proportional to any reasonable function of current, even $\int i\,dt$, with Joule heating. Also, it should be mentioned that cathode and anode fall voltages are not known for short-pulse high-current arcs which make it hard to check the erosion dependence on $\int V_{arc}\, i\,dt$.

Current: In order to understand the erosion dependence on current one should consider the following: the high-current arc in both vacuum and pressurized gaps is known [9], [27] to consist of many individual filaments, each of which is attached to the electrode and forms a microscopic crater. Even if the erosion at each crater site is due to Joule heating [21], [28] the total erosion is a function of the filament current and the temporal history of each attachment site. For example, under certain circumstances it has been shown [9], [27] that the current per filament and the attachment lifetime are approximately constant. Thus regardless of the erosion dependence on current at each individual attachment site, the total erosion would be a function of $\int i\,dt$ since the total number of sites would be a linear function of current. This also explains why no clear dependence of erosion on the thermophysical properties [T_{mp}, d, k, c, ρ] has been consistently measured in experiments. Thus to understand the erosion process correctly, one not only has to model the erosion mechanism occurring at each filament attachment site correctly, which will certainly depend on T_{mp}, d, k, c, and ρ [21], but also a model must exist which specifies the filament current and the temporal history of its attachment site. Excellent models exist for filament motion in low-current low-pressure

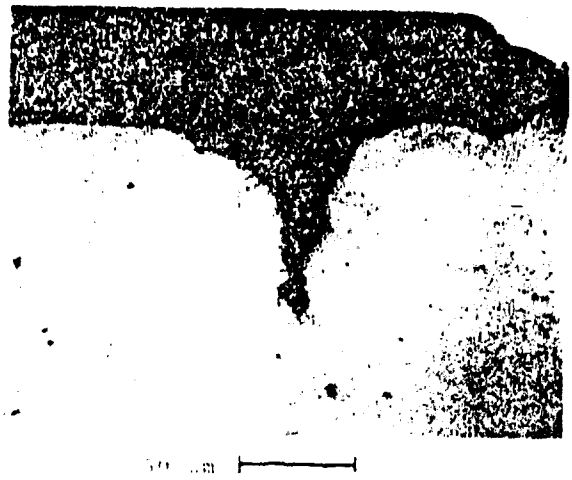

Fig. 5. Cross section of stainless steel (304) cathode in air.

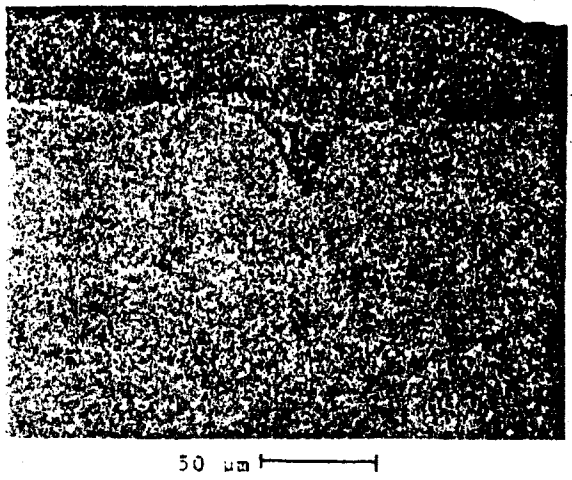

Fig. 6. Cross section of stainless steel (304) cathode in nitrogen.

arcs [28], and high-current arcs in vacuum [27], but it is not anticipated that any one model will suffice for the wide range of conditions encountered in high-energy switches.

Gas: The erosion rate for copper-graphite was slightly higher in nitrogen than in air, whereas the rates for most of the other materials were smaller in nitrogen by a factor of 2-3. In addition, the cross sections of the electrodes, shown in Figs. 5 and 6, show a significant reduction in the depth and amount of damage when the gas is nitrogen rather than air. The gas may affect the erosion in one or more of the following ways:

1) by forming chemical compounds on the electrode surface which alter:
   a) the thermal stability [29],
   b) the current density at individual attachment sites in the arc [30],
   c) the lifetime of each attachment [30];
2) by producing accelerated chemical reactions at the electrode surface [31], particularly at impurity sites or at the magnesium sulfide stringer locations in stainless steel [32]; and
3) by altering the cathode and anode fall voltages, particularly at higher pressures.

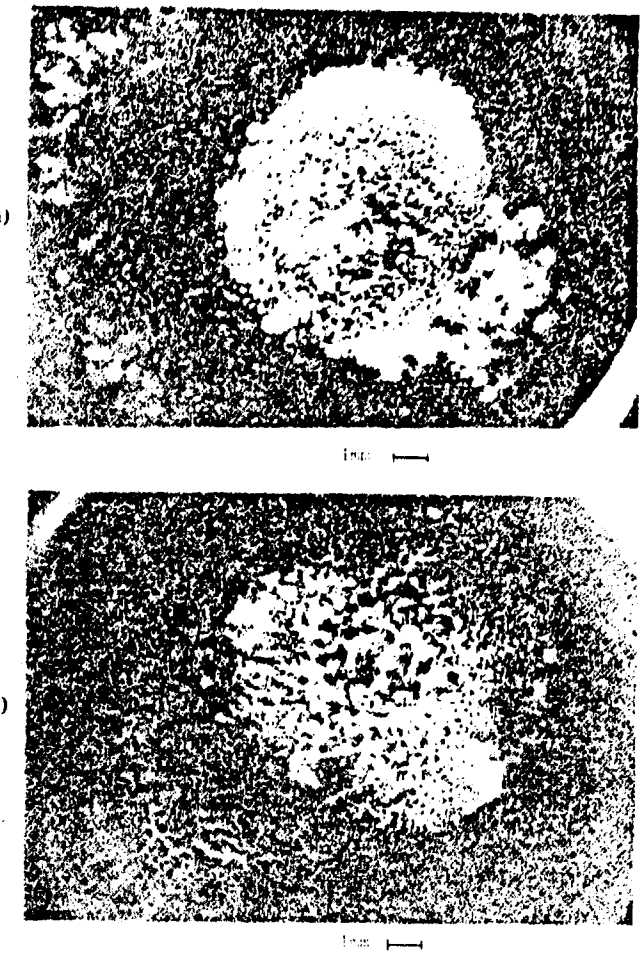

Fig. 7. Surface of brass electrodes in air; (a) anode, (b) cathode.

Surface Conditions

The surface of the electrode tips and the insulator inserts were examined after 50 000 shots. The analysis techniques utilized were Auger electron spectroscopy (AES), scanning electron microscopy (SEM), and optical microscopy.

Brass: The surfaces of the brass electrodes are shown in Figs. 7 and 8. Large-scale melting is evident, with dendrites or metallic protrusions up to 0.2 cm long existing on the surface. The self-breakdown voltage for these electrodes dropped from 20 to 3 kV in approximately 2000 shots as a result of macroscopic field enhancements. In addition, the voltage self-breakdown distribution was characterized by a series of "jumps" thought to be due to large particles being "blown" off the ends of the protrusions. Originally it was thought that the material being "pulled out" of the bulk electrode was lead, but the results of the AES analysis shown in Fig. 9 indicate the surface consists primarily of carbon, copper, and oxygen, with a notable absence of zinc and lead. From these results and those found by Marchesi and Maschio [6], it is obvious that brass has only limited use in repetitive operation at higher levels of charge transfer.

Although the mechanism for the material extraction is not completely understood, Belkin [33] showed that the electromagnetic $\vec{J} \times \vec{B}$ force resulting from the discharge can play an important role at large currents. In addition, Fitch and Mc-

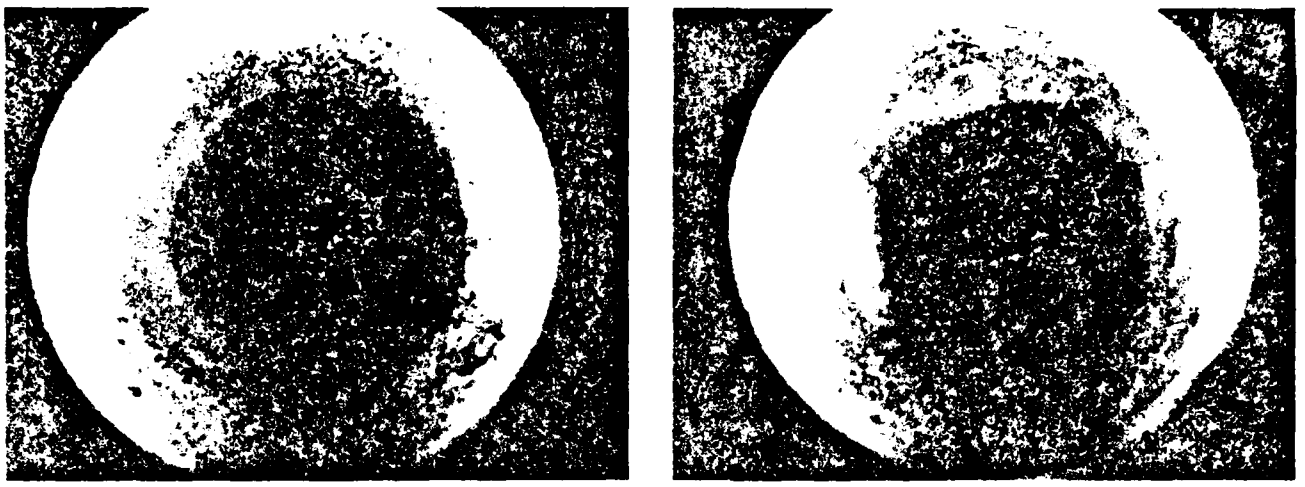

(a) (b)

Fig. 8. Surface of brass electrodes in nitrogen: (a) anode, (b) cathode.

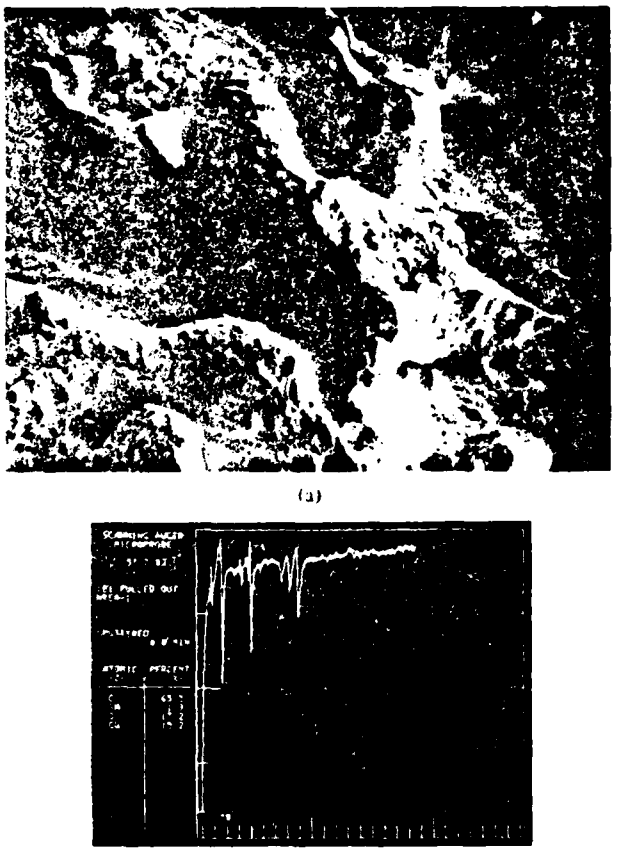

(a)

(b)

Fig. 9. Auger electron spectroscopy surface analysis of brass electrodes: (a) cathode, (b) Auger spectrum.

(a) (b)

Fig. 10. (a) Graphite and (b) copper-graphite cathode surfaces in air.

Cormick [34] observed gross material extraction from stainless steel electrodes as a result of asymmetrical current connections.

Cathode: The cathodes for most of the remaining materials are shown in Figs. 10–12. Considerable erosion has taken place, especially on the graphite materials. The stainless steel and copper-tungsten cathodes show evidence of severe melting. Although it is not easy to see in the photographs, all cathodes showed a distinct tendency to form a large-scale crater whose diameter increases with increasing gap spacing and cur-

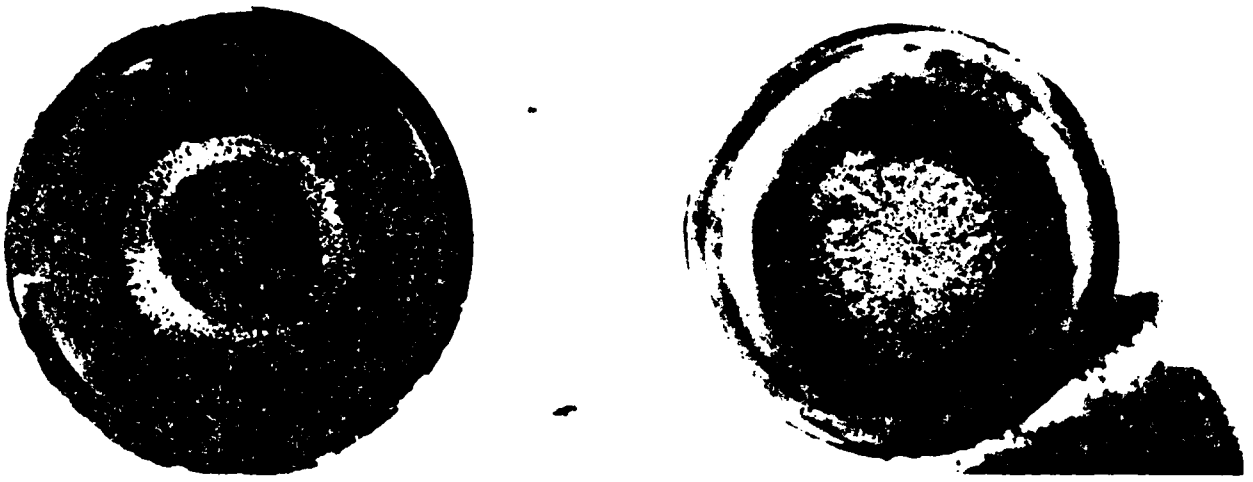

(a) (b)

Fig. 11. (a) Stainless steel (304) and (b) copper-tungsten (K-33) cathode surfaces in air.

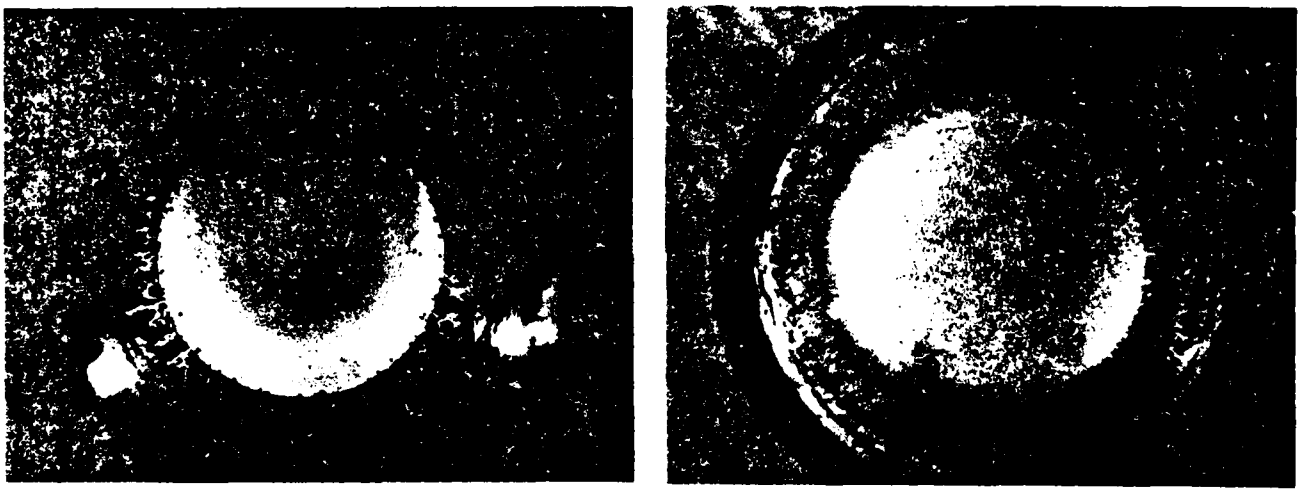

(a) (b)

Fig. 12. (a) Stainless steel (304) and (b) copper-tungsten (K-33) cathode surfaces in nitrogen.

rent. Similar macroscopic cratering was observed by Watson [35] who explained the results with the use of a hydromagnetic flow model. The idea of using a cathode cup in spark gaps is not new [36], [37], but it is interesting that the electrode erosion produces this shape. The location of the current attachment at the cathode should depend on the minimum electrical path length seen by the electron avalanche prior to breakdown. Thus the erosion pattern and the corresponding erosion rate may be highly geometry dependent.

Anode: The anodes, corresponding to the cathodes shown in Figs. 10-12, are shown in Figs. 13-15. The graphite and copper-graphite anode erosion occurs primarily in a band, 0.8 cm wide, with the inner radius located 0.3 cm from the center of the electrode. This pattern is consistent with the results of Johnson and Pfender [38] which showed that an annular-shaped attachment region of high current density can exist at the anode. The copper-tungsten and stainless steel anodes indicate that melting and vaporization have taken place over the entire surface. Like the pattern at the cathode, the diameter of the anode erosion region increases with increasing current.

Insulator: A typical insulator insert, for eight of the possible combinations of electrode material and gas, is shown in Figs. 16 and 17. The insulator surfaces are covered by a coating of recondensed electrode material. The one notable exception was graphite electrodes in air, in which case no coating was found on the insulator surface. A dramatic difference is seen in Fig. 16, in the case of a graphite electrode run in nitrogen. The entire insulator surface is covered with a thick coating of fluffy black material which is thought to consist of monoatomic layers of amorphous carbon [31].

All insulators were covered with solid particles, 10-100 μm in size, distributed within a 5-cm band centered on a plane passing through the center of the gap and parallel to the electrode surfaces. This indicates that a considerable portion of the solid or molten material is ejected parallel to the electrode

(a) (b)

Fig. 13. (a) Graphite and (b) copper-graphite anode surfaces in air.

(a) (b)

Fig. 14. (a) Stainless steel (304) and (b) copper-tungsten (K-33) anode surfaces in air.

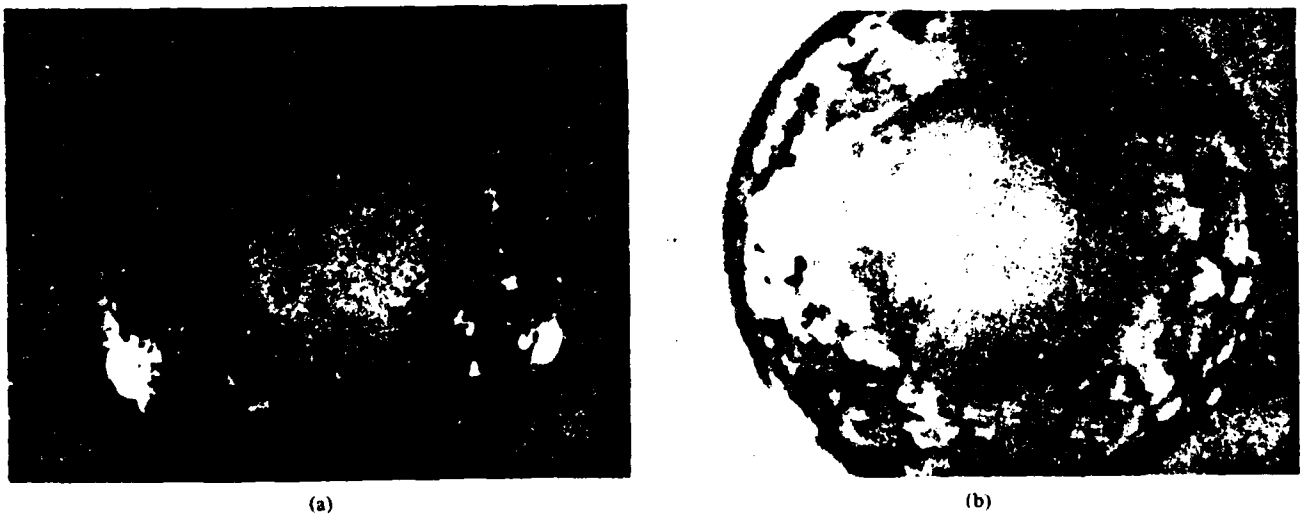

(a) (b)

Fig. 15. (a) Stainless steel (304) and (b) copper-tungsten (K-33) anode surfaces in nitrogen.

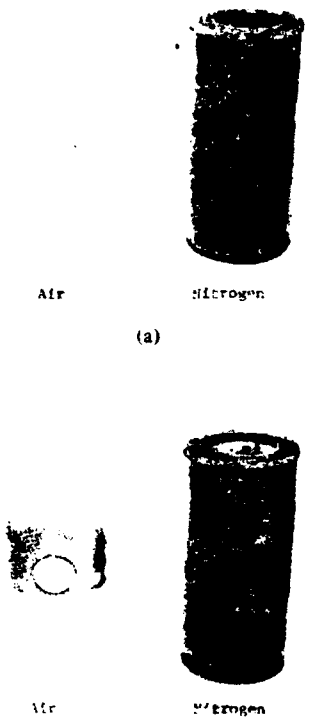

Fig. 16. Insulator inserts exposed to (a) graphite and (b) copper–graphite electrodes in air and nitrogen.

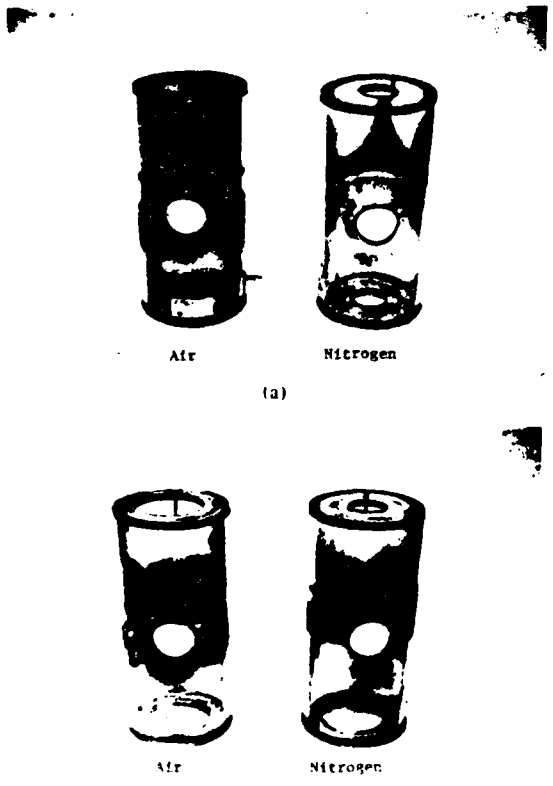

Fig. 17. Insulator inserts exposed to (a) stainless steel (304) and (b) copper–tungsten (K-33) electrodes in air and nitrogen.

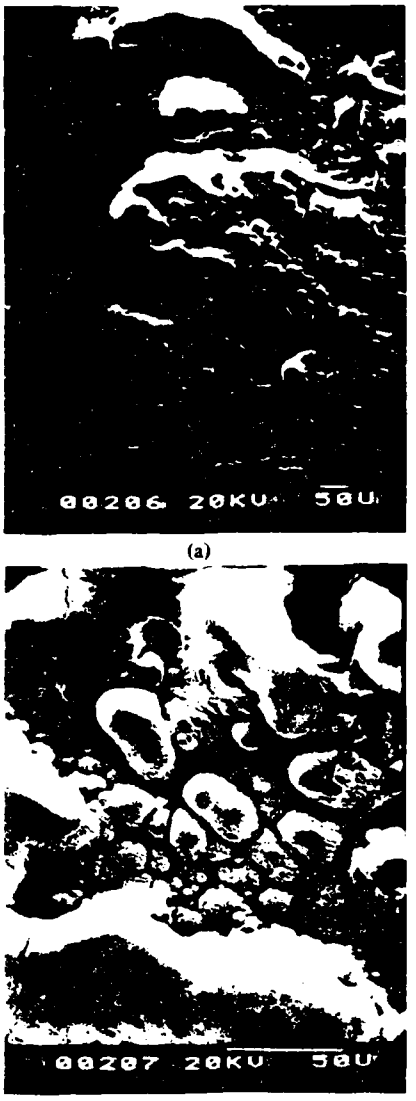

Fig. 18. Scanning electron microscope picture of stainless steel (304) electrode surface; (a) outer edge, (b) outer edge enlarged.

surfaces. Daalder [39] has reported similar results for vacuum arcs and McClure [40] has developed a model which shows that the ion recoil pressure of a vacuum arc plasma is sufficient to remove molten material from a cathode spot crater with velocities of 2×10^3 to 2×10^4 cm/s parallel to the electrode surface. The values of velocity from McClure's model are in good agreement with the experimental findings of Udris [41].

Recent studies in vacuum arcs by Farrall [42] and Shalev [43], which have characterized the size and flux of the ejected particles as a function of current, indicate that the maximum number of particles are released at, or just following, the current maximum. Since the arc attachment region will reach its maximum diameter at the current maximum, then one would expect droplets of material to separate from the electrode at the crest or edge of the macroscopic crater. An SEM examination of the surface of the stainless steel (304) electrodes shows considerable agreement between the size and shape of the electrode surface features existing at the edge of the macroscopic crater, which is shown in Fig. 18, and a 50-μm stainless steel

Fig. 19. 50-μm stainless steel (304) particle on Lucite insulator.

(304) particle found on the insulator and shown in Fig. 19. A thorough characterization of the particles found on the insulators used in this experiment is given by Jackson *et al.* [44]. The presence of similar particles has been shown to have serious effects on the flashover potential of the insulator at high pressures for particles bigger than 35 μm and densities of 20 particles/mm [45]. Thus the electrode erosion mechanism affects the switch lifetime, not only as a result of the erosion itself, but also by coating the insulating materials with conductive particles.

Conclusions

The erosion rate and surface damage of the electrodes was determined for several materials utilized in a high-energy spark gap. The results from these preliminary studies have led to the following conclusions.

1) The electrode erosion rates and mechanisms are highly polarity dependent and thus results for oscillatory and unipolar discharges can be considerably different.

2) A large amount of the erosion is in the form of solid and molten material removed parallel to the electrode surface and, apparently, from the edge of the macroscopic craters found on the cathode.

3) Cathode erosion rates are proportional to the total amount of charge transferred for a fixed repetition rate and pulse width.

4) Stainless steel (304) may be an economical replacement for copper-tungsten composites as a cathode material for the conditions studied.

5) Anode erosion rates were quite scattered, but, in general, were considerably less than the cathode erosion rates for all materials tested except stainless steel.

6) No distinct correlation was found between the thermophysical properties of the electrode materials and the amount of erosion.

In order to develop a more precise understanding of the effects of electrode erosion on switch performance, the following objectives are being considered for future work.

1) Measure the erosion rate as a function of pressure (10^{-2} to 4 atm), rep-rate (1–1000 pps), and gas flow rate for a few of the more promising electrode-gas-insulator combinations.

2) Study the attachment of the arc to the electrode surface for a single shot as a function of pulse shape and peak current.

3) Compare the relative erosion rates for oscillatory and unipolar pulses which have different peak currents but transfer the same net charge.

4) Measure the voltage drop in the arc for pulsed currents in order to calculate the energy dissipated in the gap region.

5) Measure energy delivered to electrodes as a function of pulse shape, previously done by Carder [8], and compare these results with those computed from the arc voltage measurements in 4).

Acknowledgment

The authors wish to express their sincere appreciation to the following people for their various contributions to this work and its preparation: A. Bowling, M. Byrd, J. Clare, B. Conover, J. Davis, B. Maas, C. Mueller, R. Ness, S. Prien, K. Rathbun, A. Shaukat, and A. Williams.

References

[1] T. R. Burkes *et al.*, "A critical analysis and assessment of high power switches," NSWC Dahlgren Lab., Rep. NP 30/78, pp. 189–202, 1978.
[2] L. B. Gordon *et al.*, "Material studies in a high energy spark gap," *IEEE Trans. Plasma Sci.*, vol. PS-10, pp. 286–293, 1982.
[3] J. E. Gruber and R. Suess, "Investigation of the erosion phenomenon in high current, high pressure gas discharges," Max Planck Inst. fur Plasmaphysik, Garching bei Munchen, IPP 4/72, Dec. 1969.
[4] R. A. Burden and T. E. James, "Statistical performance data for a high current 60 kV spark gap switch," in *Proc. 7th Symp. Fusion Technology* (Grenoble, France), Oct. 1972, pp. 24–27.
[5] G. S. Belkin, and V. Ya. Kiselev, "Electrode erosion in pulsed high-current discharges," *Sov. Phys. Tech. Phys.*, vol. 11, pp. 280–283, 1966.
[6] G. Marchesi and A. Maschio, "Influence of electrode materials on arc voltage waveforms in pressurized field distortion spark gaps," in *Proc. 5th Int. Conf. on Gas Discharges*, Sept. 1978, pp. 145–148.
[7] Y. Kawakita *et al.*, "A 150-kV, 100-kA spark gap switch for Marx generators," in *Proc. 3rd IEEE Int. Pulsed Power Conf.*, (Albuquerque, NM), June 1981, pp. 444–447.
[8] B. Carder, "Gas spark gap electrode heating and erosion," Physics Int. Rep., PIIR, pp. 12–74, Dec. 1974.
[9] R. Basharov *et al.*, "Erosion of cathode material in a pulsed discharge between parallel electrodes," *Sov. Phys. Tech. Phys.*, vol. 12, pp. 1383–1390, 1966.
[10] A. L. Donaldson, "Electrode erosion measurements in a high energy spark gap," M.S. thesis, Texas Tech University, Lubbock, TX, Aug. 1982.
[11] Carpenter Technology Corp. Reading, PA.
[12] Schwarzkopf Development Corp., Holliston, MA.
[13] Contacts Metals Welding, Indianapolis, IN.
[14] Poco Graphite, Decatur, TX.
[15] D. Affinito *et al.*, "Design and structure of an extended life high current spark gap," *IEEE Trans. Plasma Sci.* vol. PS-7, pp. 162–163, 1979.
[16] K. J. Bickford *et al.*, "Spark erosion characteristics of graphite and CO gas," in *Proc. IEEE Conf. 15th Power Modulator Symp.* (Baltimore, MD), June 1982, pp. 89–92.
[17] G. S. Belkin, "Vaporization of metal electrodes by pulsed currents," *Sov. Phys. Tech. Phys.*, vol. 13, pp. 1256–1260, 1969.
[18] R. A. Petr, "Erosion phenomena of arching electrodes," M.S. thesis, Texas Tech University, May 1980.
[19] H. W. Turner and C. Turner, "Choosing contact materials," *Electron. Power*, vol. 14, pp. 437–439, 1968.

[20] L. M. Williams and R. F. Smith, "Phenomena accompanying transient low-voltage discharges in liquid dielectrics," *IAEE Trans.*, part I, vol. 74, pp. 164–169, 1955.

[21] V. I. Il'in and S. V. Lebedev, "Destruction of electrodes by electric discharges of high current density," *Sov. Phys. Tech. Phys.*, vol. 7, pp. 717–721, 1963.

[22] E. W. Gray and J. R. Pharney, "Electrode erosion by particle ejection in low-current arcs," *J. Appl. Phys.*, vol. 45, pp. 667–671, 1974.

[23] K. K. Namitokov, "Electrode erosion in high-current pulsed discharges," *Sov. Phys. Tech. Phys.*, vol. 12, pp. 714–716, 1967.

[24] G. S. Belkin and V. Ya. Kiselev, "Features of electrode erosion due to high current pulses," *Sov. Phys. Tech. Phys.*, vol. 12, pp. 719–720, 1967.

[25] S. Levy, "Spark-gap erosion studies," USAELRDL Rep. No. 2454, U.S. Army Electronics Research and Development Labs, Fort Monmouth, NJ, Apr. 1964.

[26] B. Juttner, "Cathode heating by vacuum arcs. A survey," *Beitrage aus der Plasma Physik*, Band 22-Heft 5, pp. 453–462, 1982.

[27] J. C. Sherman, *et al.*, "The spontaneous formation of cathode spots in high-current triggered vacuum switches and an estimate of the cathode spot current density on copper," in *Proc. 4th Int. Conf. on Gas Discharges* (Swansea, U.K.), 1976, pp. 94–97.

[28] A. E. Guile, "Joule heating in emitting sites on various nonrefractory arc cathodes," *Proc. Inst. Elec. Eng.*, vol. 127, pp. 452–457, 1980.

[29] E. I. Zolotarev, *et al.*, "Breakdown-voltage stability of gas-filled switches for voltage pulse generator," *Sov. Phys. Tech. Phys.*, vol. 21, pp. 340–344, 1976.

[30] A. E. Guile and A. H. Hitchcock, "Arc-cathode craters on copper at high currents and with reduced gas pressures," *Proc. Inst. Elec. Eng.*, vol. 125, pp. 251–256, 1978.

[31] L. B. Gordon, "Material studies in a high energy spark gap," Ph.D. dissertation, Texas Tech University, Lubbock, TX, May 1983.

[32] "Carpenter 20Cb-3 stainless steel," Carpenter Technology Corp., Reading, PA, 1980, p. 9.

[33] G. S. Belkin and V. Ya. Kiselev, "Effect of the medium on the electrical erosion electrodes at high current," *Sov. Phys. Tech. Phys.*, vol. 23, pp. 24–27, 1978.

[34] R. A. Fitch and N. R. McCormick, "Low-inductance switching using parallel spark gaps," *Proc. Inst. Elec. Eng.* vol. 106A, pp. 117–130, 1959.

[35] A. Watson, "Fast rising heavy current spark damage to electrodes," in *Proc. 2nd IEEE Int. Power Pulsed Conf.* (Lubbock, TX), June 1979, pp. 471–474.

[36] L. S. Goucher *et al.*, "Spark gap switches for radar," *Bell. Sys. Tech. J.*, vol. 25, pp. 563–602, 1946.

[37] A. E. Bishop and G. D. Edwards, "Low-inductance 100 kV switch (spark gap) for starting, diverting, and clamping capacitor discharges," *Proc. Inst. Elec. Eng.*, vol. 113, pp. 1549–1556, 1966.

[38] D. Johnson and E. Pfender, "Modeling and measurement of the initial anode heat fluxes in pulsed high-current arcs," *IEEE Trans. Plasma Sci.*, vol. PS-7, pp. 44–48, 1979.

[39] J. F. Daalder, "Cathode spots and vacuum arcs," *Physica*, vol. 104c, pp. 91–106, 1981.

[40] G. W. McClure, "Plasma expansion as a cause of metal displacement in vacuum-arc cathode spots," *J. Appl. Phys.* vol. 45, pp. 2078–2084, 1974.

[41] Y. Udris, "On the emission of cathode material particles in low pressure arc discharges," in *Proc. Int. Conf. on Gas Discharges* (London, England), 1970, pp. 108–112.

[42] G. A. Farrall *et al.*, "The time-resolved characterization of erosion products from high-current, copper vacuum arcs," *IEEE Trans. Plasma Sci.*, vol. PS-11, pp. 132–138, 1983.

[43] S. Shalev *et al.*, "In situ determination of macroparticle velocities in a copper vacuum arc," *IEEE Trans. Plasma Sci.*, vol. PS-11, pp. 146–151, Sept. 1983.

[44] G. Jackson *et al.*, "Surface studies of dielectric materials used in spark gaps," *J. Appl. Phys.*, vol. 55, pp. 262–268, 1984.

[45] B. F. Hampton and S. P. Fleming, "Impulse flashover of particle contaminated spacers in compressed sulfur hexafluoride," *Proc. Inst. Elec. Eng.*, vol. 120, pp. 514–522, 1973.

Journal Papers and Conference Proceedings Papers

Published with AFOSR Support

(*Marks publication supported by this grant)

* A.L. Donaldson, M.O. Hagler, M. Kristiansen, G. Jackson, and L. Hatfield, IEEE Trans. on PLasma Science, PS-12, 28 (1984).

* A.L. Donaldson, M.O. Hagler, M. Kristiansen, L.L. Hatfield, and R.M. Ness, "Modeling of Self-Breakdown Voltage Statistic in High Energy Spark Gaps", accepted for publication in J. Appl. Phys.

* G.L. Jackson, L.L. Hatfield, G.R. Leiker, A. Donaldson, M.O. Hagler, M. Kristiansen, R.M. Ness, J. Marx, and P. Predecki, "Surface Analysis of Gas Filled Spark Gap Electrodes" to be submitted to J. Appl. Phys.

* C.H. Yeh, H. Krompholz, H. Hagler, and M. Kristiansen, "Recovery Measurements in a Spark Gap", Proc. 16th Power Modulator Symp. Arlington, VA, 1984 IEEE, p. 64.

* C.H. Yeh, H. Krompholz, M. Hagler, M. Kristiansen, "Recovery Studies for a High Energy Spark Gap", to be published.

H. Krompholz, J. Doggett, K.H. Schoenbach, J. Gahl, C. Harjes, G. Schaefer, and M. Kristiansen, "Nanosecond Current Probe for High Voltage Experiments", Rev. Sci. Instr., 55, 127 (1984).

G. Schaefer, K.H. Schoenbach, H. Krompholz, M. Kristiansen, and A.H. Guenther, "The Use of Attachers in Electron beam Sustained Discharge Switches - Theoretical Consideration," Laser and Particle Beams, 2, 273 (1984).

K.H. Schoenbach, M. Kristiansen, and G. Schaefer, "A Review of Opening Switch Technology for Inductive Energy Storage", Proc. IEEE, 72, 1019, (1984).

G. Schaefer, P. Husoy, K.H. Schoenbach, H. Krompholz, "Pulsed Hollow-Cathode Discharge with Nanosecond Risetime", IEEE Trans. Plasma Sci., accepted for publication in 1984.

C.H. Harjes, K.H. Schoenbach, G. Schaefer, M. Kristiansen, H. Krompholz, and D. Skaggs, "An Electron Beam Tetrode for Multiple, Submicrosecond Pulse Operation", Rev. Sci. Instr., 55, 1684, (1984).

K. H. Schoenbach, G. Schaefer, M. Kristiansen, H. Krompholz, H. Harjes, and D. Skaggs, "Investigations of E-Beam Controlled Diffuse Discharges", Gaseous Dielectrics IV, ed., L. Christophorou, Pergamon Press, p. 246, 1984.

G. Schaefer, B. Pashaie, P.F. Williams, K.H. Schoenbach, and H. Krompholz, "A New Design Concept for Field Distortion Trigger Spark Gaps", J. Appl. Phys., accepted for publication.

K.H. Schoenbach, G. Schaefer, M. Kristiansen, H. Krompholz, H.C. Harjes, and D. Skaggs, "An Electron-Beam Controlled Diffuse Discharge Switch", J. Appl. Phys., accepted for publication.

K. Schoenbach, G. Schaefer, M. Kristiansen, H. Krompholz, H.C. Harjes, and D. Skaggs, "A Rep-Rated E-Beam Controlled Diffuse Discharge Switch", IEEE 1984 16th Modulator Symposium, p. 152, Arlington, VA, June 1984.

M. Kristiansen, K. Schoenbach, and G. Schaefer, "Opening Switches", Proc. 3rd All-Union Conf. on Engineering Problems of Fusion Research, Leningrad, USSR, June 1984. - Invited